LIMITS OF INFORMATION TRANSMISSION IN PRIMARY MOTOR CORTEX

by

Robert Gregory Rasmussen

B.S. in Biomedical Engineering and Neuroscience, Johns Hopkins University, 2008

Submitted to the Graduate Faculty of

the Swanson School of Engineering in partial fulfillment

of the requirements for the degree of

Doctor of Philosophy

University of Pittsburgh

2015

UNIVERSITY OF PITTSBURGH

SWANSON SCHOOL OF ENGINEERING

This dissertation was presented

by

Robert Gregory Rasmussen

It was defended on

November 9, 2015

and approved by

Andrew B. Schwartz, Ph.D., Professor, Department of Neurobiology

Steve M. Chase, Ph.D., Assistant Professor, Department of Biomedical Engineering and Center for the Neural Basis of Cognition, Carnegie Mellon University

Zhi-Hong Mao, Ph.D., Associate Professor, Departments of Electrical and Computer Engineering and Bioengineering

Doug A. Weber, Ph.D., Associate Professor, Departments of Bioengineering and Physical Medicine and Rehabilitation

Dissertation Director: Andrew B. Schwartz, Ph.D., Professor, Department of Neurobiology

LIMITS OF INFORMATION TRANSMISSION IN PRIMARY MOTOR CORTEX

Robert Gregory Rasmussen, PhD

University of Pittsburgh, 2015

Many people consider the brain to be the ultimate computer. Much like computers, the brain receives input information from the environment via various sensory receptors. The brain then processes that input information, formulates goals, and transmits information to create output movements that seek to achieve those goals. Again similar to computers, the brain has limits in its ability to transmit information. These limits can be studied using information theory, the branch of applied mathematics that gave rise to modern day computing. Although many researchers have studied the limits of the nervous system in transmitting input sensory information, little effort has been applied towards linking information in neural populations to movement.

In this work, we created a novel method for estimating information transmitted by neural populations during a movement task using a limited number of trials per stimulus condition. Using this method, we found that the information transmitted by the population increased up to a limit, as the information required to be encoded by the task increased. We found that this limit was a function of the size of the population. Larger populations could transmit greater amounts of information. However, this relationship also appeared to reach a limit. Lastly, we found that the limit of information transmission is greater in a three-dimensional task compared to a two-dimensional task.

We also studied neural activity during a brain-computer interface where the task dimensionality changed. We found that neurons changed their tuning to identical targets depending on whether they were encountered in the 2D or the 3D context. We present evidence that

the observed changes are a motor system analogue to the phenomenon of dynamic range adaptation, which has been observed throughout various sensory systems. The neurons in the population adapted their tuning models to better utilize their limited range of firing rates to transmit information about desired output movement. Overall, this work opens up opportunities for future research investigating the role of motor cortex in transmitting contextually-encoded information.

TABLE OF CONTENTS

LIST OF TABLES

LIST OF FIGURES

PREFACE

I would first like to thank my advisor, Andy Schwartz, for his help in getting me to this point. He provided me with the freedom, support, and motivation to pursue my interests in computational motor control. His polymathic skill set has been crucial in helping me along the way from fixing seemingly unfixable equipment to simplifying my writing into something understandable. I would be remiss if I did not also thank my officemate, committee member, and collaborator, Steve Chase for his tireless assistance and advising. He has helped guide and form my scientific thinking since my first summer in the lab. Through his stories and humor he has taught me important lessons such as the importance of drinking real coffee as well as the value of working hard but not overcommitting to a single task. Thankfully, he did not have to throw a tomato in my face to teach me that lesson. I would also like to thank lab alumni Sam Clanton, Meel Velliste, and Angus McMorland for their help during my early years in the lab working on the robot project and for their programming knowledge that they bestowed upon me. Andrew Whitford deserves a special thanks for helping me set up my research project as well as training me how to win the respect of a big, grumpy monkey. My career advisor, Aaron Batista, and MSTP director, Richard Steinman, deserve a heartfelt thanks for their caring support and motivation throughout this journey. I would also like to thank the other members of Andy's Motorlab for their assistance, patience, and humor throughout my years working with them.

My friends and family were also key in helping me throughout this long endeavor. Andreea Bostan has been instrumental in motivating me as well as helping me keep my sanity along the way. She has helped me find my balance between work and fun, pushing me to work hard and to take time to enjoy the company of friends or the quiet peace of running. I would also like to thank the Swisshelm Park crew and the members of team Trail-or-Trashed

for the fun and adventures. Lastly and most important, I'd like to thank my amazing family: Mary, Mark, and Chris Rasmussen for always believing in me over the years. I would not be where I am today without their love and support.

1.0 INTRODUCTION

Information theory is a tool frequently used by researchers to study behavior and neurophysiology. Although the field was originally developed to describe telecommunications and sparked the digital age of computers and the internet, the same equations can be used to quantify the information transmitted within the nervous system. Information theory was first used to describe behaviors in judgement and reaching tasks. It was later used to describe the psychophysics of sensation. A gap exists between this work. Performance in movement tasks has been assessed quantitatively using information theory. Similarly, sensory information transmitted through the nervous system has been quantified using information theory. However, little effort has been applied toward linking information in neurons to movement.

Information as a metric has become increasingly important with the emergence of brain-computer interfaces (BCIs). BCIs show promise for restoring interaction with the external world for individuals that have lost that ability through spinal cord injuries, strokes or amputations. These BCIs leverage the nervous system's ability to encode information about movement to control movement of computer cursors or robotic arms. Over the past two decades, BCI research has rapidly progressed, allowing users to complete increasingly complex and intricate tasks. Early experiments in offline and online BCI control demonstrated two- and three-dimensional control of a computer cursor from neural populations [84, 93]. Recent studies with monkeys have demonstrated four DoFs and even six to seven DoFs control of a robotic arm in a self-feeding task as well as a reach-and-orient-to-grasp task [94, 13]. Recent studies with human subjects using anthropomorphic robotic arms have been successful at achieving seven as well as ten dimensional control [14, 101]. Faced with this demand for increasing control, it becomes important to understand the characteristics of the nervous system in encoding information about movement.

In this work, I investigated the limits of information transmission in the motor cortex. I developed a novel method for quantifying the information transmitted by neural populations about arm movements. In Chapter 2, I describe this method and use it to find a limit for information transmission in a neural population within primary motor cortex. In Chapter 3, I describe adaptations that occur in these neural populations with contextual changes in a brain-computer interface task. These adaptations appear to serve the purpose of optimally encoding and transmitting contextually relevant information in the task.

In the following sections, I first provide an overview of information theory and how information is quantified (Section 1.1). I then review how information theory has been applied to behavioral research soon after its development (Section 1.2), being used to quantify the limits of judgement (subsection 1.2.1) and motor movement (subsection 1.2.2). Not long after this behavioral information research was initiated, neurophysiologists began applying information theory to their work (Section 1.3) to quantify information transmission in single neurons (subsection 1.3.1) and, more recently, neural populations (subsection 1.3.2). Because this work focuses on information transmission in the motor cortex, I next introduce previous research on how the motor cortex encodes movements (Section 1.4). Lastly, I provide a brief introduction to a phenomenon observed within many neural systems where encoding adapts to changes in the environment to allow maximum transmission of information (Section 1.5).

1.1 WHAT IS INFORMATION?

Claude Shannon established the field of information theory with his pioneering work in 1948 [86], expanding upon the earlier work of Nyquist [69, 70] and Hartley [38]. In this work, Shannon quantifies the process of communicating a message. While the means or channel through which the message is communicated is not relevant, it is important that the message is comprised of a series of signals, each of which is one out of a set of possible signals. Information is produced when one signal is chosen from that set. When the set is finite and each signal has equal probability of being chosen, information can be measured as the number of possible signals, or any monotonic function of that number.

Shannon and Hartley chose the logarithmic function to measure information. Specifically, Shannon used the logarithm with base 2, defining the information metric as *bits*, coined by J.W. Tukey from "binary digits." This metric is simple to visualize. A switch with an "on" and an "off" position is able to store one bit of information. A group of n such switches would be capable of storing a pattern containing n bits of information. The group of switches has 2^n unique positions which translates to $\log_2 2^n = n$ bits.

Shannon also defined a communication system to transmit the informational signals. This system can be visualized as the schematic in Figure 1.1 and comprises five parts: the information source, transmitter, channel, receiver, destination. The information source chooses the signal or sequence of signals (i.e., a message) out of the set of possible signals to be communicated to the destination. In the case of a telegraph system, the information source chooses the sequence of letters to be communicated. The transmitter processes the signal to allow it to be sent over the channel. From the example of a telegraph, the transmitter translates the letters to sequences of dots, dashes, and spaces that will be sent through the wires. The channel is simply the means of transporting the signal from the transmitter to the receiver, such as wires or coaxial cable. This channel may also be subject to noise. The receiver decodes the transmitted signal. In a telegraph system, each sequence of dots, dashes, and spaces is translated to a letter. Lastly, the destination is the entity for whom the signal was intended.

Such communication systems or channels can be thought of as having a capacity or limit to the amount of information they can transmit over time. In the case of a discrete system without noise and with equally probable signals, the channel capacity, C, is measured as:

$$C = \lim_{t \to \infty} \frac{\log_2 n(t)}{t} \left(\frac{\text{bits}}{\text{sec}} \right) \tag{1.1}$$

Here, $n(t)$ is the number of unique series of signals that can be sent within a duration t seconds. An example of such a channel would be a person flipping a switch off and on. If the person flipping the switch could only flip the switch once per second, then, after time t seconds, the switch position could have been changed t times. The state of the switch over that time period could be described with a binary array of length t. Such an array has 2^t unique values. The number of unique series of signals (states of the switch) that can be

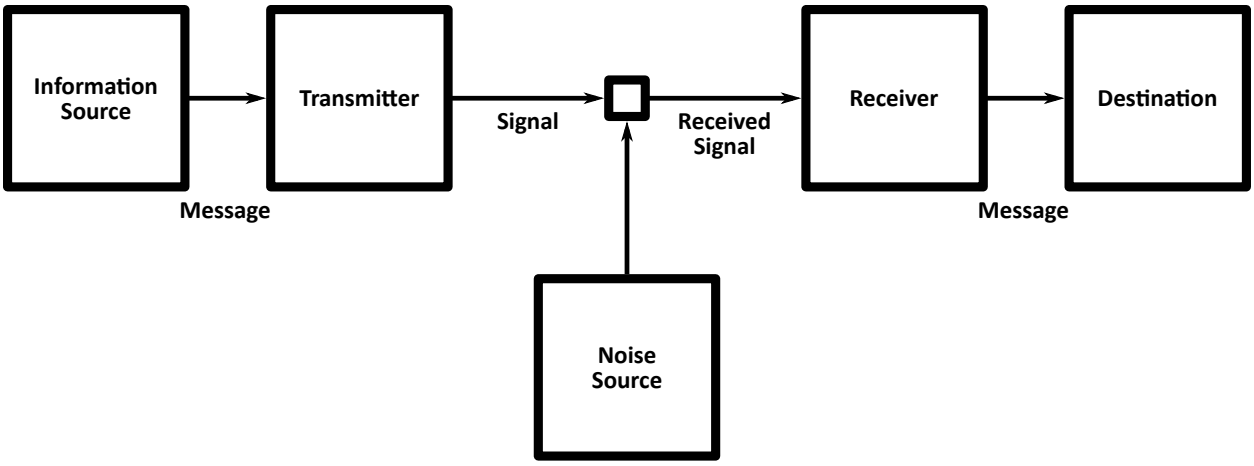

Figure 1.1: Schematic diagram of an example communication system, republished from Shannon, 1948 [86] under public domain.

sent within a time duration t seconds is $n(t) = 2^t$. The channel capacity of this system is calculated as one bit per second.

To generalize the estimation of information beyond cases of equally probable signals, Shannon introduced the concept of entropy. The entropy measure is a generalization of the measurement of information contained in a single signal when all signals are not equally likely. Considering a set of n signals as a random variable, X, with probability distribution $p(x)$ the entropy measure is calculated as:

$$H(X) = \sum_{i=1}^{n} p(x_i) \log_2 \left(\frac{1}{p(x_i)} \right) \text{ (bits)} \tag{1.2}$$

Returning to the case of equally probable signals, where $p(x) = 1/n$, it is easy to see that the generalized information measure of entropy returns the measure of $\log_2 n$ bits:

$$H(X) = n \frac{1}{n} \log_2 n = \log_2 n \text{ bits} \tag{1.3}$$

The entropy equation can be understood as calculating the average amount of information contained in the distribution. The log term, $\log_2 \left(\frac{1}{p(x)} \right)$, calculates the information contained in signal x out of all possible signals X. The summation and scaling by $p(x)$ calculates

the average of the information contained in a single signal across all possible signals. An explanatory example would be a channel that can transmit one of four possible signals $[a, b, c, d]$. The probabilities of each signal being transmitted are: $p(a) = 1/2$, $p(b) = 1/4$, $p(c) = 1/8$, and $p(d) = 1/8$. The entropy for this channel would be calculated as:

$$H(X) = \frac{1}{2}\log_2 2 + \frac{1}{4}\log_2 4 + \frac{1}{8}\log_2 8 + \frac{1}{8}\log_2 8 = 1.75 \text{ bits} \tag{1.4}$$

This value of 1.75 bits is less than the value of 2 bits that would be transmitted in the case of equally probable signals. These signals could be optimally encoded in binary as:

$$\begin{aligned} a &= 0 \\ b &= 10 \\ c &= 110 \\ d &= 111 \end{aligned} \tag{1.5}$$

This binary code could also be thought of as the best set of "yes" or "no" questions to ask to determine an unknown signal, assuming you knew the probability distribution of the signals. The average number of binary digits needed to encode the signals (or the average number of "yes" or "no" questions you would have to ask) is:

$$\frac{1}{2}1 + \frac{1}{4}2 + \frac{1}{8}3 + \frac{1}{8}3 = 1.75 \text{ bits (or questions)} \tag{1.6}$$

Again, this is less than the 2 bits (or questions) needed to encode the signals in the case of equally probable signals.

In the case where the communication system is distorted by noise, the received signal can be thought of as another random variable, Y. The information of the received signal can also be calculated with the formula for entropy. However, some of that entropy will be due to noise, as the noise distorts the probability distribution of the received signal, $p(y)$, away from the probability distribution of the sent signal, $p(x)$. This noise entropy of the transmitted signal can be calculated as the entropy of the received signal conditioned on the sent signal, $H(Y|X)$. This uses the conditional probability $p(y|x)$ and is calculated as:

$$H(Y|X) = \sum_{x \in X} p(x) \sum_{y \in Y} p(y|x) \log_2 \left(\frac{1}{p(y|x)} \right) \tag{1.7}$$

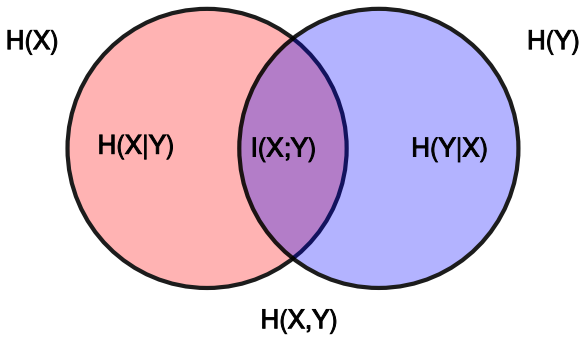

Figure 1.2: Venn diagram illustrating the relationship between entropy and mutual information. The entropy of the sent signal is shown as the red circle and the entropy of the received signal is shown as the blue circle. The overlap of the two circles is the mutual information between the sent and received signals. The entire area bounded within the two circles is the joint entropy, $H(X, Y)$. Republished from Wikimedia Commons [96] with permission.

The amount of information about the original signal that is conveyed as the received signal is calculated as the mutual information, $I(X;Y)$. The mutual information is determined as the difference between the received entropy and the noise entropy:

$$I(X;Y) = H(Y) - H(Y|X) \tag{1.8}$$

The relationships between the signal entropies, noise entropies, and mutual information can be visualized with the Venn diagram shown in Figure 1.2.

This relationship of information and signal and noise entropies can also be understood with the simple example of a noisy channel transmitting one of four possible signals $[a, b, c, d]$, each with equal probability of being transmitted. The joint probability distribution $p(x, y)$ can be visualized as a channel input-output matrix (Table 1.1). In a noiseless channel, the matrix would have have values only along the diagonal, and those values would be equal to

Table 1.1: Example input-output matrix of a noisy channel. Values in the matrix describe the joint probability $p(x, y)$.

		x (transmitter)				
		a	b	c	d	$p(y)$
y (receiver)	a	0.19	0.05			0.24
	b	0.06	0.17	0.05		0.28
	c		0.03	0.17	0.08	0.28
	d			0.03	0.17	0.20
	$p(x)$	0.25	0.25	0.25	0.25	1.00

$p(x_i)$ at $p(x_i, y_i)$. Because this example has noise, there are off-diagonal values. The noise entropy for $x = a$ is calculated as:

$$H(Y|x = a) = \frac{0.19}{0.25} \log_2 \left(\frac{0.25}{0.19} \right) + \frac{0.06}{0.25} \log_2 \left(\frac{0.25}{0.06} \right) = 0.795 \text{ bits} \tag{1.9}$$

Repeating this and averaging along each column, the total noise entropy is calculated as:

$$\begin{aligned} H(Y|X) &= \frac{1}{4} H(Y|x = a) + \frac{1}{4} H(Y|x = b) + \frac{1}{4} H(Y|x = c) + \frac{1}{4} H(Y|x = d) \\ &= \frac{1}{4} 0.795 + \frac{1}{4} 1.210 + \frac{1}{4} 1.210 + \frac{1}{4} 0.904 \\ &= 1.03 \text{ bits} \end{aligned} \tag{1.10}$$

The entropy of the received signal, $H(Y)$ is calculated as:

$$\begin{aligned} H(Y) &= 0.24 \log_2 \left(\frac{1}{0.24} \right) + 0.28 \log_2 \left(\frac{1}{0.28} \right) + 0.28 \log_2 \left(\frac{1}{0.28} \right) + 0.2 \log_2 \left(\frac{1}{0.2} \right) \\ &= 0.24 \cdot 2.06 + 0.28 \cdot 1.84 + 0.28 \cdot 1.84 + 0.2 \cdot 2.32 \\ &= 1.987 \text{ bits} \end{aligned} \tag{1.11}$$

Thus, the mutual information of this noisy channel can be calculated as:

$$I(X; Y) = H(Y) - H(Y|X) = 1.987 - 1.03 = 0.957 \text{ bits} \tag{1.12}$$

With the mutual information measure of information transmission through a communication channel, the capacity of the channel is measured as:

$$C = \sup_{p(x)} I(X;Y) \tag{1.13}$$

where the supremum, sup, is calculated over all possible choices of the distribution of sent signals, $p(x)$. The supremum can be thought of as taking the maximum up to and including the bounded limits of all possible choices of $p(x)$. Calculating the channel capacity as an information rate, bits per second, involves scaling the mutual information by the bandwidth of the channel, in Hertz (or cycles per second). If we return to the simple example of a binary switch, the range of possible choices for the distribution of sent signals is described by the range of Bernoulli distributions. In the Bernoulli distribution, the "off" position has a probability p and the "on" position has a probability $1-p$, where $0 < p < 1$. If we assume the distribution has no noise, then the mutual information is equal to the entropy of the switch system:

$$I(X;Y) = H(X) = H(X_{\text{on}}) + H(X_{\text{off}}) = (1-p)\log_2\left(\frac{1}{1-p}\right) + p\log_2\left(\frac{1}{p}\right) \tag{1.14}$$

Plotting the mutual information as a function of the "off" probability, p, we see that it is maximized at 1 bit of information when $p = 0.5$ (Figure 1.3). This is the simple case discussed earlier of when the switch has equal probability of being in the "off" or "on" position. Assuming an instantaneous response of the switch, the bandwidth of the system is the inverse of the amount of time it takes the operator to flip the switch between "off" and "on."

In the case where the the channel is distorted by additive Gaussian noise with variance (or power) N, Shannon [87] proved the channel capacity is:

$$C = W\log_2\frac{P+N}{N}\ \left(\frac{\text{bits}}{\text{sec}}\right) \tag{1.15}$$

where the channel has a bandwidth of W Hertz and has a signal variance (or power) that is bounded by a maximum value, P. This relationship can be found by calculating the mutual information from the signal and noise entropies. From before, the sent and received signals

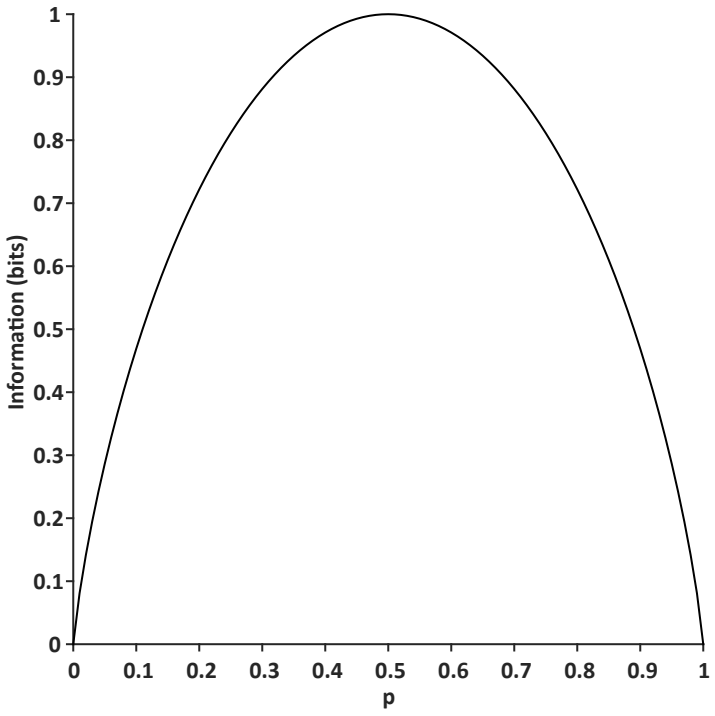

Figure 1.3: Plot showing the information transmitted through a Bernoulli switch system as a function of the probability of the "off" position, p. The information is maximized at 1 bit when $p = 0.5$, where the switch has equal probability of being "off" or "on."

are the random variables X and Y, respectively. The received signal, Y, is equal to the sent signal plus the Gaussian noise, $Z \sim \mathcal{N}(0, N)$.

The conditional probability distribution, $P(Y|X = x)$ may be simplified to a mean-shifted version of the noise distribution, $P(Z - x)$. This is due to the fact that the noise is additive and independent. In other words, the received signal may be written as $Y = X + Z$. Subsequently, the conditional probability distribution can be simplified as $P(Y|X = x) = P(X + Z|X = x)$. Because the distribution created by the addition of two random variables is equal to the convolution of their respective distributions, the conditional probability distribution may also be written as $P(Y|X = x) = P(X|X = x) \star P(Z|X = x)$. The first term in the convolution simplified to the Dirac delta function centered at x. The second term simplifies to the noise distribution, $P(Z)$ due to independence. Subsequently, the conditional distribution simplifies to the mean-shifted version of the noise distribution, $P(Y|X = x) = \delta(X - x) \star P(Z) = P(Z - x)$. Because of this property, the conditional entropy, $H(Y|X)$, is equal to the entropy of the noise:

$$H(Y|X) = H(Z) = \frac{1}{2}\log_2(2\pi N) \tag{1.16}$$

where the right side of the equation is the formula for the entropy of a Gaussian distribution with power, N.

The bound for the entropy of the received signal can be derived from the bound of the sent signal variance. Because the noise is additive, the variance of the received signal may be written as $E(Y^2) = E((X + Z)^2)$, where $E(R)$ is the expected value of a random variable R. The exponent may be expanded: $E(Y^2) = E(X^2) + 2E(XZ) + E(Z^2)$. Because the noise is also independent, the covariance simplifies as $E(XZ) = E(X)E(Z)$. Lastly, because both the signal and noise are zero-mean and the variance of the sent signal is bounded by P, the variance of the received signal is also bounded:

$$E(Y^2) = E(X^2) + E(Z^2) \leq P + N \tag{1.17}$$

Because the Gaussian distribution maximizes the entropy for all distributions with equal variance, the entropy of the Gaussian distribution with variance $P + N$ forms an absolute

bound on the entropy of the received signal:

$$H(Y) \leq \frac{1}{2}\log_2(2\pi e(P+N)) \tag{1.18}$$

Thus, the mutual information through the channel, $I(X;Y) = H(Y) - H(Y|X)$, is bounded:

$$I(X;Y) \leq \frac{1}{2}\log_2(2\pi e(P+N)) - \frac{1}{2}\log_2(2\pi eN) = \log_2\left(\sqrt{\frac{P+N}{N}}\right) \tag{1.19}$$

As discussed above, the entropy of the received signal is maximized when the distribution, $p(y)$, is Gaussian, $Y \sim \mathcal{N}(0, P+N)$ and the variance of the sent signal, $E(X^2)$, is at the bound, P. The distribution of the received signal is Gaussian if and only if the distribution of the sent signal is Gaussian. Thus, the mutual information is maximized when the sent signal is Gaussian with variance, P (i.e., $X \sim \mathcal{N}(0, P)$).

The maximum amount of information the channel can encode with a single amplitude (signal) is $\log_2\left(\sqrt{\frac{P+N}{N}}\right)$ bits. To convert this maximized information into a channel capacity of bits per second, we scale this value by the number of amplitudes (signals) the channel can send per second. In this example, the channel has a bandwidth of B Hertz (or cycles per second). Additionally, Shannon assumes that the channel may encode two distinct amplitudes in a single cycle - one amplitude for the negative swing and a separate amplitude for the positive swing. Subsequently, the channel capacity may be calculated as:

$$C = 2B\log_2\left(\sqrt{\frac{P+N}{N}}\right) = B\log_2\left(\frac{P+N}{N}\right) \ \frac{\text{bits}}{\text{sec}} \tag{1.20}$$

This can also be understood with estimating $n(t)$ for the noisy channel. In a time window of t, the channel can encode information with $2tB$ amplitudes (signals). With the noise, the number of amplitudes that can be distinguished in that time window is bounded at:

$$M = \left(\sqrt{\frac{P+N}{N}}\right)^{2tB} \tag{1.21}$$

Extending the analogy of a switch, the channel is akin to $2tB$ multi-position switches that can each encode $\sqrt{\frac{P+N}{N}}$ unique states or positions. The channel capacity can then be seen as:

$$C = \frac{\log_2 M}{t} = B \log_2 \left(\frac{P+N}{N} \right) \tag{1.22}$$

Shannon's development of the field of information theory helped pave the route of the information age. The simple concept of binary switches encoding information is widespread through computers and other modern technology, where various forms of information are stored and transmitted as "bits" of information, encoded as sequences of 1's and 0's. Shannon's work also created a new way to study and understand animal behavior and the nervous system.

1.2 INFORMATION IN BEHAVIOR

Soon after Shannon's work in developing information theory, physiologists began applying his methods of quantifying information to their research. It makes sense to apply information theory to physiology. A goal of physiology is to understand how input stimuli are translated to output behaviors. In essence, the animal being studied functions as a communication channel. The input stimulus functions as the signal being sent and the resultant behavior of the animal functions as the delivered signal. Physiologists may then measure the throughput information to understand the effective channel between stimulus and behavior. Furthermore, the researchers may adjust the distribution of the input stimuli to find the limits of information transmission through the behavioral system.

1.2.1 Judgement of stimuli

The application of Shannon's information theory to behavioral responses was first proposed by Miller and Frick [65]. One of the earliest studies of directly applying Shannon's work to behavioral research was Garner and Hake's study of the information contained in judgements [31]. In their work, they studied the perception of loudness by comparing the discretized

Table 1.2: Stimulus-response matrix republished from Garner and Hake's study on judging loudness of sounds [31] with permission. The stimuli (k) are counted in the columns and the responses (j) are counted in the rows. The last row and last column sum the total number of each stimulus category and each response category, respectively.

		k (stimulus)				
		1	2	3	4	N_j
j (response)	1	76	20			96
	2	24	68	20		112
	3		12	68	32	112
	4			12	68	80
	N_k	100	100	100	100	400

levels presented to subjects with their selected levels of response. To calculate the information transmission of the auditory judgement channel, they introduced the practice of creating a stimulus-response matrix.

In the stimulus-response matrix, individual responses are summed for all possible combinations of stimuli and responses. For example, in Garner and Hake's study, one of four unique stimuli were presented and subjects chose one of four response categories, which were summarized in a 4×4 matrix. One such matrix from their work is recreated in Table 1.2. In this matrix, the stimuli (k) are counted in the columns and the responses (j) are counted in the rows. The total number of each stimulus category and each response category are summed as N_k and N_j, respectively. For example, of the 100 times that stimulus 4 was presented, the subject incorrectly judged it as 3 a total of 32 times. A perfect auditory judgement channel would have 100's along the diagonal.

Garner and Hake assumed the responses and stimuli to be random variables, J and K, respectively. With this assumption, the stimulus-response matrix describes the probability distributions, $p(j)$ and $p(j|k)$. The information transmission of the channel can then be

measured as the difference between the stimulus entropy and the noise entropy in the rows of the matrix. Note that the data in Table 1.2 is identical to the data in Table 1.1, scaled by the 400 trials. Thus, the mutual information is again equal to:

$$I(J;K) = H(J) - H(J|K) = 1.987 - 1.03 = 0.957 \text{ bits} \tag{1.23}$$

Out of the maximum 2 bits of information that could be transmitted, the auditory judgement channel transmitted 0.96 bits of information.

Later work by Garner [30] completes a more thorough analysis of the information transmitted in loudness judgements for different numbers of sound stimuli. When accounting for response differences between different observers as well as the effects due to previous stimuli, they found that the information transmission reaches a maximum near 2.3 bits as the number of stimulus categories, or input information, increases. It is important to note that this maximum cannot be called the "channel capacity." Changing the number of stimuli presented is not the equivalent of evaluating different stimulus distributions, $p(k)$. Instead, changing the number of stimuli also changes the overall "channel" being considered. Because of this fact, the maximum transmission they found represents the limit of information transmission for the task with equally probable input stimuli.

Seven years after publishing the introduction of information theory to behavioral research, Miller published a review on the capacity of information processing in behavior and the role the "magic number" seven has played in that work [64]. Miller's review discusses how the information processing in behavior consistently found a limit near 2.8 bits or seven signals. Miller plotted the data from the multiple studies in his review, showing the output information transmitted as a function of the input information. These plots are recreated in Figure 1.4.

1.2.2 Movement responses

While much of the early work in applying information theory to behavioral research involved judgement responses about stimuli, Paul Fitts took a different approach to estimate the informational capacity in the motor system's control of movement [27, 28]. Fitts applied

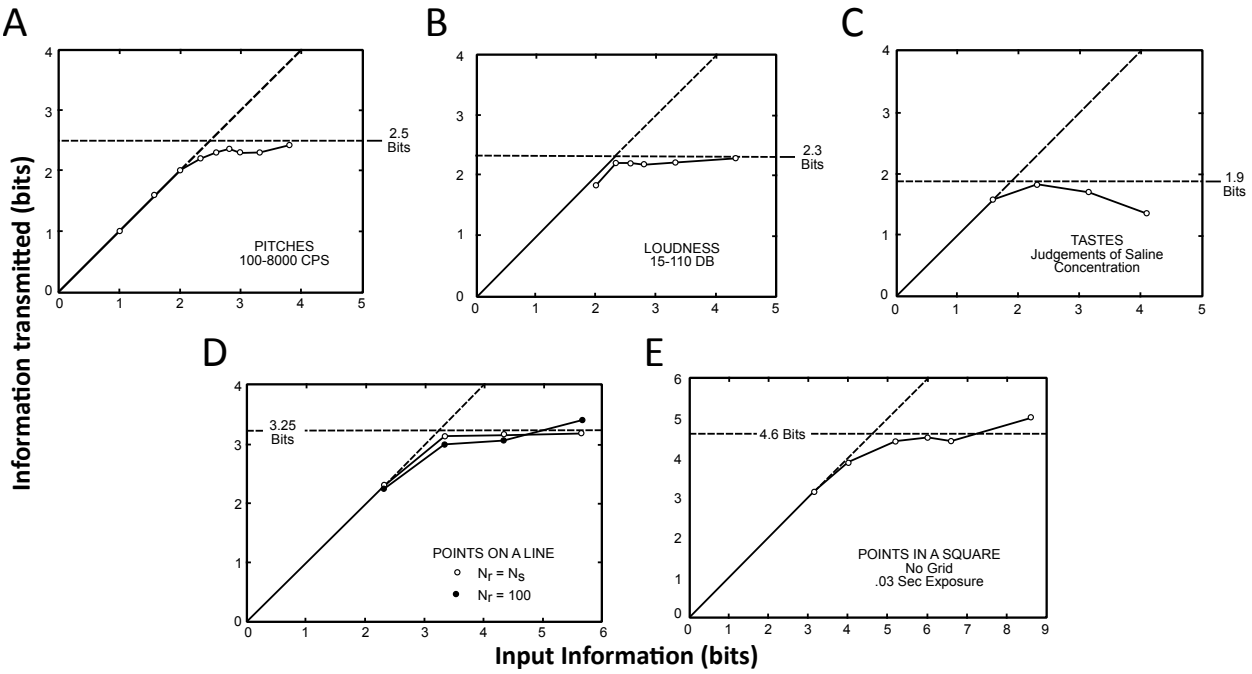

Figure 1.4: Limits of information transmission in behavior. Multiple plots republished with permission from Miller's review [64] showing output information transmission as a function of input information. (A) Data from Pollack [75, 76] on information transferred when making judgements on auditory pitch. (B) Data from Garner [30] on judgements of auditory loudness. (C) Data from Beebe-Center, et al. [4] on judgements of saltiness. (D) Data from Hake and Garner [37] on information transmitted on judgements of the linear position of a pointer. (E) Data from Klemmer and Frick [51] on information transmitted on judgements of the position of a dot in a square.

an approximation of Shannon's formulation of the communication channel capacity in the presence of Gaussian noise (Equation 1.22) to describe performance in a movement task. The primary task in Fitts' experiments involved tapping two targets with a stylus (Figure 1.5). The movements required to hit the targets were of amplitude A and each target had a width of W.

With this task setup, Fitts proposed a measurement of the task difficulty based upon information theory. Fitts termed this metric as the index of difficulty (ID):

$$ID = \log_2\left(\frac{A}{W/2}\right) \text{ bits} \tag{1.24}$$

In order to estimate the "bandwidth" of the motor system channel, Fitts calculated the movement time, MT, for subjects completing the task. Fitts divided ID by MT to estimate the capacity of the motor system channel. He termed this metric as the index of performance (IP):

$$IP = \frac{1}{MT}\log_2\left(\frac{A}{W/2}\right) \frac{\text{bits}}{\text{sec}} \tag{1.25}$$

Although Equation 1.25 resembles Equation 1.22, the similarity is not exact. MacKenzie investigated the information-theoretic basis of Fitts' work [59]. MacKenzie noted that in Fitts' derivation of the index of performance, he referenced Goldman's [36] approximation to Equation 1.22:

$$C = B\log_2\left(\frac{P}{N}\right) \tag{1.26}$$

Goldman noted that Equation 1.26 is only an approximation to Equation 1.22, valid when "the transmitted power is large in comparison with the noise." Unfortunately, Fitts' experiments used conditions where the signal (movement amplitude) was small relative to the noise (target width), including conditions where $A = W$.

Fitts scaled the target width by half in Equation 1.24 and Equation 1.25 in attempt to correct for the inaccuracies. Fitts argued that this correction "insures that the index will be greater than zero for all practical situations." In other words, ID would be less than zero when $A < W/2$ with the correction rather than when $A < W$. Notably, in the experiments that Fitts devised, conditions where $A < W/2$ were impossible. With this correction, Fitts found that the index of performance was relatively consistent across a wide range of indices of

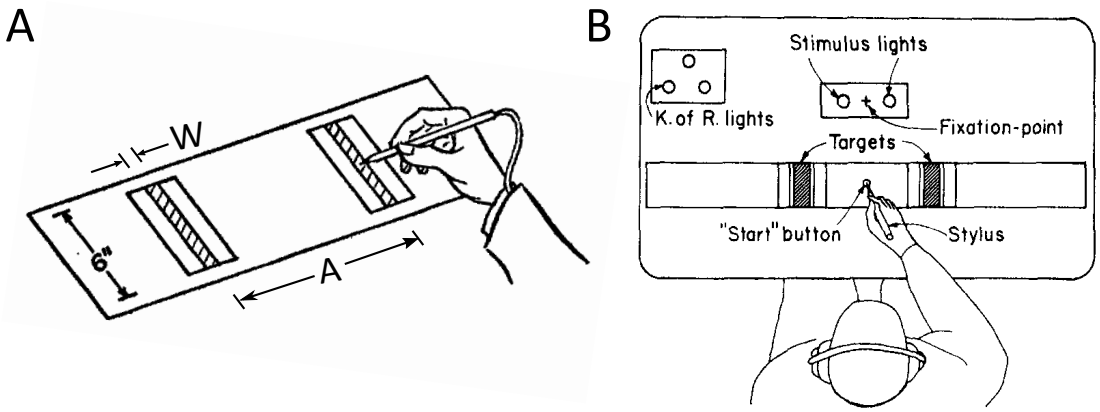

Figure 1.5: Movement tasks in Fitts' experiments republished with permission. The tasks involved tapping the two targets with the stylus. (A) Illustration of the movement task from Fitts' 1954 study [27]. Subjects were instructed to reciprocally tap the two targets with the stylus as fast as possible while maintaining accuracy. (B) Illustration of the movement task from Fitts' 1964 study [28]. Subjects were instructed to rapidly move the stylus from the start button to one of the two equidistant targets as indicated by the stimulus lights. Subjects were provided with knowledge of results (i.e., hits, overshoot errors, and undershoot errors) from the set of lights next to the stimulus lights. The amplitude of movement, A, was calculated as the distance between the start button and the center of the target.

difficulty, with the index of performance values gradually falling off outside of the midrange values of ID. Fitts proposed that this index of performance described the channel capacity of the subject completing the task, being able to transmit a maximum of around 10.3 to 11.5 bits per second.

In later studies, Fitts and Peterson calculated the index of performance by fitting the movement times and the indices of difficulty sampled in their tasks, to the linear equation:

$$MT = a + bID \tag{1.27}$$

where a and b are the regression coefficients. The index of performance is calculated as the inverse of the slope, $IP = 1/b$. Ideally, the intercept, a, would be equal to zero as the reaction time is already subtracted from the total trial time to give the movement time. The intercept may be viewed as an indication of the accuracy of the model, or as an additive factor in the task that does not vary with ID (e.g., target dwell time) [60]. Fitts and Peterson found negative values for the intercept (-70 to -42 ms) in their studies [28]. These fits predicted unrealistic, negative movement times for indices of difficulty near zero (i.e., when $A \approx W/2$).

At the suggestion of Welford [98], Fitts and Peterson tested an alternative definition for the index of difficulty:

$$ID = \log_2 \frac{A + 0.5W}{W} \tag{1.28}$$

The change was suggested based upon observations that the alternative definition reduces the magnitude of the intercept, a, in Equation 1.27. Using this alternative formulation, Fitts and Peterson found a positive intercept value of 6 ms. The model then realistically predicted near zero values of MT for values of ID near zero (i.e., when $A \approx W/2$). This formulation also returned an improved fit to the data from Fitts' 1954 experiment [27], returning an R^2 value of 0.980 versus 0.966 [59].

Later, MacKenzie [59, 60] proposed an improved model that most closely resembles Equation 1.22:

$$ID = \log_2 \frac{A + W}{W} \tag{1.29}$$

Comparing Equation 1.22 to Equation 1.29, the amplitude of the movement, A, is analogous to the signal going through the motor channel. In other words, a perfect movement would

have a distance of A. However, the constraints of the task allow errors in the movement signal. The width of the target, W, is analogous to the noise added to the movement signal sent through the motor channel. Not only does this formulation provide a closer analogy to Equation 1.22, it also provides an improved fit to the data. Reanalyzing the data from Fitts' 1954 experiment [27], MacKenzie demonstrated the improved fit to the data using Equation 1.29 ($R^2 = 0.987$) versus the using either Equation 1.28 ($R^2 = 0.980$) or Equation 1.24 ($R^2 = 0.966$) [59].

Multiple studies have demonstrated that the movement endpoint does follow a normal distribution [27, 99, 16]. Moreover, when the target widths were significantly large or small, the distribution of target endpoints was not well-described by the target width. Subsequently, the output or "effective" target width, W_e, is derived from the observed distribution of target endpoints [99]. The common formulation for the effective target width can be understood by the equation for the entropy of a normal distribution. The entropy for a normal distribution with standard deviation, σ, is $\log_2(\sqrt{2\pi e}\sigma) \approx \log_2(4.133\sigma)$. Subsequently, the effective target width is computed as $W_e = 4.133\sigma_w$, where σ_w is the observed standard deviation of the movement endpoints. Thus, the index of performance may be re-formulated by replacing the target width, W, with the effective target width, W_e. This formulation of the index of performance is currently the most widely used version and has been adopted as the ISO standard for measuring throughput of movements.

An important footnote in Fitts' 1954 paper describes the applicability of his work to different aspects of movement: "Although only amplitude is considered here, the present rationale can be extended to the question of the rate of information involved in the selection of the direction, the force, or the duration of movements." Along the lines of choosing the direction of movements, MacKenzie and Buxton [60, 61] studied the extension of Fitts' work to two-dimensional tasks. In these tasks, the targets had both a width, W, a height, H, and were at a distance, A, from the starting point (Figure 1.6). In their studies, they investigated what would be the appropriate choice for the "noise" in the amplitude signal of the movement. They investigated how well Equation 1.29 fit the data when the W used in the equation was W, $\min(W, H)$, $W + H$, $W \times H$, or W', the width of the target along the direction of movement. They discovered that the data was best fit when the smaller of

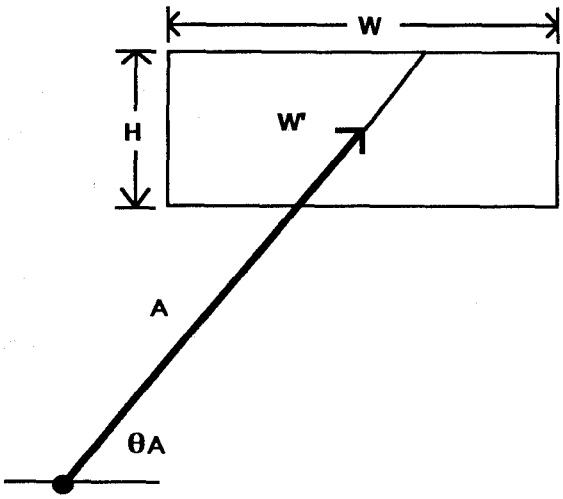

Figure 1.6: Two-dimensional Fitts-like task in MacKenzie and Buxton's experiments [60, 61] republished with permission.

W or H was used as the "noise" in Equation 1.29. This can be thought of as although the subjects may still be aiming towards the center of the target, their movement endpoint is most constrained by the smaller value.

Extending this finding to a more extreme case, Accot and Zhai [2, 3] demonstrated the applicability of Fitts' indices of difficulty and performance in a "goal-passing" task. This task is illustrated in Figure 1.7. In the task, the subject was required to move a stylus between the two goals at a distance of A apart and with a width of W. The objective of the goal-passing task was to move the stylus across the target within the width of the target. This is different from the task in Fitts' experiments where the width of the target was collinear with the amplitude and the subjects were required to stop the stylus upon the target. Comparing the task to that of MacKenzie and Buxton, the target has a width of infinity and a height of W. Accot and Zhai found that Fitts' indices of difficulty and performance still fit their experimental data in this extreme case.

Accot and Zhai further extended their goal passing task to the case of an infinite series of goal passing tasks. One such task was drawing a path within a bounded curve (Figure 1.8).

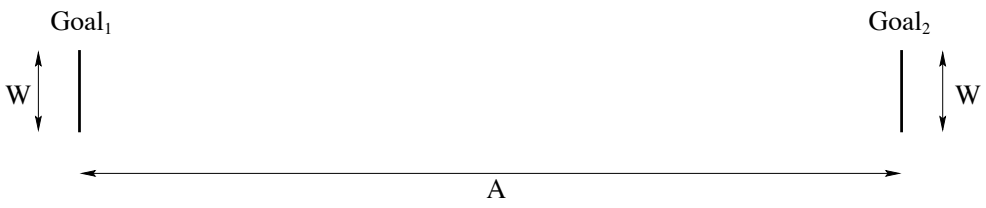

Figure 1.7: Goal-passing task in Accot and Zhai's experiments [2, 3] republished with permission.

They developed a "steering law" that describes the index of difficulty, ID_C, for drawing a path within a curve, C:

$$ID_C = \int_C \frac{ds}{W(s)} \tag{1.30}$$

Equation 1.30 is a line integral along the curve, C, where ds can be thought of as the infinitesimal arc length along the curve. Thus, the curve is parameterized by s, where the width of the curve, W, is a function of s. They found that the steering law well described the performance of subjects in tracing multiple curves of varying directions and widths.

As a side note, their work did not thoroughly investigate the role of curvature in the estimates of the indices of difficulty and performances. In fact, many studies have demonstrated a two-thirds power law relationship between tangential movement velocity and movement curvature [56, 95]. In other words, the movement velocity is linearly proportional to the

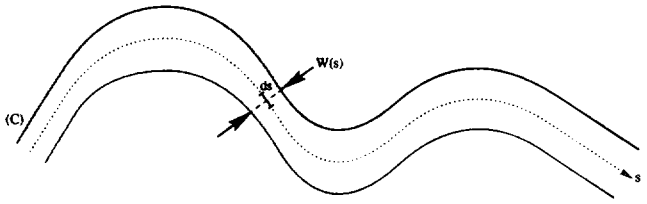

Figure 1.8: Steering law task in Accot and Zhai's experiments [2] where subjects drew a path within the curve, C, with varying width, W. Republished with permission.

two-thirds power of the radius of curvature of that movement. This result implies that the index of difficulty increases for movements with smaller radii of curvature. Although the steering law does not account for the radius of curvature, the results may be explained by considering the effective width of the curve observed during the task. Indeed, multiple studies have demonstrated that the variance (or effective width) in traced ellipses decreases with the radius of curvature [56, 62]. Thus, this decrease in effective width would translate into an increase in the index of difficulty which may explain the decrease in movement velocity. Despite a thorough literature search, no known study has investigated whether this decrease in effective width fully explains the two-thirds power law.

Nonetheless, looking at the curves in the tasks studied by Accot and Zhai, it can be inferred that their work shows the applicability of Fitts' work to a goal-passing task for encoding direction. In such a task, targets would be arcs on a circle. Movements would start at the center of the circle. Successfully completing the task would involve passing the the boundary of the circle at the location of the target arc. Georgopoulos and Massey studied such a task [35]. The setup of their task is illustrated in Figure 1.9. Unlike the measurements of movement capacity in the Fitts-like studies, Georgopoulos and Massey return to the estimation of information transmission by using stimulus-response matrices. One such matrix from their study is shown in Table 1.3. Calculating the information transmission as the number of stimulus directions increased from 4 to 100, they found a maximum information transmission of 4.5 bits with an input information of 6.64 bits (Figure 1.10). Notably, although their results show the information transmission beginning to diverge away from the unity line, the curves do not show a plateau as seen in the curves of Figure 1.4. Unfortunately, their results do not include the effect of the number of stimulus directions on the subjects' movement times. This information would allow for the calculation of output information in bits per second, which would likely reach a plateau at the motor system's limit of information transmission for the task.

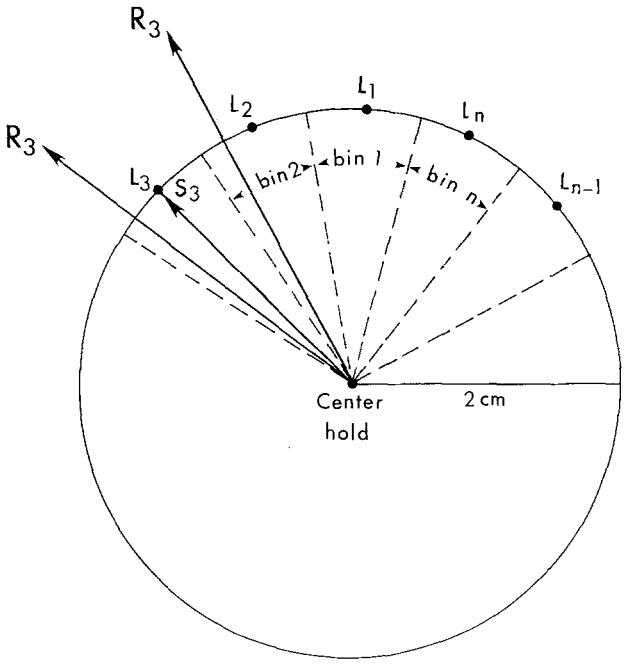

Figure 1.9: Two-dimensional goal passing task in Georgopoulos and Massey's experiments [35] republished with permission. Stimuli and responses are placed into bins. Movement directions required in each trial are indicated by illumination of one of the n lights, eg. L_3. The stimulus direction for light 3 is indicated as S_3 and falls into bin 3. Two possible responses to S_3 are each shown as R_3. Note that one response is successful, falling in bin 3, whereas the other falls in bin 2.

Table 1.3: Stimulus-response matrix republished with permission from Georgopoulos and Massey's study of a two-dimensional goal passing task [35].

		Stimulus Bin												
		1	2	3	4	5	6	7	8	9	10	11	12	N_R
Response Bin	1	4												4
	2		5											5
	3			5										5
	4				5									5
	5					5								5
	6						5	1						6
	7							4						4
	8								5	3				8
	9									2	3			5
	10										2			2
	11											4	2	6
	12	1										1	3	5
	N_S	5	5	5	5	5	5	5	5	5	5	5	5	60

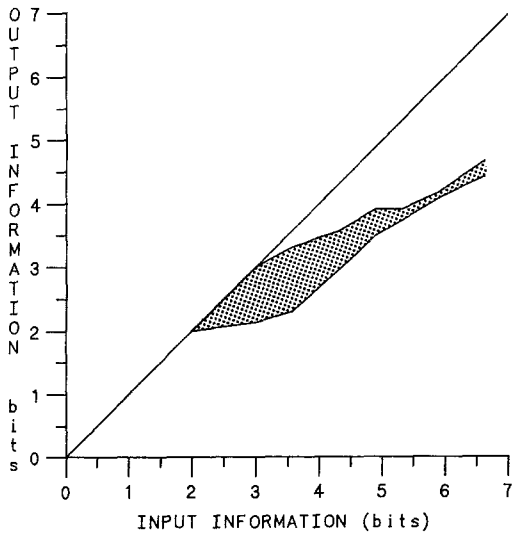

Figure 1.10: Information transmitted in the two-dimensional goal-passing task in Georgopoulos and Massey's experiments [35] republished with permission. Data are from 16 subjects, with the lower and upper curves showing the worst and best results amongst the subjects, respectively. Not all subjects completed each target set.

1.3 INFORMATION IN NEURONS

In addition to the field of animal behavior, information theory has been more directly applied to the study of the nervous system. The application of information theory to neurophysiology makes sense. It is easy to visualize the neural system as a typical communication channel. In concordance with information theory, the brain receives an input signal in the form of varied stimuli, transmits that signal through neurons, and eventually creates an output signal in the form of an action.

1.3.1 Single neurons

One of the early experiments that used information theory to characterize neuronal function was the work of Werner and Mountcastle [100]. They studied the spiking impulse response of cutaneous afferent neurons during applied tactile stimulation. From their initial studies detailed in the same paper, they found that the firing rate of the neuron (Hertz) varied linearly with the log of the applied skin indentation (microns). Upon finding this relationship, they applied Shannon's concepts of mutual information and entropy [87] to quantify the information about the stimulus transmitted by the neuron. Under this formulation, both the neural responses and the stimulus categories were considered to be random variables (R and S, respectively).

Entropy is classically thought of as a measurement of the average amount of information contained in a single sample from a random variable. When considering the response of a neuron as a random variable, there is information contained in the firing rate. This information is quantified in $H(R)$:

$$H(R) = \sum_{r \in R} p(r) \log_2 \left(\frac{1}{p(r)} \right), \tag{1.31}$$

The noise entropy, $H(R|S)$, is calculated as:

$$H(R|S) = \sum_{s \in S} p(s) \sum_{r \in R} p(r|s) \log_2 \left(\frac{1}{p(r|s)} \right) \tag{1.32}$$

Similar to Equation 1.7, Equation 1.32 uses the conditional probability distribution, $p(r|s)$, describing how "noisy" the neural response is to individual stimuli. Although this information is generally thought of as the noise information, although it may be attributable to other, unknown stimuli. When we subtract the information not attributable to the stimuli from the total information, we calculate the mutual information, $I(R;S)$, between R and S

$$I(R;S) = H(R) - H(R|S). \tag{1.33}$$

Werner and Mountcastle used this measurement of mutual information to quantify the information about mechanical stimuli transmitted by a single cutaneous afferent neuron.

In order to calculate the entropies and mutual information, they first needed to calculate the probability distributions, $p(r)$ and $p(r|s)$. To do this, similar to the work in estimating information transmission for judgement responses, they created a stimulus-response matrix to estimate information. In their work, they discretized the levels of the mechanical stimulation of the neurons. They also binned the responses as the number of neural impulses per response in steps of 2 impulses, for observation time windows between 250 to 500 ms. One such stimulus-response matrix from their study is shown in Table 1.4. The curvature of the data off the diagonal of the matrix demonstrates the logistic relationship Werner and Mountcastle found between the neural firing rates and the tactile stimuli. Data from these stimulus-response matrices were used to estimate the limits of information transmission as the number of stimulus bins varied. The data from the neural data in Table 1.4 are shown in Figure 1.11. These results show the neuron reaching a limit of information transmission around 2.7 bits or 6-7 discrete levels for an observation window of 500 ms. When Werner and Mountcastle studied more neurons and varied the observation window between 250 to 500 ms, they found an average maximum value of information transmission around 2.5 bits per stimulus.

1.3.2 Neural populations

Applying these methods to a population of neurons becomes exponentially more difficult with increased population size. This difficulty is commonly referred to as the "curse of

Table 1.4: Stimulus-response matrix from neural stimulation in Werner and Mountcastle's experiments [100] republished with permission. Data are from a single neuron with a observation time window of 500 ms. Note that there was no neural response for stimulation levels 1-3.

Response Categories - Impulses Per Response	Stimulus Categories - maximal = 30																											N_R
	4	5	6	7	8	9	10	11	12	13	14	15	16	17	18	19	20	21	22	23	24	25	26	27	28	29	30	
0-1	29	15	3																									47
2-3	3	11	3																									17
4-5		5	2	1																								8
6-7			8	1																								9
8-9			6	7																								13
10-1			1	10	1																							12
12-3				7	7																							14
14-5				1	7		1																					9
16-7					4	10	3																					17
18-9						8	9	2	1		1		1															22
20-1						2	16	3	2	1	1																	25
22-3							5	8	7	7	11	6	4		1													49
24-5								3	9	6	4	5	9	2	4	2												44
26-7									4	3	5	7	5	8	6	2	5	4										49
28-9									1		1	2	8	2	2	5	6	9	4									40
30-1										1				5	6	7	4	6	7	5	7	3		1				52
32-3															2	4	2	6	7	11	9	7	8	5	1			62
34-5																	2	1	5	2	5	9	11	4	3	4	3	49
36-7																1				1	3	4	6	11	9	4	8	47
38-9																	1					1	5	7	6	7	4	31
40-1																							1	2	5	8	3	19
42-3																									1	3	1	5
44-5																									2	1	1	4
N_S	32	31	23	27	19	29	34	15	24	18	23	20	27	17	21	21	20	26	23	19	24	24	31	30	27	27	20	644

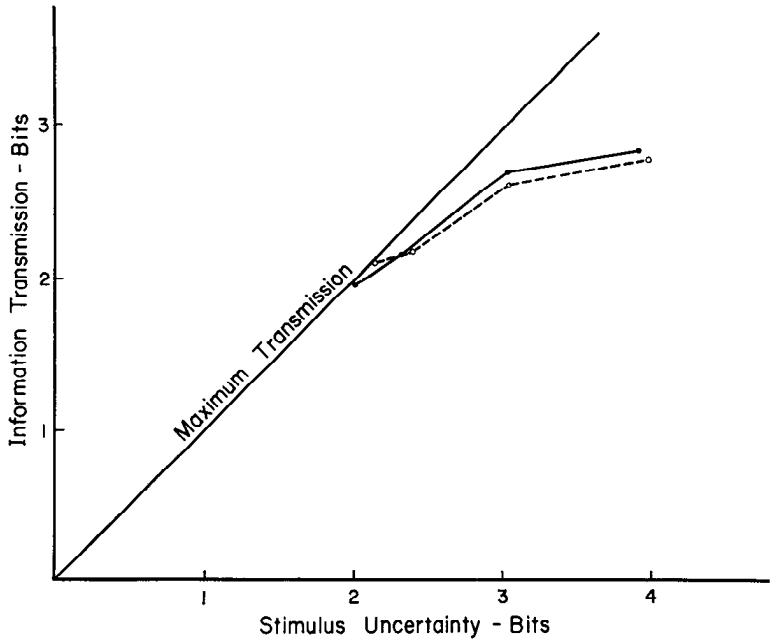

Figure 1.11: Information transmitted from neural stimulation in in Werner and Mountcastle's experiments [100] republished with permission. Data are from the same neuron as from Table 1.4. The data corresponding to that matrix are shown in the dashed line. Data from subsequent testing with the same neuron are shown in the solid line.

dimensionality." For a population of two neurons, the stimulus response matrix becomes a three-dimensional matrix with the discretized stimuli as one dimension and the binned responses of the two neurons as the other two dimensions. For a population of n neurons, each with responses in b bins, the total number of unique responses becomes b^n. Sampling enough data points to build the stimulus response matrices and estimate $p(\mathbf{r}, s)$ quickly becomes an impossible task as the population size increases.

In scenarios where the entropy is estimated with an insufficient number of data points for a large population, errors arise from both bias and variance [74]. These bias and variance errors are illustrated as a function of the number of trials collected per stimulus in Figure 1.12. These errors carry over to the estimation of the mutual information, a direct function of these entropy estimates, as shown in the equations on the preceding page. A series of methods exist that seek to correct for this sampling bias, as reviewed by Panzeri [74]. However, these methods are still limited by sampling issues. The work shows reasonably unbiased estimates of information when "the number of trials per stimulus is as small as the number of possible discrete neuronal responses." However, considering a population of 25 neurons that may respond with twenty or less spikes per stimulus presentation, the number of possible discrete neuronal responses is around 20^{25} or $\approx 10^{32}$.

Despite these corrective methods for sampling bias, the required sampling is still at astronomical levels for large neural populations. For this reason, Panzeri considered small simulated populations of $N = 8$ neurons with binary spike responses in his work. However, a more recent paper by Quian Quiroga and Panzeri [78] notes two potential alternative methods to minimize the required sampling for large neural populations:

> A major and important challenge for neurostatisticians is to find ways to further extend the feasibility of performing information computations with large populations. Two directions are particularly promising. First, it is important to explore the use of optimal dimensionality-reduction techniques that discard dimensions not carrying any relevant information. Second, the information-bias problem for large populations is exacerbated by the fact that the activity of neurons is often correlated. This problem can be diminished by simplifying the correlation structure for example, by considering pair-wise correlations between neurons and ignoring higher-order interactions.

The latter of these routes was explored by Ince, et al. [46]. In this work, they designed estimates of mutual information that considered different correlation structures of the neural

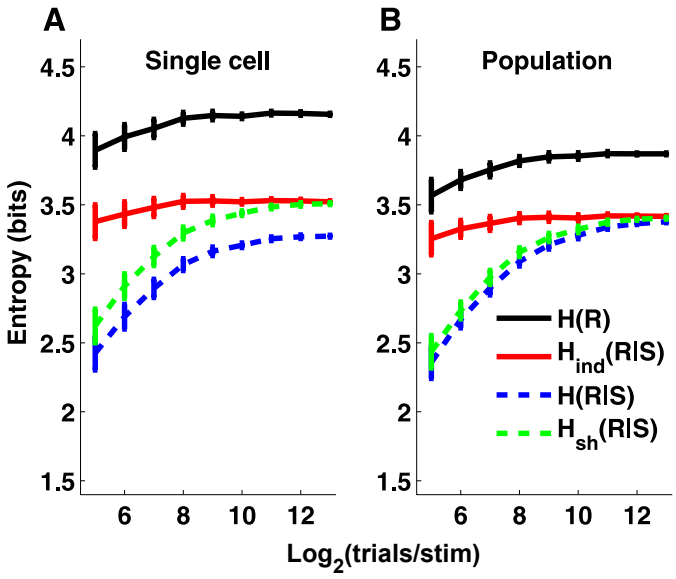

Figure 1.12: Bias and variance in undersampled estimate of entropy and information. Republished with permission from Panzeri, et al. [74]. Data shows the mean ± SD for $H(\mathbf{R})$, $H(\mathbf{R}|S)$, $H_{ind}(\mathbf{R}|S)$, and $H_{sh}(\mathbf{R}|S)$. The independent entropy, $H_{ind}(\mathbf{R}|S)$, is calculated by assuming that the elements in the response are conditionally independent, $P(\mathbf{r}|s) = \prod_i P(r_i|s)$. The shuffled entropy, $H_{sh}(\mathbf{R}|S)$, is calculated by randomly shuffling the individual elements of the response array randomly across trials for a given stimulus. (A) Data from a realistically simulated neural spike train that was discretized into 8 time bins consisting of a binary (0 or 1) spike response. (B) Data from a realistically simulated neural population of 8 cells each with a binary spike response. Both datasets evaluate the responses to 13 different simulated stimuli.

populations (Figure 1.13). The work demonstrates a faster convergence of the information estimate when assumptions are made on the correlation structure of the population. Furthermore, the convergence is faster when less correlation structure is assumed. However, bias problems arise when the correlation assumptions used for the estimate are incorrect (Figure 1.13b). Notably, the alternative information estimate displayed in the figure (I_{sh-ush}) shows convergence on par with the information estimate based upon the assumption of individual marginal (I_1) and lacks the problem of bias when the true population has more correlation structure. Despite this, the convergence occurs around 2^5 trials, or one-eighth of the number of possible discrete neuronal responses. This requisite level of sampling is still too great for large populations of 20 or more neurons. This is especially true when considering more complicated neural responses than the binary responses studied by Panzeri and Ince.

The alternative route of dimensionality reduction has the prospect of better applicability to large neural populations. In some aspects, this route was considered by both Panzeri and Ince by means of decoding the stimulus from the neural response [74, 46]. In this method, Panzeri and Ince proposed replacing the neural response, R, with the decoded estimate of the stimulus, $\hat{S}$. Subsequently, the mutual information, $I(R;S)$, was estimated as $I(\hat{S};S)$. Such decoding facilitates a transformation of the neural data onto a task-relevant space of much lower dimension. This reduced dimensionality significantly reduces the complication of sufficient data sampling as there are fewer points in the probability distribution to estimate. However, with this dimensionality reduction method, it is also necessary to have sufficient sampling to create the decoder and cross-validate the estimations. Furthermore, as the authors acknowledge, the methods used in these papers suffer from the information processing inequality in which there may be a loss of information as a result of the decoding methods. However, this drawback may be slightly alleviated by adding more information from the decoding process, such as the second most likely stimulus from the decoder [46].

An alternative method for dimensionality reduction in computing the mutual information may be that created by Faivishevsky and Goldberger [26]. In their work, they describe a gradient descent method to maximize the mutual information, $I(S;AR)$, where A is $d \times N$ matrix with $d < N$. A potential problem with this method is that it does not remove the bias

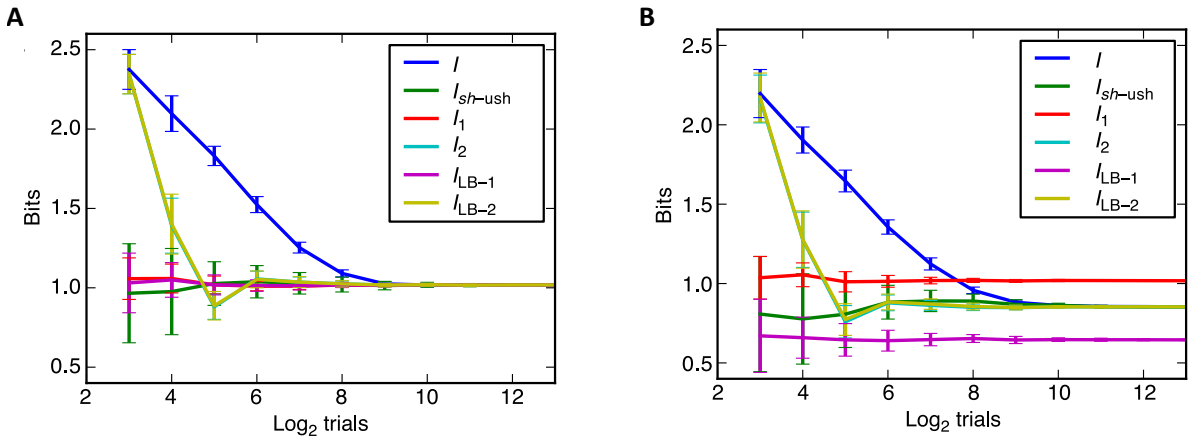

Figure 1.13: Bias in various methods of estimating mutual information. Republished with permission from Ince, et al. [46]. Figures show the mean ± SD for the estimates of mutual information: I, I_{sh-ush}, I_1, I_2, I_{LB-1}, I_{LB-2}. The shuffled minus unconditional shuffled estimate, I_{sh-ush}, is calculated as $I_{sh-ush}(S;\mathbf{R}) = H(\mathbf{R}) - H_{ush}(\mathbf{R}) + \sum_{i=1}^{C} H(r_i) - H_{ind}(\mathbf{R}|S) + H_{sh}(\mathbf{R}|S) - H(\mathbf{R}|S)$. The unconditional shuffled entropy is calculated similarly to the conditional shuffled entropy in Figure 1.12 with the exception that the data points are shuffled across all trials regardless of stimulus condition. The information estimates I_1 and I_2 are calculated by assuming only low order interactions in the population: $I_k(S;\mathbf{R}) = \sum_{\mathbf{r},s} P(s) P_k^{ME}(\mathbf{r}|s) \log_2 \frac{P_k^{ME}(\mathbf{r}|s)}{P_k^{ME}(\mathbf{r})}$. The probability distributions, $P_k^{ME}(\mathbf{x})$, calculate the maximum entropy under the constraints of marginal probabilities only up to order k. In the case of $k = 1$, the probability distribution, $P_1^{ME}(\mathbf{r}|s)$, is equal to the independent distribution, $P_{ind}(\mathbf{r}|s)$. The lower bound of the information that can be decoded with these simplified probability distributions are calculated as: $I_{LB-k}(S;\mathbf{R}) = \sum_{\mathbf{r},s} P(\mathbf{r},s) \log_2 \frac{P_k^{ME}(\mathbf{r}|s)}{P_k^{ME}(\mathbf{r})}$. The data are from simulations of a neural population similar to that in Figure 1.12b where the population was simulated with either individual marginals (A) or both individual and pairwise marginals (B).

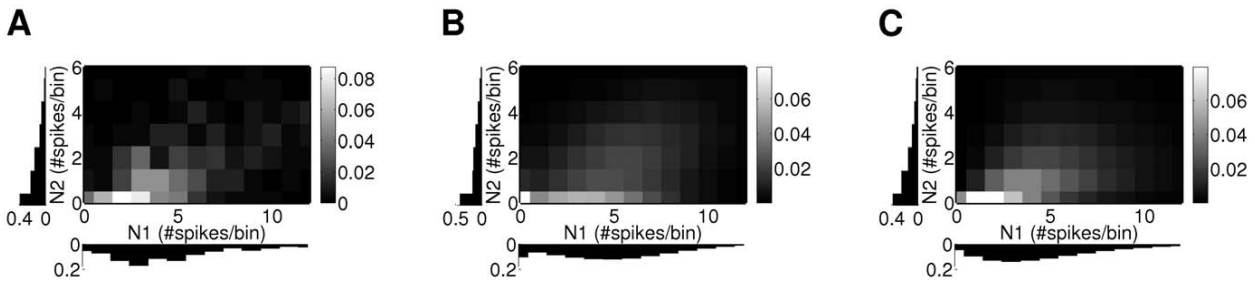

Figure 1.14: Models of population spike count distributions for a population of $N = 2$. Republished with permission from Onken, et al. [73]. (A) Normalized empirical distribution of spike counts for a pair of neurons. (B) Distributions from the multivariate normal distribution model fit to the sample mean and sample covariance of the empirical data. (C) Distributions from the best fitting Clayton copulas with negative binomial marginals to the empirical data.

in information estimates with undersampled datasets. Nonetheless, this method and other dimensionality reduction methods including principle component analysis, factor analysis, as well as linear discriminant analysis may prove promising in:

1. reducing the neural response to a task relevant subspace
2. subsequently minimizing errors in the mutual information estimate from bias and loss in the information processing inequality.

Another potential route to simplifying the estimation of the mutual information for populations of neural activity is similar to the approach discussed above (making assumptions about the level of correlation amongst the neurons), however, this approach makes further assumptions about the shapes of both the correlation structure as well as the marginal distributions. Specifically, the method involves constructing negative binomial fits to the marginal conditional distributions, $p(R_i|s)$ and the covariances are simplified using copulas [73]. The resultant fit using this method compared to the empirical distribution and discrete multivariate normal fit for a pair of neurons is shown above (Figure 1.14). Studies on this method by Onken, et al. [73] demonstrate the Clayton family of copulas to have a superior

fit in terms of log likelihoods on validation data compared to other families of copulas as well as alternative methods of best fit discrete multivariate normal and Poisson latent variables models (Figure 1.15).

A potential benefit of this method is that it describes the probability distribution of populations of neurons with only one free parameter needed to describe the neuronal interactions and two free parameters to describe the negative binomial marginal distributions. With this, it may be feasible to estimate the mutual information with a limited sampling of the population response. Nonetheless, the copula method forces strong assumptions about the correlation structure within the population. The validity of these assumptions has not been well confirmed aside from the work of Onken, et al. in comparing the method to others with populations of 6 neurons. Furthermore, the optimization techniques for fitting the copula method may be computationally unfeasible for large populations of neurons [73].

1.4 NEURAL CODING OF ARM MOVEMENT

As previously discussed, neurons within the sensorimotor system can be considered to be communication channels, transmitting information about perceived input or desired output. The neurons comprising this channel translate the perceived input into neural impulses which are transmitted between neurons to transmit information through the system. The stochastic nature of the neural spikes creates the noise that imposes limits on the ability of the sensorimotor system to transmit information. For desired output, the final step in generating the desired output is through movement. A major source of the descending commands for voluntary movement is the primary motor cortex (M1). Part of these descending commands originate from cortico-motoneuronal (CM) cells in M1. CM cells descend to the spinal cord from cortical layer V where they may make direct connections with motorneurons that synapse with muscles at neuromuscular junctions [57, 47, 79]. Aside from the direct synaptic connections of CM cells, there are extensive indirect connections made by cells in M1 that contribute to and convey information about movement output [45, 83]. With this in mind, it is important to understand how neurons in M1 encode the desired movement output.

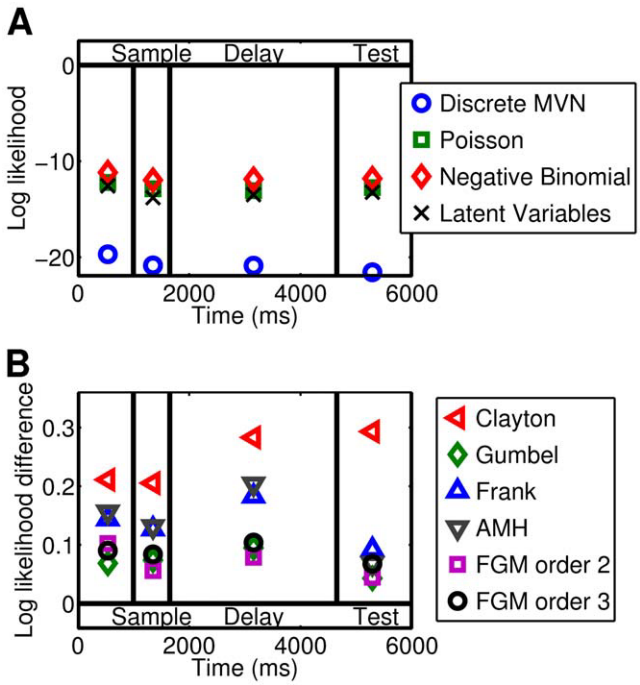

Figure 1.15: Validation of copula models of neural distributions. Republished with permission from Onken, et al. [73]. (*A*) Log likelihoods of a validation dataset, averaged over 20 stimuli, for the discrete multivariate normal distribution (Discrete MVN), the multivariate Poisson latent variables distribution (Latent Variables), and the best fitting copula model with Poisson (Poisson), and with negative binomial marginals (Negative Binomial). (*B*) Difference between the log likelihood of a model with negative binomial marginals and independence assumed between neurons and the log likelihoods of the best fitting parameters for different families of copula models with negative binomial marginals.

Georgopoulos, et al. studied M1 neuronal activity in their 1982 work [33]. They investigated how the firing activity of single neurons in monkey motor cortex modulate with the direction of movement in a 2D center-out task. This task is similar to that shown earlier in Figure 1.9, with the exceptions that circle radius was 8 cm and the monkeys were required to terminate their reach within 12.5 mm of the target lights.

In their work they found that the relationship between neural activity and arm movement was well-described with a cosine function:

$$f(\theta) = b_0 + M_D \cos(\theta - \theta_0) \tag{1.34}$$

where $f(\theta)$ is the firing rate of the neuron in response to a movement in direction θ, b_0 is the average, or "baseline," firing rate of the neuron, M_D is the "modulation depth" of the neuron, and θ_0 is the "preferred direction" of the neuron. For movements towards the neuron's preferred direction, the neuron reaches its maximal firing rate, $b_0 + M_D$, while it reaches its minimal firing rate, $b_0 - M_D$, for movements directly away from its preferred direction. Results from an example neuron in their work are replicated in Figure 1.16.

Georgopoulos, Kettner, and Schwartz later expanded their study relating motor cortical activity and arm movement to tasks involving three-dimensional movement [34, 50, 85]. In their work, they find that the neural response also follows a cosine tuning function for the 3D movements:

$$f(\mathbf{d}) = b_0 + M_D \cos\theta_{\mathbf{p},\mathbf{d}} \tag{1.35}$$

where $f(\mathbf{d})$ is the firing rate of the neuron in response to a movement in the direction of the 3D unit vector, $\mathbf{d}$. The parameters, b_0 and M_D, have the same meaning as in Equation 1.34. The angle, $\theta_{\mathbf{p},\mathbf{d}}$, is the minimum angle between the two 3D unit vectors representing the preferred direction, $\mathbf{p}$, and the direction of movement, $\mathbf{d}$. This cosine tuning function can be identically represented as a linear tuning function:

$$f(\mathbf{d}) = b_0 + M_D \mathbf{p}^\intercal \mathbf{d} \tag{1.36}$$

Results from their work are replicated in Figure 1.17. The neural tuning response of these models can be visualized with tuning volumes (Figure 1.18). With such a tuning volume, the two-dimensional cosine tuning functions can be visualized as slices through the volume.

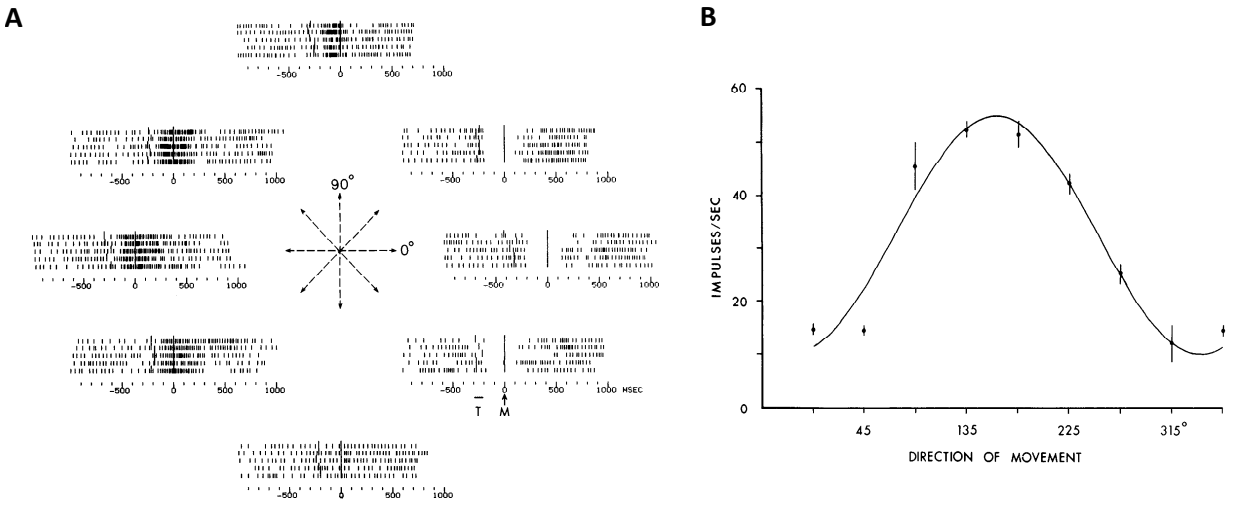

Figure 1.16: Neural responses to two-dimensional movements in a center-out task. Republished with permission from Georgopoulos, et al. [33]. (A) Spike raster plots of a neuron's response to arm movement. The plots are radially placed to align with the movement direction. The rasters are centered at the time of movement onset, M, with the time of target illumination, T, indicated with the oversized vertical lines along each trial row. (B) Average firing rate $\pm$ SEM for the neuron plotted as a function of movement direction. The sinusoidal curve illustrate the cosine tuning function fit to the neuron's data. Firing rates were calculated in time windows from target illumination to target acquisition.

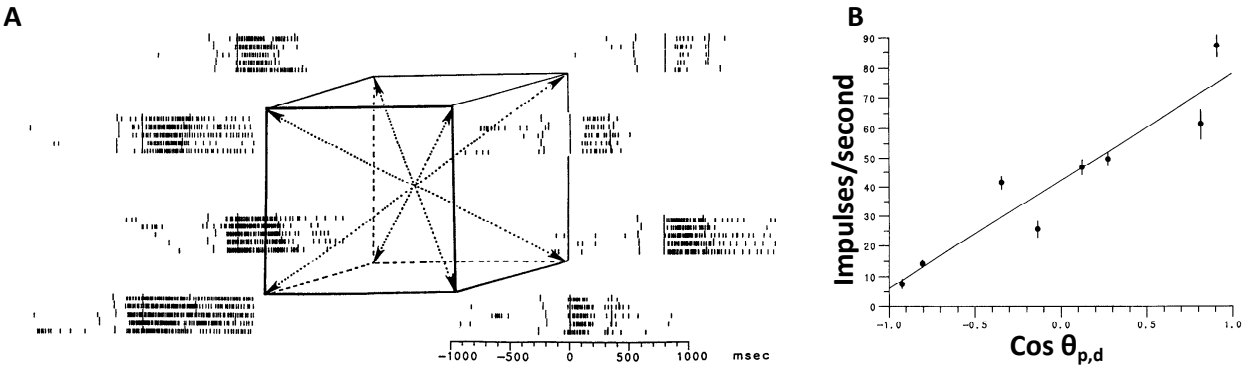

Figure 1.17: Neural responses to three-dimensional movements in a center-out task. Republished with permission from Schwartz, et al. [85]. (A) Spike raster plots of a neuron's response to arm movement. The rasters are similarly arranged and centered as in Figure 1.16a with the exception that the 8 targets were in three-dimensional space. (B) Average firing rate $\pm$ SD for the neuron plotted as a function of $\cos\theta_{\mathbf{p,d}}$. The solid line shows the tuning function fit to the data.

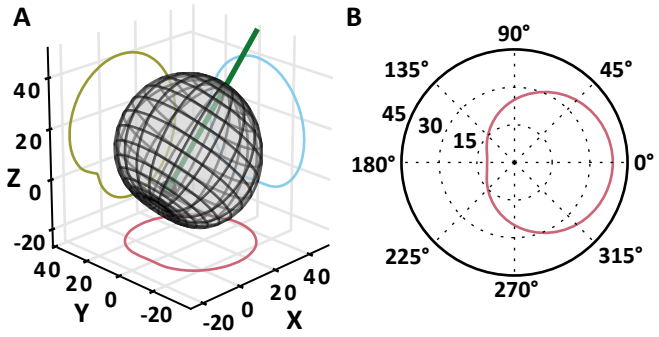

Figure 1.18: Tuning response of an example neuron. (A) 3D polar plot or tuning volume for the neuron. The radius of the volume at a particular point represents the neuron's firing rate for movements in the direction of the point. The units along the axes are $M_D \cdot p_i \cdot d_i$, for $i = X$, Y, or Z. The preferred direction vector is shown in green. The cross-sections of the tuning volume through the xy-plane, xz-plane, and yz-plane are drawn upon the corresponding axes grids. (B) The cross section of the tuning volume through the xy-plane redrawn as a 2D polar plot.

Later work by Moran and Schwartz demonstrated that the M1 neurons were also tuned to the speed of the movements [67]. The speed had both an additive and a gain scaling effect:

$$f(\mathbf{d}, s) = b_0 + s \cdot b_s + sM_D\mathbf{p}^\intercal\mathbf{d} \tag{1.37}$$

where the firing rate $f(\mathbf{d}, s)$ is a function of the movement direction $\mathbf{d}$ and the speed of the movement, s. The parameters, b_0 and M_D, have the same meaning as in Equation 1.34. The new parameter, b_s, measures the magnitude of the additive effect of speed on the neural response. Work by others have demonstrated that M1 neural activity modulates with acceleration [29], joint kinematics and dynamics such as angular velocity [81] and torque [54], as well as EMG activity [11] and muscle contractions [49, 71].

1.5 CONTEXTUAL CHANGES IN NEURAL CODING

The other type of information that neurons in the nervous system transmit is information about perceived inputs. Similar to the areas in motor cortex encoding information about desired movement output, neurons in various sensory areas of the nervous system encode information about sensory inputs. For example, neurons in the visual cortex and retina encode light intensity [53, 43], neurons in the inferior colliculi encode sound pressure levels [80], and neurons in barrel cortex encode environmental perturbations of the whiskers [89].

When considering these sensory areas as information encoders, an interesting question arises. What happens when the distribution of the sensory input, $p(s)$, changes? If the neural tuning functions for the sensory inputs are constant, then information is not optimally transmitted for most distributions, $p(s)$. In order to optimally encode information about the environment, the neural tuning functions (the equivalent of the transmitter in Figure 1.1) would need to change with changes in stimulus distributions.

This is indeed what happens. This phenomenon has been described with a few different names such as "gain rescaling" or "dynamic range adaptation," but the effect observed has been identical: the neural coding of stimuli changes with changes in the stimulus distribution. You have probably experienced this phenomenon yourself when leaving from a dark movie

theater or after turning off your house lights for the night. Initially, the change in the light stimulus distribution is dramatic and you are effectively blinded. Thinking about the neural encoding of light on a scale of 0 to 1, from dark to light, everything is at 1 when you leave the theater and everything is at 0 when you turn off the lights. There is no contrast to the signal; you receive no information about the environment. Then, after a surprisingly brief time (although it certainly may feel like forever), the neural communication channel transmitting light information adapts to the new stimulus statistics. The neural code adjusts so that the scale of 0 to 1 now spans the range of light intensity in the environment. There is now contrast in the signal and you can now receive information about the environment.

Stepping aside from anecdote, this phenomenon has been studied in the retina and the primary visual cortex. When the levels of light intensity in the environment changed, researchers observed changes in the neural encoding of light intensity in these regions [88, 72, 91]. The encoding changed so as to span the intensity levels in the environment with the range of neural firing rates. Similarly, in the inferior colliculi, researchers found that the neural encoding of sound pressure levels adjust based upon the distribution of observed sound pressure levels [55, 17]. Data from one such study by Dean, Harper, and McAlpine [17] are shown in Figure 1.19. In the whisker barrel cortex, the tuning function relating neural firing rates to whisker motion change with changes in stimulus variance [63]. There has only been one study thus far that has investigated dynamic range adaptation in motor cortex [39]. This study demonstrated that the neural encoding of force in an isometric grip task changed with the number and magnitude of discrete forces levels required in the task.

Researchers have looked at adaptations to changes in stimulus statistics from an information theory point of view [7, 24, 97]. Their work has demonstrated that the dynamic range adaptation observed in sensory areas maximizes information transmission. Brenner, Bialek, and de Ruyter van Steveninck [7] estimated the information transmission for theoretical neural response functions. They kept a constant stimulus distribution and adjusted the "stretch factor", θ, of the theoretical neural response function. They estimated the information for values of the stretch factor less than, at, and greater than 1. The value of the stretch factor, $\theta = 1$, indicated the neural response function fit from their studies in an H1 neuron in the visual system of a blowfly. Values less than one narrowed the response function and values

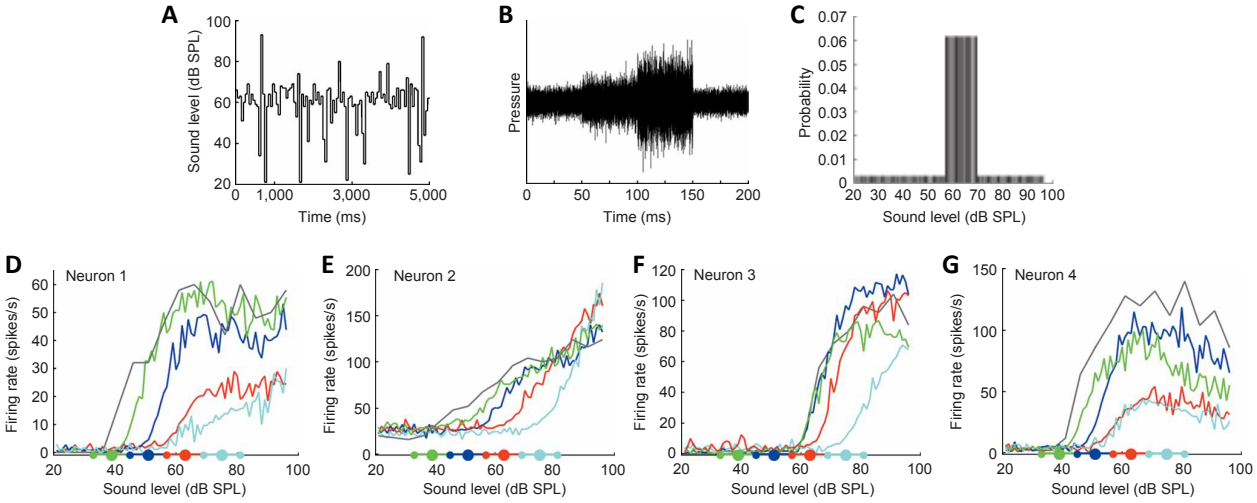

Figure 1.19: Dynamic range adaptation in the inferrior colliculi. Data republished with permission from Dean, Harper, and McAlpine [17]. (A) The sound stimulus presented to the guinea pigs showing the sound pressure levels in dB over 5 seconds. (B) A zoomed in view of the presented stimulus over 200 ms showing the sound pressure. (C) The probability distribution, $p(s)$, of the presented sound stimulus from a trial. (D-G) Tuning functions for four neurons for four trials each showing firing rate as a function of sound pressure level. The stimulus distributions for each trial are shown on the x-axis. Each distribution had the same shape as in C with the center and edges of the maximum probability range shown with the large and small circles, respectively. The color of the tuning curve corresponds to the color of the probability distribution. The gray curve shows the baseline tuning function of each neuron. Note how the tuning functions shift, providing contrast over the highly probable range of sound pressure levels.

greater than one widened the response function. The results from their work are republished in Figure 1.20. Their results demonstrate that the information transmission of the H1 neuron is maximized by the tuning function empirically derived after the neuron underwent dynamic range adaptation. These studies by Brenner and others add evidence to the theory that the nervous system functions as a communication channel, optimally encoding and transmitting information.

1.6 RESEARCH OBJECTIVES AND OUTLINE

The objective guiding the research presented in this dissertation is to study characteristics of the motor cortex in encoding and transmitting information. This goal has particular relevance for brain-computer interfaces (BCIs). BCIs are becoming increasingly complex with increasing degrees of freedom controlled by users. With this in mind, it is important to understand where informational limits exist in neural populations used in BCIs. In Chapter 2, I develop a method for quantifying the information transmitted by motor cortical populations as monkeys move their arms. With this metric, I find that the population reaches an informational limit as the demands of the task increase. Furthermore, this limit is a function of the recorded population size as well as the number of dimensions controlled in the task. In Chapter 3, I investigate the changes in neural coding as the number of dimensions controlled in a brain-computer interface task change. The nature of these changes appears to be akin to the dynamic range adaptation observed in sensory systems (Section 1.5). In Chapter 4, I discuss the impact these information constraints may have on BCI performance. It appears that performance is a function of the population size controlling the BCI and of the dynamic ranges of the neurons comprising the population.

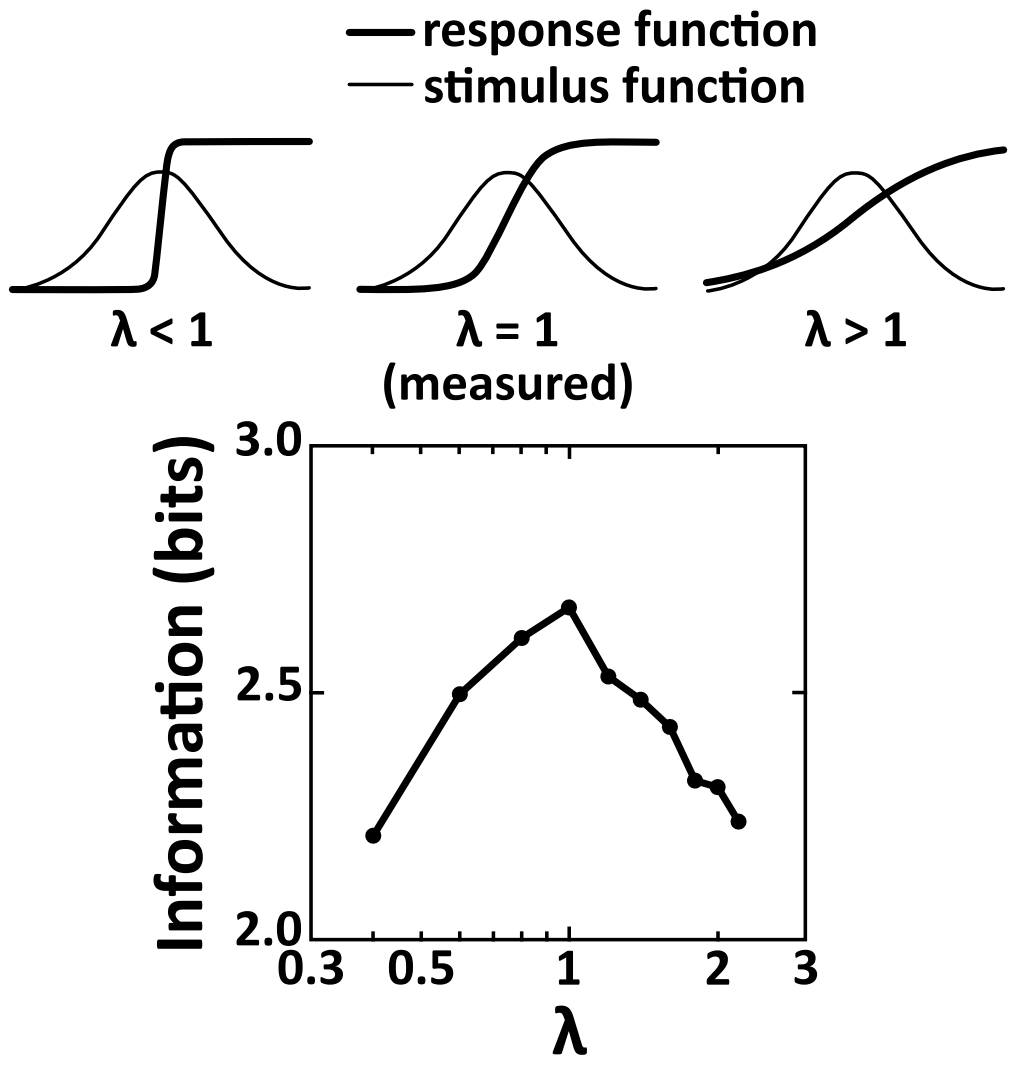

Figure 1.20: Dynamic range adaptation optimizes information transmission. Results from Brenner, et al. [7] republished with permission. The top three plots demonstrate the effect of changing the stretch factor, λ, of the response function with a constant stimulus function. The response function curve shows firing rate as a function of stimulus and the stimulus function curve shows stimulus probability as a function of stimulus. Increasing values of λ stretch the response function. The value, $\lambda = 1$, indicates the emperically derived response function. The bottom plot shows the information transmission of the neural response as a function of the stretch factor. The emperically measured response maximizes the information transmission for the neuron.

2.0 ARM REACHING TASKS

The nervous system can be thought of as a computer. Various sensory receptors deliver information about the environment. The nervous system then processes that input information to formulate goals. Finally, the system transmits information that controls the output movements that seek to achieve those goals. Similar to computers, the nervous system has limits on its ability to transmit information. These limits are studied using information theory, the branch of applied mathematics that gave rise to modern day computing. Although many researchers have studied the limits of the nervous system in transmitting input sensory information, little effort has been applied towards linking information in neural populations to movement. In this work, we propose a novel method for quantifying the information transmitted by neural populations during arm movements. Using this metric, we found that the information transmitted by the population reaches a limit as the demands of the task increase. Furthermore, we found that this limit is a function of the recorded population size as well as the number of dimensions controlled in the task.

2.1 INTRODUCTION

The field of information theory has long been an important tool for investigating issues in physiology. In 1948, Claude Shannon developed information theory to describe the transmission of information in systems [86]. Soon after this work, physiologists began applying information theory to studies of sensory and motor functions [31, 42, 41, 15, 51]. Paul Fitts applied information theory to describe the information capacity of the motor system [27]. In Fitts's work, he made the assumption of movements occurring at the motor system's channel

capacity. Shannon quantified the capacity of a channel with bandwidth B as:

$$C = B \log_2(1 + S/N). \tag{2.1}$$

where the channel has signal power S and is perturbed by additive Gaussian noise of power N. Fitts' eponymous law quantifies the index of performance, or channel capacity, of the motor system as:

$$IP = \frac{1}{MT} \log_2 \left(\frac{2D}{W} \right) \tag{2.2}$$

where MT is the movement time to reach a target of width W at a distance D. Researchers later adapted adapted the Shannon formulation of Fitts' law [60, 92]. This formulation better matches Equation 2.1, replacing the term in the log with unity plus the ratio of distance to width.

Later, neurophysiologists Werner and Mouncastle used information theory to quantify the limits of information transmission in cutaneous afferent neurons [100]. Since this early work, many neurophysiologists have sought to quantify the limits of information transmission throughout the nervous system and its relation to neural coding [20, 21, 58, 1, 6]. These applications consider environmental stimuli and the corresponding neural responses to be random variables, S and R. Under this construct, the neural responses contain information quantified as entropy:

$$H(R) = -\sum_{r \in R} p_R(r) \log_2 p_R(r). \tag{2.3}$$

A portion of this total information is unrelated to the measured environmental stimuli and is generally thought of as noise, although it may be attributable to other, unknown stimuli. This "noise information" is quantified as conditional entropy:

$$H(R|S) = -\sum_{s \in S} \sum_{r \in R} p_{R,S}(r, s) \log_2 p_{R|S}(r|s). \tag{2.4}$$

The remaining portion of the neural information is the information transmitted about the stimuli by the neural responses. This information transmission is quantified as mutual information:

$$I(R; S) = H(R) - H(R|S). \tag{2.5}$$

Channel capacity is related to mutual information as the supremum of the mutual information over all possible distributions $p_S(s)$.

In our work, we sought to quantify the mutual information of a population in primary motor cortex (M1) in Fitts-like motor tasks. Considering the targets as the stimuli for the neural responses, we find that as the stimulus entropy increases, the information transmission of the population reaches a limit. Furthermore, this limit scales with the size of the population and the dimensionality of the task.

2.2 METHODS AND MATERIALS

2.2.1 Behavioral paradigm

Two monkeys (*Macaca mulatta*) each performed a center-out reaching task (Figure 2.1a) while hand position was tracked optically and neural activity was recorded with multielectrode arrays. Each monkey controlled a computer cursor on a stereoscopic 3D monitor viewed through a mirror, through movement of their optically tracked hand. The monkeys completed the center-out reaches either in a 2D or 3D context (Figure 2.1c, d). The movement of the cursor was constrained to the xy-plane during the 2D context although the monkeys' arms were not similarly constrained.

Trials started with the monkey holding the cursor near the origin of the task space for a period of 25 ms (Figure 2.1b). The task space origin was displayed as a sphere with a radius of 7.7mm (Monkey C) or 6.3-8.7mm (Monkey N). After the hold period, the origin sphere disappeared and a randomized target from the current target set appeared on the monitor. The monkey then reach towards the target during a reach period of either 1 second (Monkey C) or 3 seconds (Monkey N). The reach period was shorter for Monkey C as that monkey had significantly more experience with center-out reaching tasks than Monkey N. Although the reach period for Monkey N was longer, over 98.7% were completed in 1 second. Histograms of the reach times for the 2D and 3D trials for all sessions from Monkeys C and N are shown in Figure 2.2 and Figure 2.3, respectively. The long tails of the histograms for Monkey N

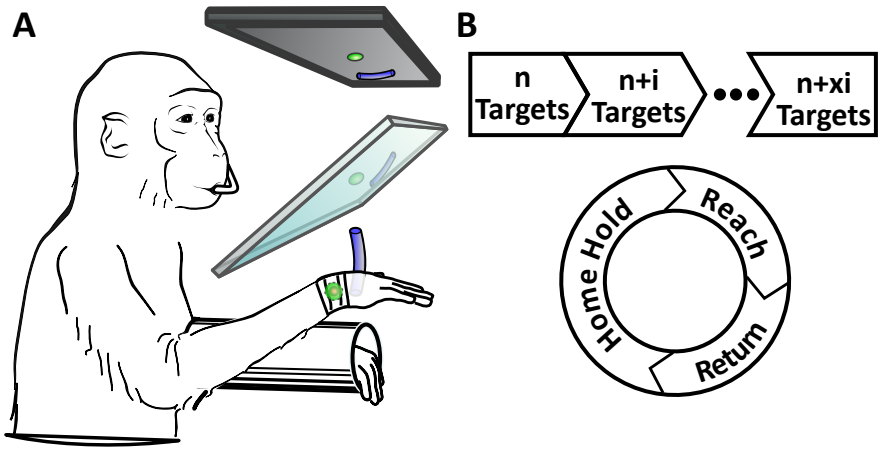

Figure 2.1: Experimental Setup (A) The monkey sat in front of a mirror reflecting the image of a 3D stereoscopic monitor. The monkeys controlled movement of a cursor on the monitor by moving their arms. The movement of the arm was tracked using infrared markers attached to their hands. (B) Recording sessions began with a block of trials for a set of targets. After successfully completing the block of trials (40-100 trials per target), the next block of trials with a larger target set began. This incremental increase in the target set after successful completion of a block of trials continued until the end of the recording session. For some recording sessions for Monkey C, blocks of 3D trials would immediately precede or follow the blocks of 2D trials. Each trial started with holding the cursor at the home position followed by target presentation and a reach period. The monkey then returned the cursor back to the home position to start the next trial.

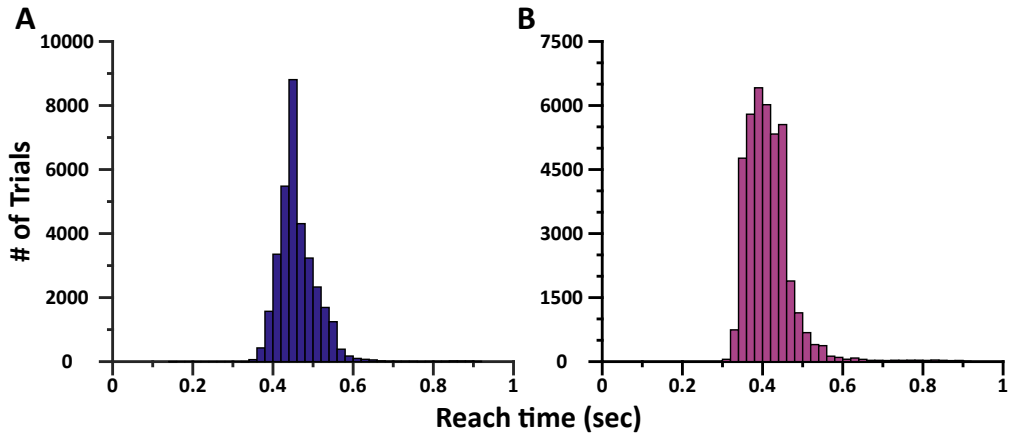

Figure 2.2: Reach times for Monkey C. (A) Histogram of reach times of the 2D trials from all recording sessions. (B) Histogram of reach times of the 3D trials from all recording sessions.

are likely due to corrective movements during the reach. The average ($\pm$ SD) reach time was 436 ± 60 ms for Monkey C and 528 ± 135 ms for Monkey N. Average reach times as a function of target direction for a single recording session for Monkey C and Monkey N are shown in Figure 2.4. Both Monkey show slightly slower movements in the 2D trials for targets between 0-90°, although the average movements for those targets are still very rapid (near 500 ms for Monkey C and 700 ms for Monkey N).

Similar to the center-out reaching tasks used by Georgopoulos and Massey [35], there was no target hold period. Each trial ended when the cursor left the task space. In the 3D context, the task space was a sphere of radius 77mm (Monkey C) or 63-67mm (Monkey N) centered at the origin. In the 2D context, the task space was a circle of the same radius centered at the origin. Targets were placed on the edge of the task space. In the 3D context, the targets were spherical caps (Figure 2.5a), similar to contact lenses. In the 2D context, the targets were circular "arc" segments (Figure 2.5b). Trials were considered successful if the cursor left the task space within the boundary of the target and before the end of the reach period. The task design is akin to applying Fitts' study of the selection of movement amplitude to the selection of movement direction (see footnote 4 of [27]). The applicability of Fitts' law in such a task design was demonstrated by Accot and Zhai with their "goal

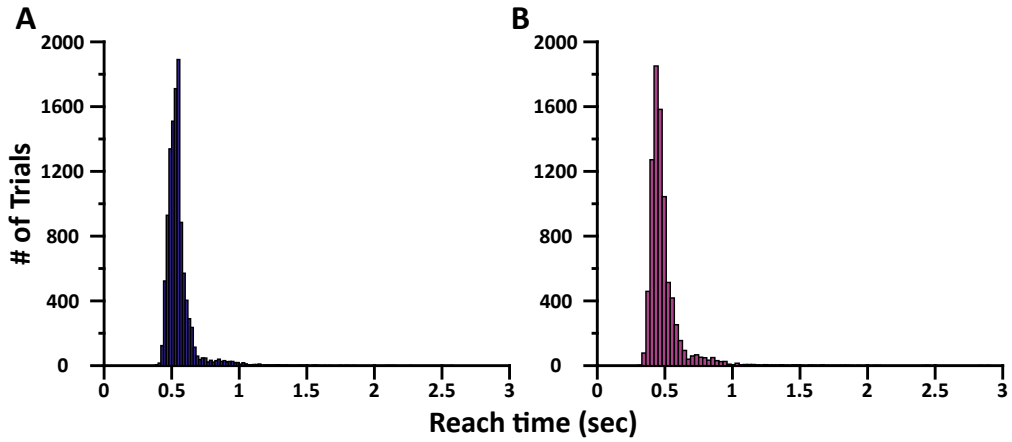

Figure 2.3: Reach times for Monkey N. (A) Histogram of reach times of the 2D trials from all recording sessions. (B) Histogram of reach times of the 3D trials from all recording sessions.

passing" tasks [2, 3]. The monkey was given a liquid reward for successes with a variable ratio schedule, where the reward was randomly administered for approximately 75% of the successful trials. After either a success or failure, the reach target disappeared and the origin sphere reappeared. The monkey was required to reach to the origin to start the next trial.

Within each recording session, target sets were switched after the completion of a target set. Target sets ranged between 40 to 100 trials per target. The number of targets in a target set ranged between 4 to 30 targets. The size of the targets scaled inversely with the number of targets in the set to maximally cover the perimeter of the task space without overlap. In the 2D context for a target set consisting of k targets, the central angle of each circular segment target was $2\pi/k$ radians. In the 3D context, the target placement and size were determined from an online database of putatively optimal packings of points on a sphere [90].

2.2.2 Data recording

Each monkey was implanted with one 96-channel Utah array (Blackrock Microsystems, Salt Lake City, UT). The implantations were visually placed in the arm area of primary motor

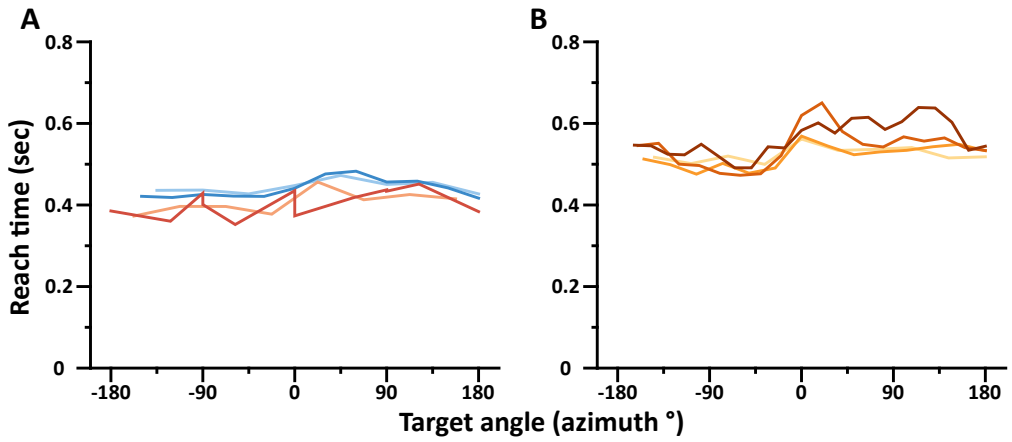

Figure 2.4: Reach times from center-out tasks in 2D and 3D. The plots show the average reach times for targets as a function of the target direction in the xy-plane. (A) Reach times from a recording session from Monkey C. The data shown in this plot are from the recording session shown in Figure 2.15b. The blue curves show the average reach times for the targets in the 2D trials. The red curves show the average reach times for the targets in the 3D trials. The darker curves are from the 12-target blocks of trials and the lighter curves are from the 8-target blocks of trials. (B) Reach times from a recording session from Monkey N. The data shown in this plot are from the recording session shown in Figure 2.11b. The curves are colored from light to dark orange, with darker curves illustrating blocks of trials with larger target sets (10, 14, 18, and 22 targets).

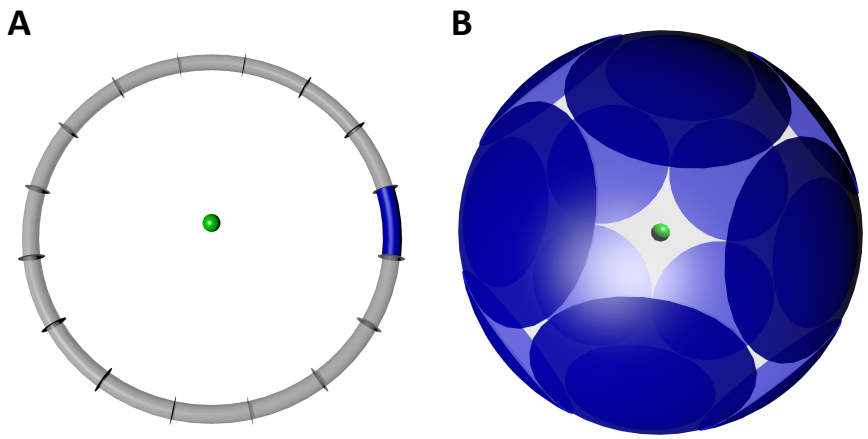

Figure 2.5: Targets in center-out task (A) Illustration of an example set of 16 targets from the 2D task. The cursor is shown in green. The gray torus is drawn to illustrate the edge of the task space and was not shown to the monkeys. Trials ended when the monkey moved the center of the cursor beyond the edge of the task space. One of the 16 targets is highlighted in blue. The remaining 15 targets are demarcated by the discs dividing the torus. (B) Illustration of an example set of 16 targets from the 3D task. The translucent gray sphere is drawn to illustrate the edge of the task space and was not shown to the monkeys. Trials ended when the monkey moved the center of the cursor beyond the edge of the task space. The 16 targets are shown in translucent blue.

cortex (Monkey C: right hemisphere, Monkey N: left hemisphere). Recordings were amplified, filtered, and sorted online with a 96-channel Plexon MAP system (Plexon, Dallas, TX). An infrared marker placed on the back of the hand of the monkey (Monkey C: left, Monkey N: right) was tracked with an Optotrak 3020 optical tracking system (Northern Digital, Waterloo, ON) at a frame rate of 60 Hz. The position of the 3D marker was used in real time to drive the cursor on the 3D monitor. All procedures were performed with the approval of the Institutional Animal Care and Use Committee of the University of Pittsburgh.

2.2.3 Estimation of information transmission

With the advent of multielectrode recording systems, more researchers have sought to measure the information transmission of populations of neurons. These efforts are complicated by the exponential growth in the amount of data needed to describe $P(\mathbf{R}, S)$ with linear increases in population size, where $\mathbf{R}$ is the multivariate random variable in $\mathbb{R}^n$ describing the activity of n neurons. To combat these limitations, various methods have been described to correct for undersampling [74, 78, 46]. Although these methods help with estimating the mutual information, they still require a significant number of trials per stimulus condition for large populations. Quian Quiroga and Panzeri proposed two main ideas for minimizing the sampling required for estimating mutual information [78]. One was to use dimensionality reduction to simplify the stimulus-response matrix. The other was to simplify the assumed correlation structure between the neurons. In our work, we used both of these proposed methods to simplify the quantification of mutual information.

Analysis was conducted only on successful trials. Firing rates for each unit were calculated in windows from target appearance to target acquisition. We first reduced the dimensionality of the neural data by removing units that did not modulate with movement direction. Units in the population were determined to modulate with movement direction based upon their estimated modulation range under linear tuning models. The tuning models were fit with data from all completed blocks of trials in a given recording session. Units with an estimated tuning range above 4 Hz in the xy-plane were kept for analysis. The tuning range in the xy-plane was calculated as $2m\cos(\phi)$, where m is the estimated modu-

lation depth of the unit and ϕ is the minimum angle between the unit's estimated preferred direction and the xy-plane.

We next used factor analysis to further reduce the dimensionality of $\mathbf{R}$ and reduce the noise in the data. The factor analysis model assumes that the high dimensional neural activity, $\mathbf{r} \in \mathbb{R}^n$, is driven by a low dimensional set of factors, $\mathbf{z} \in \mathbb{R}^d$. The number of factors that drive the neural activity is commonly referred to as the intrinsic dimensionality [82]. In factor analysis, each factor is assumed to be distributed as a standard normal distribution:

$$\mathbf{z} \sim \mathcal{N}(\mathbf{0}, I) \tag{2.6}$$

where I is the identity matrix. The neural activity, given the factors, is also assumed to follow a normal distribution:

$$\mathbf{r}|\mathbf{z} \sim \mathcal{N}(\Lambda\mathbf{z} + \boldsymbol{\mu}, \Psi) \tag{2.7}$$

The models were created from all the square-root transformed firing rates in a recording session. The model parameters were fit using the expectation-maximization algorithm [18]. For our analyses, we used 8 factors to describe the population activity. The number of factors used was lower than the estimated intrinsic dimensionality of the population in order to facilitate the estimation of the distribution of the factors for each target, $P(\mathbf{Z}|S = s)$, with few trials.

The intrinsic dimensionality was estimated for each recording session using the methods described by Sadtler, et al. [82]. We compared factor analysis models with dimensionalities ranging from 2 to 20. For each potential dimensionality, we used 4-fold cross-validation in which we estimated the model parameters from 75% of the session's data. We then computed the log-likelihood of the remaining data from the session with the model. The intrinsic dimensionality was determined as that with the greatest log-likelihood averaged across the four folds. We compared the difference in the log-likelihood at the intrinsic dimensionality to that at the choice of 8 factors to validate that the assumed dimensionality was reasonable (Figure 2.6). This figure demonstrates that the log-likelihood at the choice of 8 factors was within one standard deviation of the log-likelihood at the intrinsic dimensionality for all sessions from Monkey C and within two standard deviations for over 70% of the sessions from Monkey N.

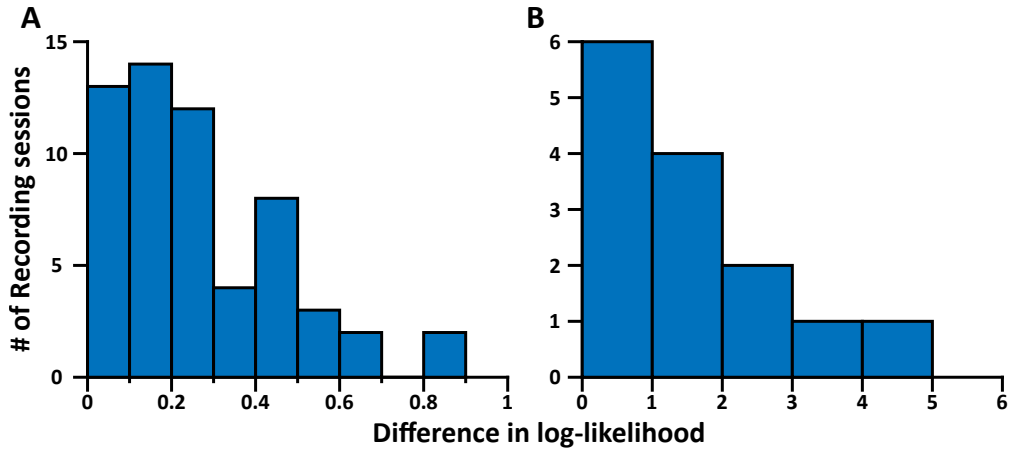

Figure 2.6: Difference from intrinsic dimensionality in the center-out reaching tasks. The plots show the histograms of the difference in the log-likelihood at the intrinsic dimensionality to that at the choice of 8 factors for recording sessions from Monkey C (A) and Monkey N (B). The difference in the log-likelihoods is scaled in units of the standard deviation of the log-likelihood at the intrinsic dimensionality.

In order to estimate the conditional entropy, $H(\mathbf{Z}|S)$, we made the assumption that the conditional probability distribution, $P(\mathbf{Z}|S)$, was a multivariate normal distribution:

$$\mathbf{z}|S = s_i \sim \mathcal{N}(\boldsymbol{\omega}_i, \Sigma_i) \tag{2.8}$$

One key advantage of the assumption of a conditional distribution model is that, unlike other methods [74, 78, 46], it does not require choosing a bin-size for binning the firing rate response. This allows for easy comparison of the results across different stimulus sets, and populations without complications arising from differently sized bins. Note that the estimation of the covariance differs from the covariance assumed in factor analysis of $I - \Lambda^\intercal C^{-1}\Lambda$, where $C = \Lambda\Lambda^\intercal + \Psi$. We made this assumption under the hypothesis that covariance of the stimulus-conditioned low-dimensional data is unique from the covariance of the entire low-dimensional dataset.

After estimating the mean, $\boldsymbol{\omega}_i$, and covariance, Σ_i, for each of the k targets in a set, the conditional entropy was calculated as:

$$H(\mathbf{Z}|S) = \sum_{i=1}^{k} \frac{d}{2k} \left(1 + \ln(2\pi) + \frac{1}{d} \ln |\Sigma_i|\right) \tag{2.9}$$

With the normality assumption of the conditional probability distribution, the neural response for a target set has a multivariate Gaussian mixture distribution:

$$p_{\mathbf{Z}}(\mathbf{z}) = \sum_{i=1}^{k} \frac{1}{k} \mathcal{N}(\boldsymbol{\omega}_i, \Sigma_i) \tag{2.10}$$

Unlike the conditional entropy, there is no closed-form solution for the response entropy under the assumed model. However, work by Huber, et al. has demonstrated an approximation for the entropy of Gaussian mixture models [44]. This method utilizes the second-order Taylor series expansion of the entropy formula. We estimated the population entropy, $H(\mathbf{Z})$, from the Gaussian mixture model using the methods described by Huber. The mutual information $I(\mathbf{Z}; S)$, was computed as the difference between the population entropy, $H(\mathbf{Z})$, and the entropy of the population conditioned on the target stimuli, $H(\mathbf{Z}|S)$. We used this value of mutual information as the estimate for the true quantity of information transmitted by the population about the target stimuli, $I(\mathbf{R}; S)$.

The estimation method designed for this study can be summarized with the following steps:

1. Record neural spikes for multiple blocks of varying target sets
2. For each trial, bin the spike data in windows from target appearance to acquisition
3. Divide each spike bin by the window duration to determine firing rate
4. Compute the square-root transform of the firing rates
5. Reduce the transformed population data to 8 dimensions using factor analysis
6. For each block, separate the reduced data by target
7. For each block and target-separated data set, compute the mean and covariance
8. Use Equation 2.9 and the target covariances to solve for the conditional entropy in the block

9. Use the target means and covariances and the second-order Taylor series expansion to solve for the total entropy in the block

10. Subtract the conditional entropy from the total entropy to solve for the information transmission

2.3 RESULTS

2.3.1 Stable estimation of information transmission with few trials

In order to evaluated the stability of our estimation methods for sessions with as few as 40 trials per stimulus condition, we collected a dataset with 100 trials per stimulus condition from Monkey C. This dataset consisted of 10 targets for both a 2D and 3D task, giving 20 unique stimuli. For each of the 2D and 3D tasks, we took 500 random subsamples (from 15 to 99 trials) of these 100 trials and estimated the information transmission for those subsamples. In order to estimate when the bias stabilizes, the random subsets were sampled without replacement. Plotting the average and standard deviation of the transmission estimate against the number of trials per stimulus (target), we see that the estimate stabilizes around 60 trials per stimulus condition for the 3D task and near 80 trials per stimulus for the 2D task (Figure 2.7). Sampling with replacement introduces a positive bias in the mutual information due to the lower conditional entropy. However, this sampling demonstrates that the variance of the mutual information estimate stabilizes near 30 trials per stimulus for the 3D and and 60 trials per stimulus for the 2D task (Figure 2.8). For both the 2D and 3D trials, the majority of the bias and variance decays by 40 trials per stimulus. For this reason, we chose 40 trials per stimulus as a reasonable number to estimate mutual information and compare the value between changes in the set of stimuli. Unless otherwise stated, the results that follow are estimates of the mutual information from 40 trials per stimulus. Recording sessions with more than 40 trials per stimulus were similarly randomly subsampled without replacement at 40 trials per stimulus.

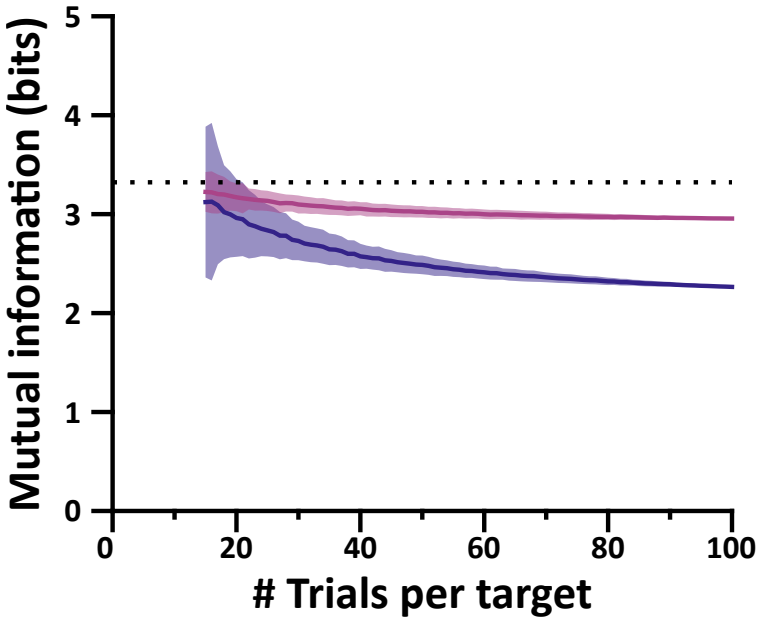

Figure 2.7: Information estimation bias with few trials per stimulus. The data in this plot show the decay of bias in the estimation of mutual information with more trials per target. The dark blue line shows the average of the estimated mutual information for the 2D trials as a function of the number of trials per target (stimulus) used in the estimate. The shaded blue region shows the variance of this estimate. The pink line shows the average of the estimated mutual information for the 3D trials as a function of the number of trials per target used in the estimate. The shaded pink region shows the variance of this estimate. These averages and variances were calculated from generating 500 random subsamples without replacement from the original dataset of 100 trials per target.

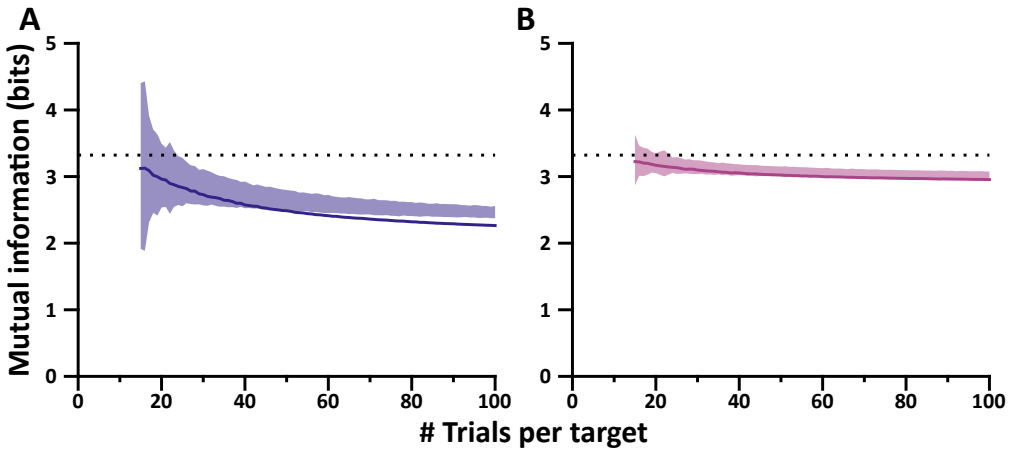

Figure 2.8: Information estimation variance with few trials per stimulus. The data in these plots show the decay of variance in the estimation of mutual information with more trials per target. (A) The dark blue line is identical to the dark blue line in Figure 2.7, showing the average mutual information in the 2D trials as a function of the number of trials per target. The shaded blue region shows the variance centered around the mean for estimates of the mutual information in the 2D trials for random subsamples taken with replacement from the original dataset of 100 trials per target. This differs from the variances in Figure 2.7 which were estimated from random subsamples taken without replacement. (B) The pink line is identical to the pink line in Figure 2.7, showing the average mutual information in the 3D trials as a function of the number of trials per target. Similar to the shaded region in A, the pink shaded region shows the variance centered arond the mena for estimates of the mutual information in the 3D trials for random subsamples taken with replacement from the original dataset of 100 trials per target.

2.3.2 Information transmission reaches a limit for center-out movements

In our studies, we stepped through different levels of stimulus entropy by increasing the number of presented targets. The targets were non-overlapping and decreased in size with increases in the number of targets. Because each target was presented an equal number of times for each dataset, the stimulus entropy was calculated as $\log_2 k$, where k is the number of targets. Data from multiple sessions from Monkey C and Monkey N are plotted in Figure 2.9a,b, respectively. Because the information transmitted about the stimuli cannot be greater than the information contained in the stimuli, the unity lines in each of these plots represent the maximum possible information transmission.

In these plots, the mutual information is seen to track along the unity line for low values of stimulus information. As the stimulus information continues to increase, the information transmitted by the population begins to diverge from the unity line, similar to previous studies of the information limits in judgements [64] and in afferent neurons [100]. This effect is more readily apparent in the estimates of mutual information from single recording sessions as the information transmission appears to approach a plateau with increasing stimulus information. Data from 3 different recording sessions from Monkey C are shown in Figure 2.10. Data from 2 different recording sessions from Monkey N are shown in Figure 2.11. In both of these figures, the mutual information tracks along the unity line before diverging and reaching a limit with increasing stimulus information.

2.3.3 Information limit scales with neural population size

One of the key differences between the results for Monkeys C and N was the larger maximum information transmission for Monkey N. This deviation was most pronounced for the 3D trials for Monkey N where the information transmission still tracked the unity line near 4.9 bits of stimulus information. We theorized that this difference was due to the larger population size of Monkey N. The relationship between information transmission and population size can be observed across sessions for each monkey (Figure 2.12). In these plots, we show the data from Figure 2.9 with each data point darkened to reflect the population size in the corresponding recording session. Darker points represent larger population sizes. In these

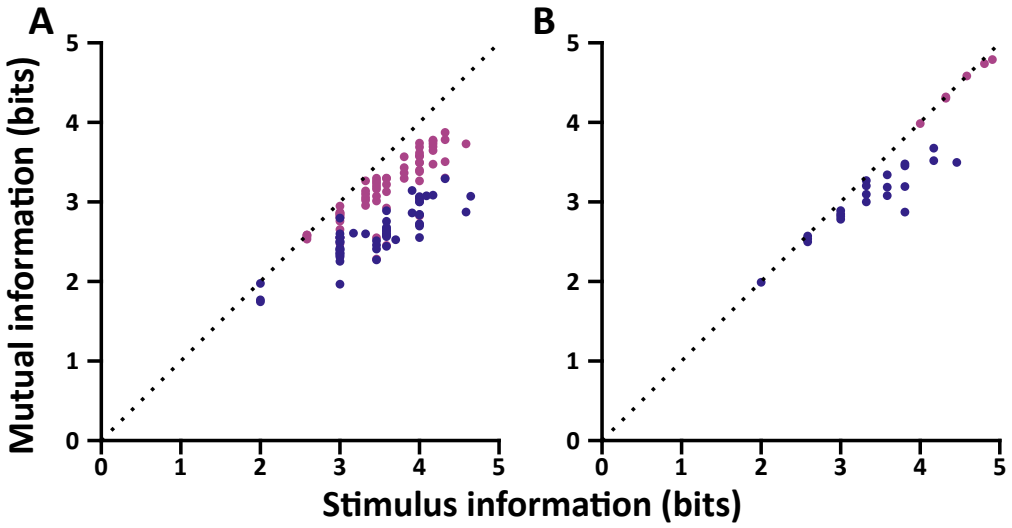

Figure 2.9: Information transmission in center-out tasks. The plotted data shows the mutual information estimated using the methods described above against the stimulus information for a given block of trials. Data from blocks of 2D trials are shown in dark blue and those from blocks of 3D trials are shown in pink. The unity line representing the absolute limit of information transmission is shown as the dotted black line. (A) Information transmitted in recording sessions from Monkey C. (B) Information transmitted in recording sessions from Monkey N.

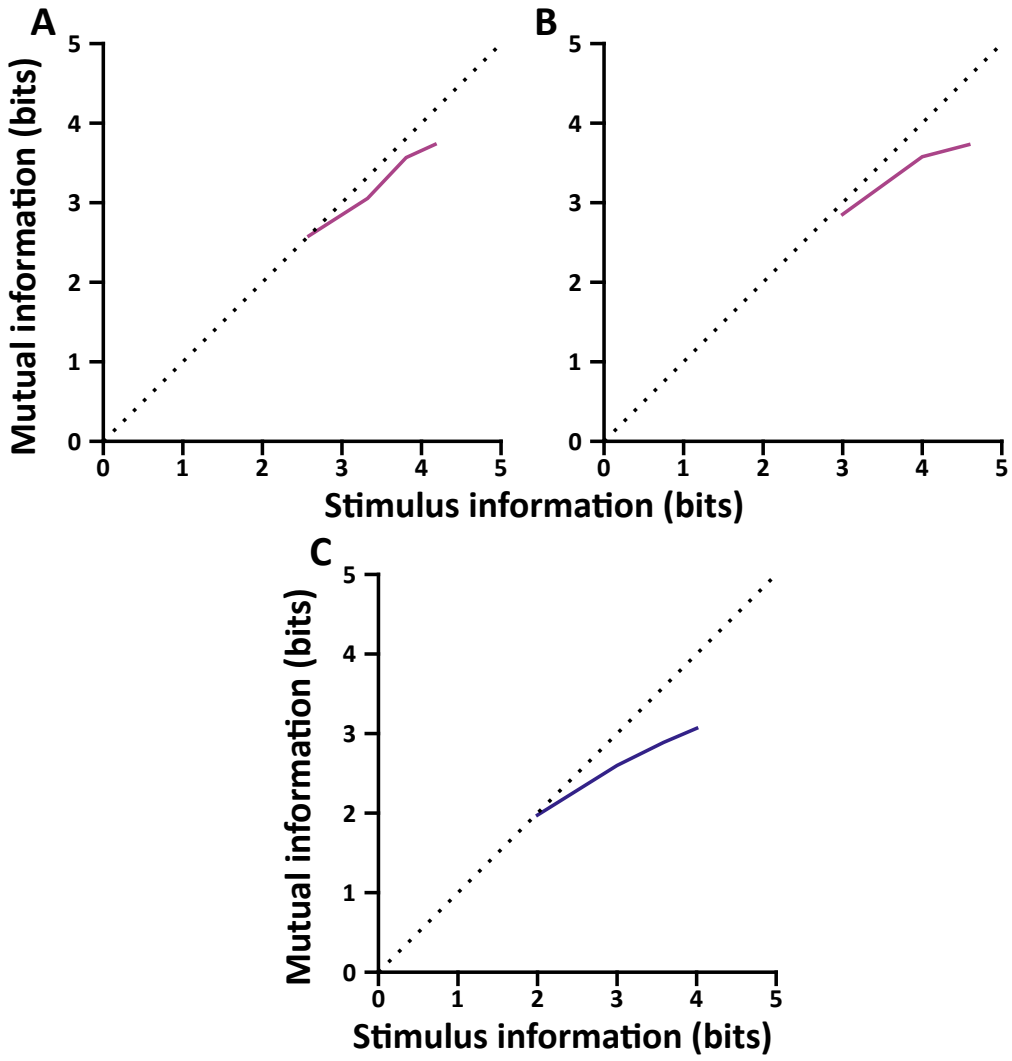

Figure 2.10: Information transmission limits in Monkey C (A) Information transmitted in a single recording session from Monkey C sampled at stimulus information levels of 2.59, 3.32, 3.81 and 4.17 (6, 10, 14, and 18 targets) in a 3D task with 40 trials per target and a population of 28 units. (B) Information transmitted in a single recording session from Monkey C sampled at stimulus information levels of 3, 4, and 4.59 bits (8, 16, and 24 targets) in a 3D task with 40 trials per target and a population of 29 units. (C) Information transmitted in a single recording session from Monkey C sampled at stimulus information levels of 2, 3, 3.59, and 4 bits (4, 8, 12, and 16 targets) in a 2D task with 40 trials per target and a population of 31 units.

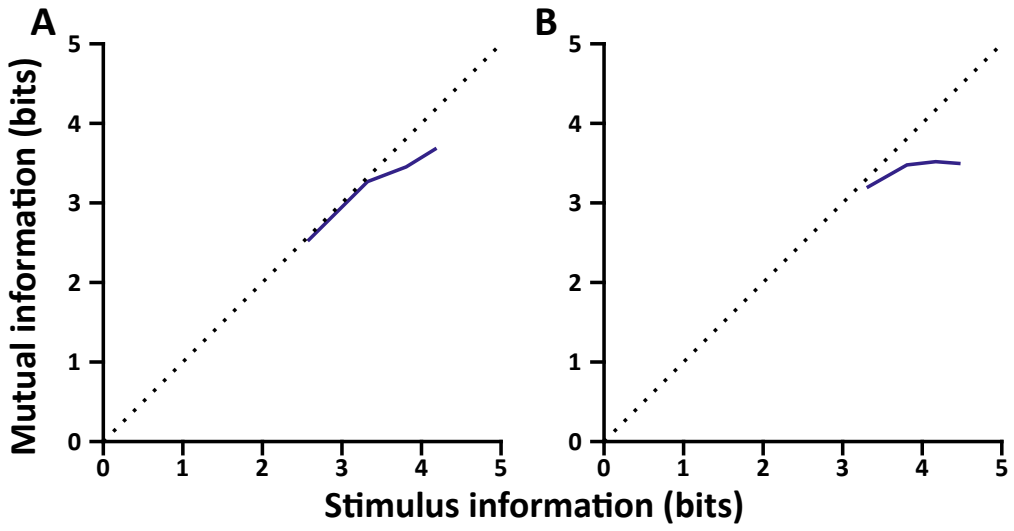

Figure 2.11: Information transmission limits in Monkey N (A) Information transmitted in a single recording session from Monkey N sampled at stimulus information levels of 2.59, 3.32, 3.81 and 4.17 (6, 10, 14, and 18 targets) in a 2D task with 40 trials per target and a population of 50 units. (B) Information transmitted in a single recording session from Monkey N sampled at stimulus information levels of 3.32, 3.81, 4.17, and 4.46 bits (10, 14, 18, and 22 targets) in a 2D task with 40 trials per target and a population of 47 units.

plots, the darker data points appear to reach a higher limit of information transmission than the lighter data points, suggesting the relationship between population size and information transmission.

In order to further test this theory, we took 500 random subsamples without replacement of the recorded population from Monkey N at different population sizes (in steps of one from 9 to 19 and in steps of two from 21 to 45). We used the data from the recording session shown in Figure 2.11b. We then recalculated the information transmission for these subsamples, using the same methods described above. Plotting the average recalculated transmission levels along against the stimulus entropies, we see that the information transmission increases when the population size increases (Figure 2.13a). Furthermore, the maximum level of information transmission decreases with decreases in population size. When we plot these maximum levels against the population size, we see that although adding more units to the population increases the transmission level, there are diminishing returns (Figure 2.13b).

To evaluate this effect, we fit a power law to the data for the stimulus information of 4.46 bits ($I = an^b + c$, where I is the mutual information and n is the population size). The data and the fit power law are shown in Figure 2.14). The data is well-fit by the power law ($r^2 = 0.999$) and the exponent term of the fit has a negative value, $b = -0.576 \pm 0.061$ (95%CI). The negative value implies that the information transmission has an asymptotic limit with increasing population size. The limit predicted from this analysis was 3.909 ± 0.073 (95%CI) bits of information ($\approx$15 discrete stimuli). To summarize, for a two-dimensional task, the information transmitted by a neural population appears to reach a limit of 3.9 bits as both the number of units and targets increases.

2.3.4 Information limit scales with task dimensionality

Another effect observed in Figure 2.9 is the significant difference between the estimated mutual information between the 2D and 3D trials. To further evaluate this effect, we conducted recording sessions from Monkey C where blocks of trials from both the 2D and 3D task were collected. We show the estimated information transmission from two such trials in Figure 2.15. Despite the identical neural populations within each of these recording sessions,

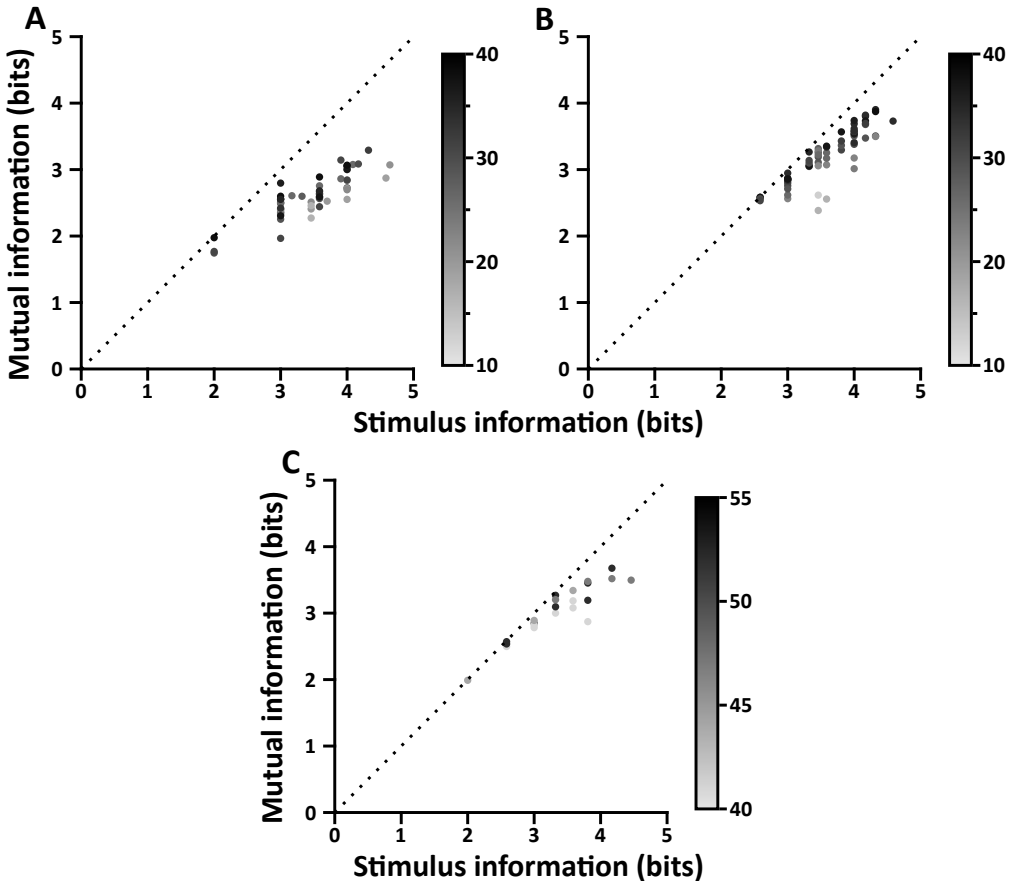

Figure 2.12: Effect of population size on information. The data points are the same from Figure 2.9 where each point is darkened to reflect the population size in the corresponding recording session. The color maps are shown to the right of each plot, indicating the number of units in the population. Darker data points have a greater population size. Unity is shown as the dotted black line. (A) Data from Monkey C for the blocks of 2D trials. (B) Data from Monkey C for the blocks of 3D trials. (C) Data from Monkey N for the blocks of 2D trials.

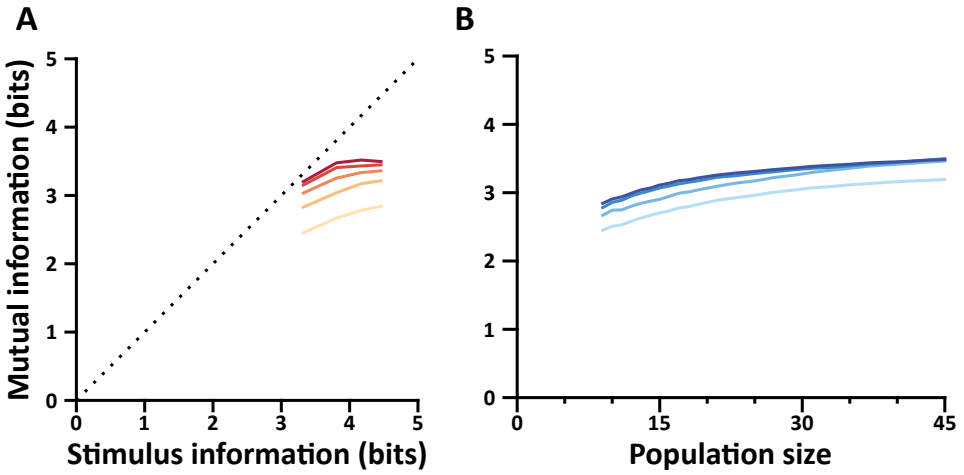

Figure 2.13: Information transmission increases with population size. Data shown are from the recording session from Monkey N illustrated in Figure 2.11b. (*A*) Average information transmission from random subsamples of the population are shown against the stimulus information. The five curves correspond to population sizes of 9, 19, 29, 39, and the original population size of 47 units. The curves are plotted in light yellow to dark red with the darker curves corresponding to the larger population sizes. Unity is shown as the dotted black line. (*B*) Average information transmission from random subsamples of the population are shown against the sampled size of the population. The four curves correspond to the four blocks of trials at different stimulus information levels of 3.32, 3.81, 4.17, and 4.46 bits (10, 14, 18, and 22 targets). The curves are plotted in light to dark blue with the darker curves corresponding to the greater stimulus information level.

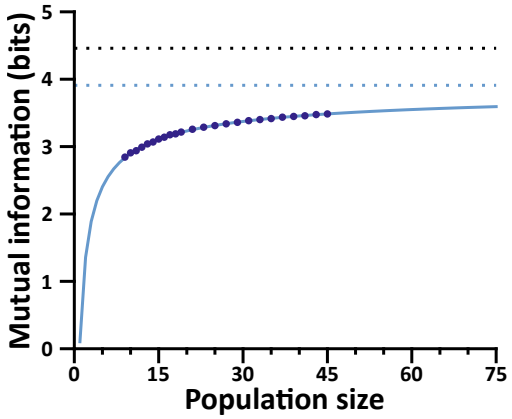

Figure 2.14: Power law fit of population effect. The dark blue data points are the data from the darkest orange curve in Figure 2.13b, where the stimulus information level was 4.46 bits (22 targets). The power law fit is shown as the light blue curve. The asymptotic limit of 3.91 bits predicted from the fit power law is shown as the dotted light blue line. The dotted black line illustrates the stimulus information level of 4.46 bits, the absolute limit on information transmission for the 22 target set.

the mutual information reaches a greater limit for the 3D trials and the 2D trials. Effectively, the neural populations are able to encode more information in a higher dimensional task. We attempted to extend this analysis to higher than three dimensions using wrist orientation as the additional dimensions. Unfortunately, we had difficulty in training the monkeys to orient their wrists during center-out movements.

2.3.5 Properties of information estimates

In estimating the information about the target stimuli transmitted by the neural population, we also estimated the conditional, or noise entropy of the the population for individual stimuli. In Figure 2.4, we showed that some of the target stimuli had a minor bias in the reach times. In order to investigate whether there was a similar bias in the estimated conditional entropies, we plotted the estimated conditional entropies as a function of the target angle in the xy-plane. Figure 2.16 shows the conditional entropies for the same recording sessions and targets shown in Figure 2.4. Visually comparing these figures, we find that there is no similar trend in the conditional entropies as there was in the reach times.

However, for the 3D trials in Figure 2.16a, a bias does emerge when considering the position of the targets along the z-dimension. In Figure 2.17a, we show the same conditional entropies as shown in the light red curve in Figure 2.16a with the conditional entropies for the targets that lie above the xy-plane highlighted with dark red dots. These points demonstrate a minor bias towards greater conditional entropies for targets in the positive z-dimension. In examining potential causes of this bias, we found that the modulation depths and preferred directions had a minor, but not significant, bias towards the negative z-dimension (Figure 2.17b).

To further evaluate this effect, we estimated the mutual information between the population and the stimuli for populations where each unit was left out of the population. The data shown in Figure 2.18 are from the recording session for Monkey N with an original population of 47 units. The 47 data points correspond to each unit where the mutual information was estimated from the remaining 46 units. The difference between the original and new estimates of mutual information are plotted against the modulation depth of the

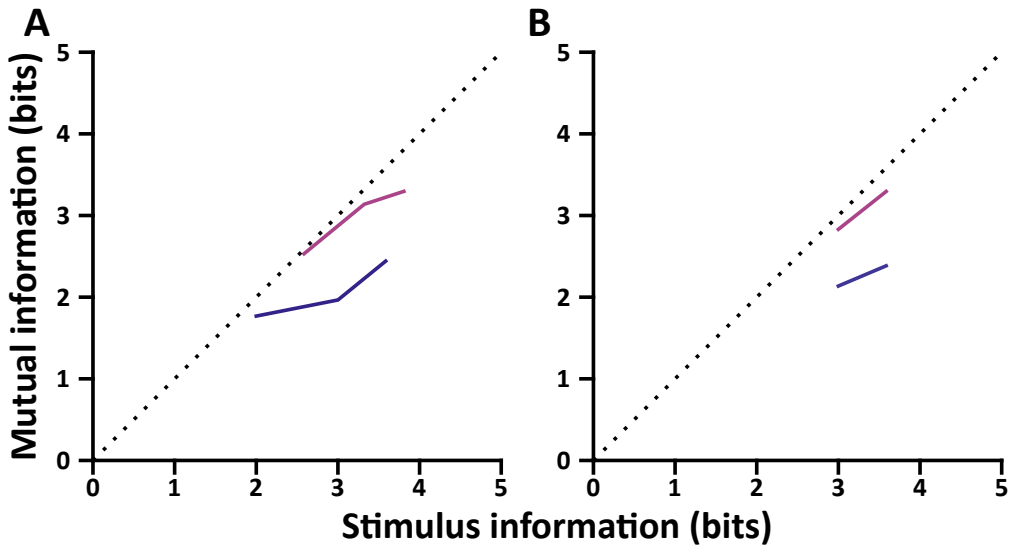

Figure 2.15: Effect of task dimensionality on information. Unity is shown as the dotted black line. (A) Data from one session from Monkey C. The dark blue line shows the estimated mutual information sampled at stimulus information levels of 2, 3, and 3.59 bits (4, 8, and 12 targets) in a 2D task. The pink line shows the estimated mutual information sampled at stimulus information levels of 2.59, 3.32, and 3.81 bits(6, 10, and 14 targets) in a 3D task. Each block in the recording consisted of 40 trials per target. The neural population consisted of 24 units. (B) Data from one session from Monkey C. The dark blue line shows the estimated mutual information sampled at stimulus information levels of 3 and 3.59 bits (8 and 12 targets) in a 2D task. The pink line shows the estimate mutual information sampled at stimulus information levels of 3 and 3.59 bits (8 and 12 targets) in a 3D task. Each block in the recording consisted of 60 trials per target. The neural population consisted of 31 units.

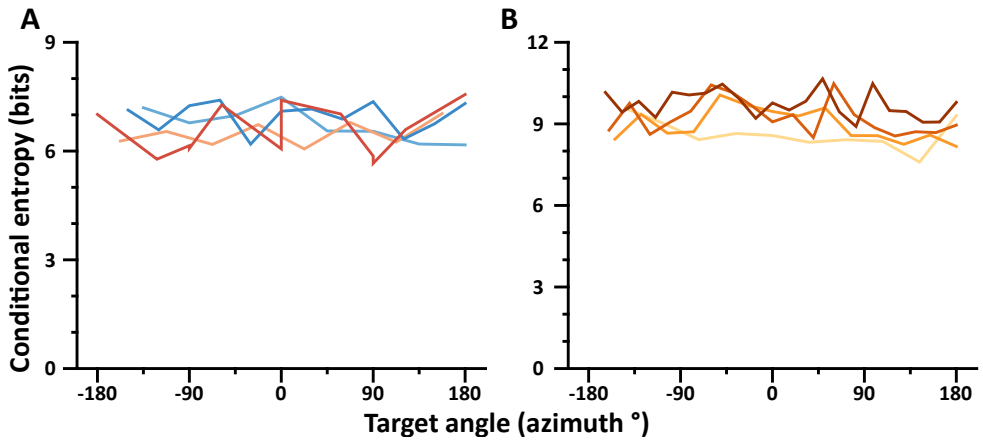

Figure 2.16: Conditional entropies for center-out tasks in 2D and 3D. The plots show the estimated conditional entropies for targets as a function of the target direction in the xy-plane. (A) Conditional entropies from the same recording session from Monkey C shown in Figure 2.15b. The color scheme of the curves are the same as in Figure 2.4a. (B) Conditional entropies from the same recording session from Monkey N shown in Figure 2.11b. The color scheme of the curves are the same as in Figure 2.4b.

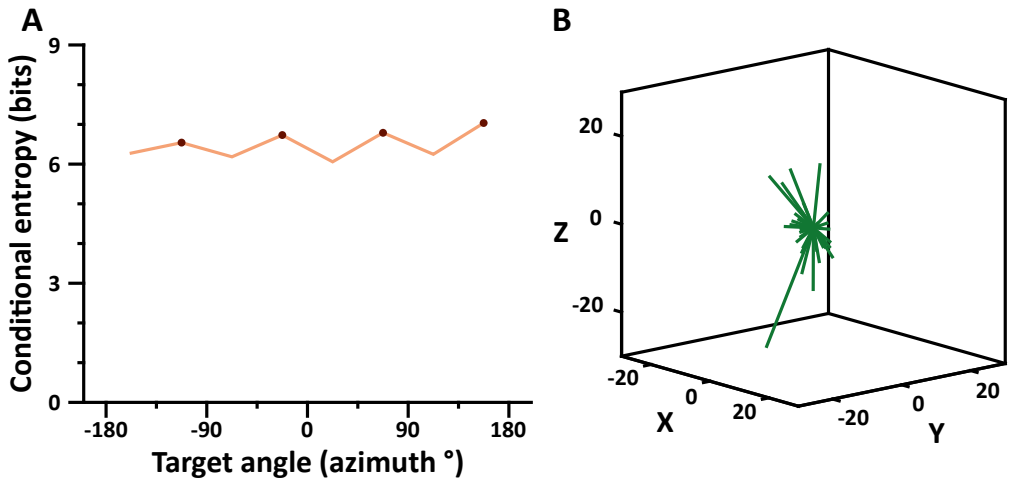

Figure 2.17: Conditional entropy and tuning bias for Monkey C. (A) The curve shows the same conditional entropies from the light red curve shown in Figure 2.16a as a function of the target direction in the xy-plane. The data points for the targets that lie above the xy-plane are shown as the dark red circles. (B) The green vectors show the preferred direction vectors scaled by modulation depth in Hertz for the population of units from A.

unit. The linear fit of the data points has a positive slope and is significant against the null hypothesis of zero slope (F-test, $P = 0.009$). This result demonstrates that units with greater modulation depths contribute more to the information transmitted about the stimuli. This is consistent with the data from Figure 2.17 as well as theories of how neurons encode information within their limited dynamic range [7].

2.4 DISCUSSION

In this work, we developed a novel method for estimating the mutual information between a neural population and the target stimuli and a center-out task. Estimating information transmission is difficult due to the curse of dimensionality. An insurmountably large number of trials would be needed to describe the information transmitted by a small population. Alternative methods have been proposed to reduce the number of trials needed. However, these methods still require a significant number of trials and the estimates produced from those methods are difficult to compare across different sets of stimuli. The method we developed works well for data with a limited number (≈ 40) trials per target. Furthermore, this method is easily adaptable to allow for comparisons amongst different sets of target stimuli. This method may be a useful tool for evaluating neural populations and their capabilities to transmit information about movement. It provides a common metric from which researchers can compare different populations and different movement tasks. This method may also be useful to predict and evaluate performance in a brain-computer interface task.

We used this method of estimating mutual information to find that the information about the target stimuli transmitted by the population increases up to a limit as the information in the set of target stimuli increases. This result is not unexpected. Werner and Mountcastle's early studies of somatosensory neurons[100] and George Miller's well-known review of information transmission in judgements[64] found similar results. Noise in the neural system leads to an effective limit on its ability to transmit increasing amounts of information about input stimuli or output actions.

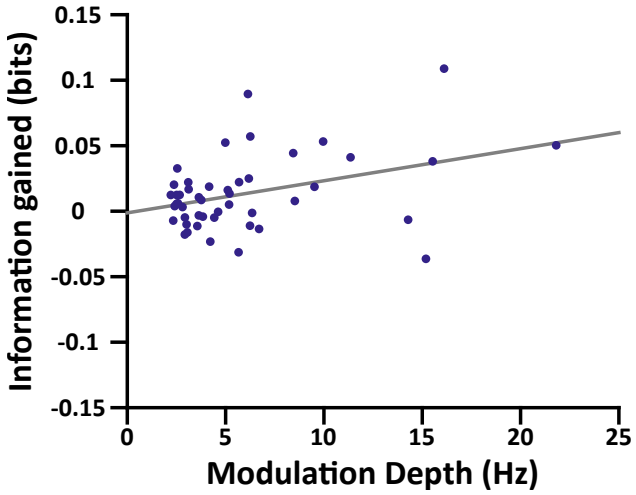

Figure 2.18: Information gain versus modulation depth. The dark blue points in this plot illustrate the information gained from single units in a population as a function of the modulation depth of that unit. The data is from the recording session shown in Figure 2.11b for the block of trials at the stimulus information level of 4.32 bits (22 targets). The information gain was calculated via taking the estimate of mutual information from the entire population and subtracting the mutual information estimated with each unit left out. The information gain for an individual unit was that difference when that unit was left out. The gray line illustrates the linear fit of the data.

We next demonstrated that this limit is a function of the size of the population. The information transmitted by the population increases as the size of the population increases. Again, this result is not unexpected. The additional units in the population contribute additional information about the stimuli despite the noise in the neural system. In other words, each unit is able to transmit information. Adding a unit to the population has an additive effect on the information transmitted by the entire population. This occurs when the unit contributes more to the total entropy than to the noise entropy, effectively reducing the uncertainty from the noise in the rest of the population. This result is similar to the results of Georgopoulos, et al.[34] in which they found the 95% confidence interval for predicted movement direction shrank when the population used to predict the movement direction increased in size.

However, we found that this relationship between population size and information transmission appears to also reach a limit. These results suggest that an infinitely large population of motor cortical neurons could transmit only a limited amount of information. Initially, this result appears counterintuitive, especially considering that the success rate for the trials was greater than that predicted by this limit. This finding cannot be explained by the fact that the analysis was restricted to successful trials. In fact, this restricted analysis increases the estimated mutual information rather than decreases it. One possible reason for this result may be the choice of the time window, where noise in the neural firing rates towards the beginning or end of the time window may lower the estimate of the information transmission. Another possible reason for this result may be that the motor cortex does not transmit all of the information involved in a movement. Studies have demonstrated that areas in the cortex other than M1 contribute to the activation of movements [19]. Moreover, Georgopoulos, et al.[34] found a similar, asymptotic relationship between population size and the 95% confidence interval for predicted movement direction. Another reason for this result may be that the choice of 8 factors may underestimate the intrinsic dimensionality of populations larger than those measured. Subsequently, extrapolating the results to an asymptote may not be accurate for such larger populations. Additional studies with larger populations and more trials per stimulus condition may help to determine the accuracy of the exponential model we fit to the results.

We lastly demonstrated that the information transmitted by the motor cortical population is greater in a 3D versus a 2D context. For identical values of stimulus information (i.e., number of targets), the information transmitted by the population was greater when the targets were arranged in three dimensions, lying on the surface of a sphere, rather than in two dimensions, lying on the edge of a circle. There may be two reasons for this result. First, if we assume that the units maintained identical linear tuning models between the two contexts, the observed range in firing rates for individual units would have been greater in the 3D versus the 2D context. This greater tuning range gives the units the capacity to encode more information, as demonstrated in the results shown in Figure 2.18. This increased capacity may be understood with the analogy of switching from a binary to a hexadecimal information channel. The binary channel has a "tuning range" of two values while the hexadecimal channel has a range of sixteen values. Assuming the channels are noiseless, each signal from the binary channel would only transmit one bit of information whereas each signal from the hexadecimal channel would transmit four bits of information. Second, the discrete targets that we studied are a subset of the continuous range of targets. According to the linear tuning model, the signal entropy is maximized by uniform target distributions in the 3D context. For individual, noiseless, linearly-tuned units, the firing rates for a uniform 2D target distribution follow an arcsine distribution. For uniform 3D targets, the firing rates are uniformly distributed over the tuning range for that unit. For uniform 4D targets, the firing rates would follow a Wigner semicircle distribution. The flat, uniform distribution of firing rates is the maximum entropy distribution for a given tuning range. If the tuning ranges were identical amongst the 2D, 3D, and 4D contexts, the signal entropy would be maximized in the 3D context. This maximum entropy distribution maximizes the information transmitted by individual, noiseless units[68]. Nonetheless, it is possible for the information transmission in 4D to be greater due to an increase in utilized tuning range in higher-dimensional context or from the true neural tuning deviating from cosine tuning model.

It should be noted that the limits on the information transmission found in this work are not equivalent to the channel capacity of the neural population. Channel capacity is measured as the maximization of the mutual information over changes in the stimulus dis-

tribution. In our work, the mutual information was only measured for uniform stimulus distributions. The increase in the number of targets during the 2D or 3D context represents a change in the channel itself rather than changes to the stimulus distribution. The channel also changes when the task context changes from 2D to 3D trials. Despite these changes in the channel, the neural population was identical. Thus, we were able to measure the limiting effect of the neural population as the demands of the task increased in complexity.

3.0 BCI TASKS

Neural populations from various sensory regions demonstrate dynamic range adaptation in response to changes in the statistical distribution of their input stimuli. These adaptations increase the transmission of information about sensory inputs. Here we show a similar effect in the firing rates of primary motor cortical cells. These neurons show changes in their directional tuning properties. Virtual reaching movements are made in both two- and three-dimensional contexts. The range of directions encompassed by the tuning curves of these neurons changed with the dimensionality of the task. These contextual changes in neural tuning provide evidence that the activity of primary motor cortical neurons operates as a high-level control signal, encoding contextually relevant information within a limited dynamic range.

3.1 INTRODUCTION

The range of natural stimuli a person or animal encounters in a single day is constantly changing. A common example is walking out of a movie theater. The levels of light switch from the faint light of the theater to the bright lobby. Despite these changing levels, you are still able to see as you walk out of the theater and through the lobby. This ability can be explained by the behavior of neurons that encode information about light intensity. Neurons in primary visual cortex and the retina encode the intensity of light with their firing rates[53, 43]. These tuning relationships typically follow monotonic curves between firing rates of zero and the maximum firing rates of the neurons (i.e. the dynamic range of the neurons). The resolution in the relationship is determined by how many steps in the

firing rate can be distinguished. This a function of the slope of the curve and the amount of noise in the firing rate.

When the levels of light intensity change from the dark theater to the bright lobby, one of two possibilities occur: the tuning curves remain the same, or they can change. Indeed, the neural tuning curves shift and adjust their slopes to provide resolution over the new range of light intensity[88, 72, 91]. This phenomenon is commonly referred to as dynamic range adaptation and is analogous to the process of histogram equalization in digital image processing. In addition to these examples in the visual system, dynamic range adaptation has been documented in a variety of other sensory regions that encode information about input stimuli, such as auditory[55, 17] and somatosensory areas[63]. This phenomenon has been described as optimizing the transmission of information about input stimuli within the limited tuning ranges of the neurons[7, 24, 97].

In sensory systems, meaningful input variables can be described concretely. In motor systems, controlled parameters are still being debated. Force was one of the earliest output variables that has been described where many studies demonstrated firing rates of neurons in primary motor cortex (M1) modulate with output force levels in monotonic relationships[22, 23, 40, 32]. Hepp-Reymond, et al. later demonstrated an example of dynamic range adaptation in single, force-tuned neurons in an isometric pinching task[39].

More recently, the direction of arm movement has received attention as a controlled variable[33, 34, 85]. These studies demonstrated a cosine-tuning relationship between movement direction and neuronal firing rates. Each unit was described as having a preferred direction where the firing rate was maximal for movements in that direction and minimal for movements in the opposite direction. In this classical model, the firing rates linearly modulate between the minimum and maximum rates with the cosine of the angle between the movement direction and preferred direction. This tuning model has been demonstrated for movements in both two- and three-dimensional arm reaches. Notably, the model predicts a lower range in firing rates for 2D movements than 3D movements when the preferred direction is not coplanar with the 2D movement space. This raises the unique question of whether changing the output movement statistics from 3D movements to purely 2D movements would lead to dynamic range adaptation.

In an effort to enforce a direct relationship between firing rates and movement direction, we investigated this question using a brain-computer interface (BCI). We trained monkeys to move a cursor on a 3D computer screen under brain control, using either a population vector algorithm (PVA) or optimal linear estimator (OLE) decoder[10]. The monkeys controlled the cursor by modulating the firing rates of neurons recorded in the motor cortex as they performed a classic center-out task in both 2D and 3D environments. We found that neurons within M1 undergo a change in tuning between the 2D and 3D contexts. We then leveraged the simultaneity of the recordings to test several hypotheses about population-based mechanisms of these changes. We found that the results are consistent with dynamic range adaptation.

3.2 MATERIALS AND METHODS

3.2.1 Behavioral Paradigm and Recording

The behavioral training and decoding methods closely followed those of Jarosiewicz, et al[48]. Briefly, two male Rhesus monkeys were trained to perform a center-out reaching task in a 3D virtual environment. The monkeys sat in a primate chair facing a mirror that reflects a 3D image from a stereoscopic computer monitor. Before electrode implantation, the monkey was trained to move its hand, fitted with an optical marker, to move a cursor from the center of an imaginary cube to targets at lying at one of the eight corners for a liquid reward[81].

Once the monkeys became proficient at the 3D center-out reaching task, they were implanted with chronic recording arrays. Both monkeys were implanted with a 96-channel array (Cyberkinetics Neurotechnology Systems, Inc.). The implantations were visually placed in the proximal arm area of primary motor cortex. Recordings were amplified, filtered, and sorted on-line with a 96-channel Plexon MAP system (Plexon Inc.). Each monkey was trained to perform the center-out task with both arms restrained by modulating the spiking activity of the recorded units to control cursor velocity. Both monkeys were proficient at the brain-control task in both contexts from training sessions prior to starting this study.

Each trial began with the monkey holding the cursor at the task space origin for a randomized period (50-160 ms). The target was presented after this period. The task required the monkey to reach the target within the 2s reach period and hold the cursor at the target position for a randomized period (0-100 ms). The cursor was then automatically returned to the home position for the start of the next trial. A water reward was delivered for successful trials. The targets were placed at a distance of 85mm from the center. The cursor and targets' radii were 8mm each. All procedures were performed in accordance with the guidelines of the University of Pittsburgh's Institutional Animal Care and Use Committee.

3.2.2 Decoding Algorithm

Each recording session began with a calibration brain control session. The calibration session followed the methods described by Chase, et al[10]. The decoding parameters were initially randomized. Eight targets from the 3D context (those lying on the corners of a cube) were then presented, individually in random order, and remained until the end of the movement period. Although the cursor did not move much during the movement period due to the randomized parameters, the firing rates were still modulated to target presentation. Once a cycle set comprising one presentation of each of the 8 targets was completed, the firing rates were regressed using the regress function in Matlab (Mathworks, Inc.) against the target direction according to the linear tuning model:

$$r_i = b_{0,i} + m_i \boldsymbol{d} \cdot \boldsymbol{p}_i \tag{3.1}$$

In a subset of recording sessions, separate calibration sessions were conducted for the 2D and 3D trials. These calibration sessions were conducted immediately prior to the start of the respective context block. The calibration session for the 2D trials differed from the previously described calibration methods only in that the target set comprised 8 targets spaced equally around a circle centered in the xy-plane. For all other recording sessions, the decoding parameters derived from the initial calibration session were used for the entirety of the recording session.

Linear decoders (PVA and OLE) were used to decode neural signals into cursor movement. The recorded population was assumed to follow the linear tuning function described

in Equation 3.1. For each unit, i, spike counts were measured at 30 Hz and converted into firing rates, r_i, by dividing by the sampling interval. Rates were averaged across the last five time bins and normalized by subtracting the fit baseline firing rate and dividing by the fit modulation depth:

$$u_i = \frac{r_i - b_{0,i}}{m_i} \tag{3.2}$$

The normalized rates of the N units comprising the population were grouped in the vector $\boldsymbol{u} = [u_1, u_2, \ldots, u_N]^\intercal$. Similarly, the preferred direction vectors of the N units were grouped in the matrix $P = [\boldsymbol{p}_1, \boldsymbol{p}_2, \ldots, \boldsymbol{p}_N]$. For the PVA decoder, normalized rates, $\boldsymbol{u}$, were converted to cursor velocity, $\boldsymbol{v}$, as:

$$\boldsymbol{v} = k_s \frac{n_D}{N} P^\intercal \boldsymbol{u} \tag{3.3}$$

where n_D is the number of movement dimensions (either 2 or 3) and k_s is the speed factor to convert the normalized speed to a physical speed in mm/s (values used in our study ranged from 65 to 120). For the OLE decoders, the normalized rates were converted to cursor velocity as:

$$\boldsymbol{v} = k_s \left(P^\intercal P\right)^{-1} P^\intercal \boldsymbol{u} \tag{3.4}$$

Cursor position, $\boldsymbol{c}$, was updated every sampling interval as:

$$\boldsymbol{c}(t) = \boldsymbol{c}(t - \Delta t) + \Delta t \boldsymbol{v}(t) \tag{3.5}$$

For trials in the 2D context, the z-component of the decoded velocity was set to zero to constrain movement to the xy-plane.

3.2.3 Tuning Range Analysis

The analyses in this work focuses on the firing rates of the recorded units, r_i. These rates are functions of many different variables: the task context (i.e., number of movement dimensions, n_D), the target direction ($\boldsymbol{d}$), the trial number for the target (j), and the time points within the trial (t). For a given monkey and recording session, the rates of the N units comprising the population were grouped in the vector $\boldsymbol{r} = [r_1, r_2, \ldots, r_N]^\intercal$. In this work, we analyzed the average firing rate over the trial duration, $\langle \boldsymbol{r} \rangle_t$. These time-averaged firing rates were also averaged over the trials for a given context and target, $\langle \boldsymbol{r} \rangle_{t,j}$. These trial- and time-averaged

firing rates remain a function of the task context and target, $\boldsymbol{f}(n_D, \boldsymbol{d}) = \langle \boldsymbol{r} \rangle_{t,j}$. We defined the target set, $\mathbb{A}$, as the target set in the 3D context, $\mathbb{A} = \{\boldsymbol{d} : n_D = 3\}$. This set comprised 26 targets, $|\mathbb{A}| = 26$. We defined the target set, $\mathbb{B}$, as the target set in the 2D context, $\mathbb{B} = \{\boldsymbol{d} : n_D = 2\}$. This set comprised 16 targets, $|\mathbb{B}| = 16$. There were 8 targets which were common to the two sets, $|\mathbb{A} \cap \mathbb{B}| = 8$. We defined that set intersection as the set of common targets, $\mathbb{C} = \mathbb{A} \cap \mathbb{B}$. The 3D planar range for the units in the population was defined as:

$$\begin{aligned} \boldsymbol{\rho}_{3\mathrm{D}} = \quad & \max\{\boldsymbol{f}(n_D, \boldsymbol{d}) : n_D = 3, \boldsymbol{d} \in \mathbb{C}\} \\ & - \min\{\boldsymbol{f}(n_D, \boldsymbol{d}) : n_D = 3, \boldsymbol{d} \in \mathbb{C}\} \end{aligned} \tag{3.6}$$

Although all targets in the 2D context lie in the xy-plane, we calculated the 2D range over the set of common targets to directly compare the ranges:

$$\begin{aligned} \boldsymbol{\rho}_{2\mathrm{D}} = \quad & \max\{\boldsymbol{f}(n_D, \boldsymbol{d}) : n_D = 2, \boldsymbol{d} \in \mathbb{C}\} \\ & - \min\{\boldsymbol{f}(n_D, \boldsymbol{d}) : n_D = 2, \boldsymbol{d} \in \mathbb{C}\} \end{aligned} \tag{3.7}$$

Our analysis compared the difference between the 3D planar range ($\boldsymbol{\rho}_{3\mathrm{D}}$) and the 2D range ($\boldsymbol{\rho}_{2\mathrm{D}}$) for the units comprising the population. For comparisons of the full tuning ranges, the 2D full range was calculated over the entire set of 16 2D targets, $\boldsymbol{d} \in \mathbb{B}$:

$$\begin{aligned} \boldsymbol{\rho}_{2\mathrm{D}}^{\mathrm{full}} = \quad & \max\{\boldsymbol{f}(n_D, \boldsymbol{d}) : n_D = 2, \boldsymbol{d} \in \mathbb{B}\} \\ & - \min\{\boldsymbol{f}(n_D, \boldsymbol{d}) : n_D = 2, \boldsymbol{d} \in \mathbb{B}\} \end{aligned} \tag{3.8}$$

Similarly, the 3D full range was calculated over the entire set of 26 3D targets, $\boldsymbol{d} \in (A)$:

$$\begin{aligned} \boldsymbol{\rho}_{3\mathrm{D}}^{\mathrm{full}} = \quad & \max\{\boldsymbol{f}(n_D, \boldsymbol{d}) : n_D = 3, \boldsymbol{d} \in \mathbb{A}\} \\ & - \min\{\boldsymbol{f}(n_D, \boldsymbol{d}) : n_D = 3, \boldsymbol{d} \in \mathbb{A}\} \end{aligned} \tag{3.9}$$

3.2.4 Optimal Re-aiming Points

In order to test a re-aiming hypothesis that would explain the change in observed tuning ranges, we devised a method to estimate the optimal re-aiming points for that hypothesis. For each recording session that used the identical set of units to control the BCI task between contexts, the firing rate data from active control in the 3D context was used to fit a log-linear tuning model[52] to each unit in the population. The log-linear tuning model is similar to the linear tuning model in Equation 3.1 with the exception of the exponential relationship in the log-linear model:

$$r_{ll,i}(\boldsymbol{d}) = \exp(b_{ll,0,i} + m_{ll,i}\boldsymbol{d} \cdot \boldsymbol{p}_{ll,i}) \tag{3.10}$$

The subscripts, ll, are used to distinguish the equation and its tuning parameters from those used in the linear tuning model. The tuning parameters were fit for each neuron using the glmfit function in Matlab with the distribution and link parameters set as Poisson and log, respectively. For each of the 8 shared targets, an optimal re-aiming point for the 2D context was estimated using the log-linear tuning models and the decoders from each recording session. The optimization was run in Matlab as a constrained minimization to move the cursor closest to the target after one time-step. The optimization was constrained to ensure that the single re-aiming point for each target and recording session lies in S^2, the space of unit vectors in $\mathbb{R}^3$. The constrained minimization could be written as:

$$\min \left\{ \left\| 85\boldsymbol{d} - \frac{\Delta t k_s n_D}{N} \sum_{i=1}^{N} \boldsymbol{p}_i \frac{r_{ll,i}(\boldsymbol{d}^*) - b_{0,i}}{m_i} \right\| : \boldsymbol{d}^* \in S^2 \right\} \tag{3.11}$$

The scalar, 85, is used to scale the target direction to the target distance of 85mm used in the studies. Also, note that the predicted firing rates, $r_{ll,i}$, are derived from the log-linear tuning model in Equation 3.10 and decoded using the tuning parameters used in the original decoder. Thus, for all target directions, $\boldsymbol{d}$, in the set of common targets, $\mathbb{C}$, we derived optimal re-aiming points, $\boldsymbol{d}^*$, which we grouped into the set, $\mathbb{D}$. The optimal re-aiming ranges were calculated as:

$$\boldsymbol{\rho}_{\text{re-aim}} = \max\{\boldsymbol{r}_{ll}(\boldsymbol{d}^*) : \boldsymbol{d}^* \in \mathbb{D}\} - \min\{\boldsymbol{r}_{ll}(\boldsymbol{d}^*) : \boldsymbol{d}^* \in \mathbb{D}\} \tag{3.12}$$

Similarly, the tuning range predicted by the log-linear model was calculated as:

$$\boldsymbol{\rho}_{ll} = \max\{\boldsymbol{r}_{ll}(\boldsymbol{d}) : \boldsymbol{d} \in \mathbb{C}\} - \min\{\boldsymbol{r}_{ll}(\boldsymbol{d}) : \boldsymbol{d} \in \mathbb{C}\} \tag{3.13}$$

For each unit and recording session, we calculated the sign of the difference in tuning ranges predicted by re-aiming, $\text{sgn}(\rho_{\text{re-aim},i} - \rho_{ll,i})$, and the sign of the observed difference in tuning ranges, $\text{sgn}(\rho_{\text{2D},i} - \rho_{\text{3D},i})$, summing the results in a contingency table.

3.2.5 Leave-One-Out Prediction Error

In order to analyze whether the population structure changes between the task contexts, we utilized factor analysis models to estimate the population structure in the two contexts. For each recording session, we created factor analysis models from the square-root transformed time-averaged firing rates, $\boldsymbol{q} = \sqrt{\langle \boldsymbol{r} \rangle_t}$. The models describe the high-dimensional neural activity, $\boldsymbol{q} \in \mathbb{R}^N$, with a low-dimensional set of factors, $\boldsymbol{z} \in \mathbb{R}^w$, where $w < N$. Each factor is assumed to be distributed as a standard normal distribution:

$$\boldsymbol{z} \sim \mathcal{N}(\boldsymbol{0}, I) \tag{3.14}$$

where I is the identity matrix. The neural activity, given the factors, is also assumed to follow a normal distribution:

$$\boldsymbol{q}|\boldsymbol{z} \sim \mathcal{N}(\Lambda \boldsymbol{z} + \boldsymbol{\mu}, \Psi) \tag{3.15}$$

The models were created from the data for the sets of unique targets from either the 2D (8 unique targets) or 3D context (18 unique targets). The models were created with $w = 8$ factors using the expectation-maximization algorithm[18]. The number of factors was chosen based upon a four-fold cross validation analysis of the factor analysis model (Figure 3.20). The factor analysis models were used to predict the square-root transformed firing rate for a neuron, $\boldsymbol{q}_i$, from the remaining population's activity, $\boldsymbol{q}_{-i}$, following the methods of Yu, et al.[102]. The prediction error for a given trial was calculated as the sum of squared differences between the model prediction and the observed square-root transformed firing rates across all N neurons in the population

$$\text{Prediction error} = \sum_{i=1}^{N} (\hat{\boldsymbol{q}}_i - \boldsymbol{q}_i)^2 \tag{3.16}$$

For each trial from the set of identical targets, we calculated the prediction error with both the concordant and discordant model.

3.2.6 Intrinsic Manifolds

To further study the changes in the population structure between contexts, we adapted the methods of Sadtler, et al.[82] to estimate the intrinsic manifolds of the neural populations under active brain control in the 3D and 2D contexts. Spiking activity for each unit were placed in 40ms bins, in windows from 200-800ms after target appearance for each successful trial. The spiking activity was square-root transformed for each recording session. We analyzed the data for the set of 8 identical targets in the two contexts. For each context, we randomly split the data in half, ensuring an equal number of data points from each target as well as an equal number of total data points between each context. The rates were then reduced to 10 (Monkey A) or 12 (Monkey C) factors for each half of each context via factor analysis with the expectation-maximization algorithm[18]. The choice of the number of factors was based upon a four-fold cross-validation analysis of the data log-likelihood under various choices of number of factors (Figure 3.21). For two recording sessions from Monkey A, a lower number of factors was used (6 and 9 factors). From the factor analysis of each half, the intrinsic manifold was taken as the column space of Λ. We then computed the average principal angles between the intrinsic manifolds from two halves of each context as well as between the factors from the first halves of the two contexts[5]. Combining the average principal angles from all recording sessions, we estimated the cumulative distribution functions of the average principal angles from within the 2D and 3D contexts as well as between the two contexts.

3.2.7 Information transmission for individual units

In order to compare the information transmission of the individual units between the two contexts, we estimated the mutual information, I, between the set of common targets and the firing rate of the unit for each unit and context. The mutual information was estimated by subtracting estimates of the conditional entropy of the firing rate from the total entropy

of the firing rate:

$$I_{i,n_D} = H(R_{i,n_D}) - H(R_{i,n_D}|\boldsymbol{D}) \tag{3.17}$$

The conditional entropy was estimated by first modeling the square-root transformed firing rate in response to a target as a Gaussian distribution:

$$p(Q_{i,n_D}|\boldsymbol{D} = \boldsymbol{d}) \sim \mathcal{N}(\mu_{i,n_D,\boldsymbol{d}}, \sigma_{i,n_D,\boldsymbol{d}}) \tag{3.18}$$

Subsequently, the entropy of the firing rate for each of the common targets was computed as the entropy of a Gaussian distribution

$$H(R_{i,n_D}|\boldsymbol{D} = \boldsymbol{d}) = \frac{1}{2}\ln(2\pi e\sigma_{i,n_D,\boldsymbol{d}}) \tag{3.19}$$

The conditional entropy was then calculated as the average of the entropies of the firing rate for each of the 8 common targets, weighting each equally. In order to calculate the total entropy of the firing rates, we modeled the rates as an equally weighted mixture of the previously calculated Gaussian distributions. Because there exists no closed-form expression for the entropy of a mixture of Gaussians, we estimated the entropy using the second-order Taylor-series expansion method formulated by Huber, et al.[44] For each unit, we compared the difference between the information transmission calculated from the 2D context, $I_{i,\text{2D}}$, and that from the 3D context, $I_{i,\text{3D}}$. The histograms of the differences between the two information estimates for each monkey are shown in Figure 3.22. The estimates were divided by $\ln(2)$ to convert the values from nats to bits.

3.3 RESULTS

Two male Rhesus macaques implanted with Utah arrays were trained to perform 2D and 3D center-out tasks in virtual reality, under brain control (Figure 3.1a, b). To map the neural activity to movement of the cursor, the activity of each unit was assumed to follow the 3D linear tuning model. With the fitted models of neural activity, cursor movement was updated online with predictions from the decoders as described in more detail in the methods section. For the 2D task, the z-component of the decoded movement was zeroed to constrain

movement to the xy-plane. There were 26 targets in the 3D context and 16 targets in the 2D context. The two target sets included 8 common targets, allowing for direct comparison between the two task contexts (Figure 3.1c, d). For 5 recording sessions from Monkey A and 4 from Monkey C, the population of units controlling the cursor movement was the same between contexts. The average population size for these sessions was 28.6 units for Monkey A (min: 26; max: 32) and 37 units for Monkey C (min: 33; max: 45). For the rest of the recording sessions (Monkey A: 13; Monkey C: 7), the majority of the units comprising each population were the same between contexts. For these sessions, we focused our analyses on the units that contributed to controlling the cursor movement for both contexts. The average size of this overlapping population was 25.6 units for Monkey A (min: 13; max: 32) and 36 units for Monkey C (min: 30; max: 45). Six units that appeared to lose signal during the recording session were removed from these analyses (Figure 3.2).

3.3.1 Firing Rates Change with Context

Our first finding is that firing rates during movement to the 8 common targets depend on whether the task context is 2D or 3D. Firing rates for each successful trial were calculated in time windows from target presentation until target acquisition. The rates were averaged across trials for each target, to compute the trial-averaged firing rates. For the set of identical targets between contexts, we calculated the average firing rate separately for each context. In Figure 3.3, we plot the average firing rates to the targets that lay in the xy-plane for both contexts. The blue lines show the trial-averaged firing rates of the neurons to all targets from the 2D context, plotted as a function of target direction (azimuth). The pink lines show the trial-averaged firing rates of the neurons for the 8 targets in the xy-plane, again as a function of azimuth. The horizontal dotted lines show the minimum and maximum trial-averaged firing rates amongst the entire set of 26 targets during the 3D context. As expected, the azimuthal preferred directions are nearly identical between the two contexts. This is consistent across all units for both monkeys (Figure 3.4). However, the ranges in the tuning curves are not also identical between the two contexts. Instead, the range of firing rates for all 16 targets during the 2D context approaches, and occasionally exceeds, the range

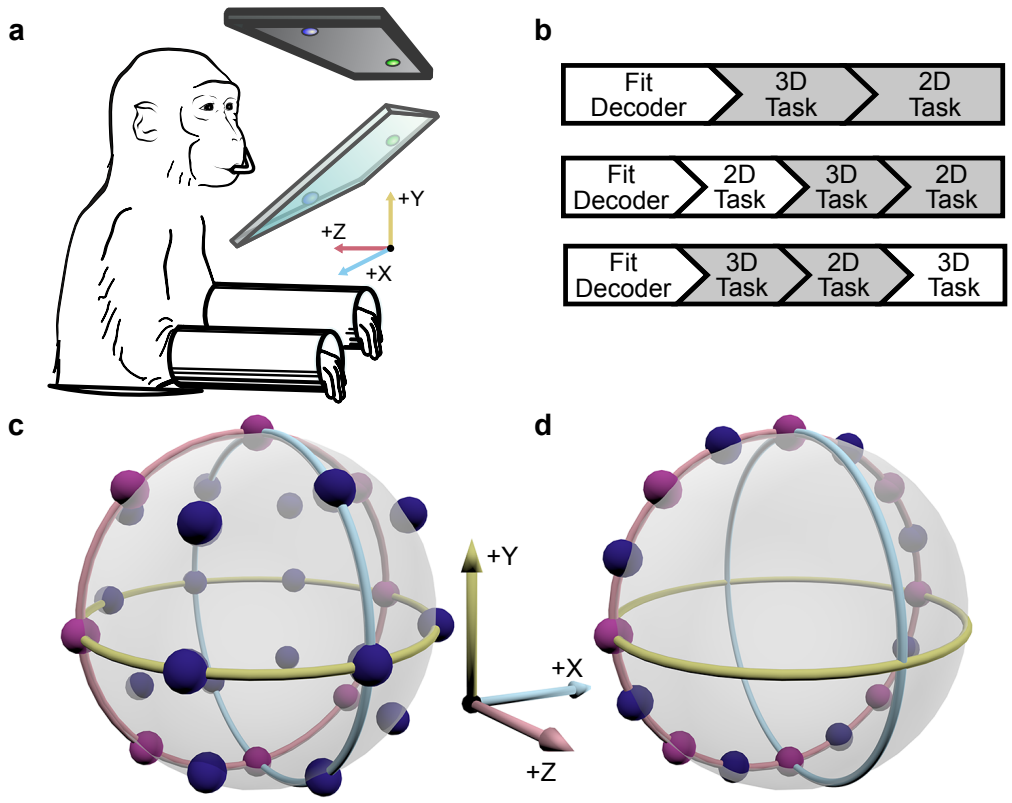

Figure 3.1: Experimental setup. (**a**) The monkey controlled a computer cursor on a stereoscopic monitor viewed through a mirror, using neural signals. (**b**) Each recording session began with a brief calibration session to build the decoder. The decoder was used for a block of 3D trials (between 9-13 trials per target), followed by a block of 2D trials (between 15-27 trials per target). In some sessions, an additional block of 2D trials would proceed the blocks of 3D and 2D trials, or an additional block of 3D trails would follow the blocks of 3D and 2D trials. We focused our analyses on the first block of 3D trials and the block of 2D trials immediately following it (the gray boxes). In the supplementary materials, we demonstrate that our findings are invariant to the order of the blocks of trials. (**c**) Locations of the 26 targets in the 3D context. (**d**) Locations of the 16 targets in the 2D context. The 8 targets that were common to the 2D and 3D contexts are shown in pink. The red, yellow, and light blue hoops represent the xy-plane, xz-plane, and yz-plane, respectively.

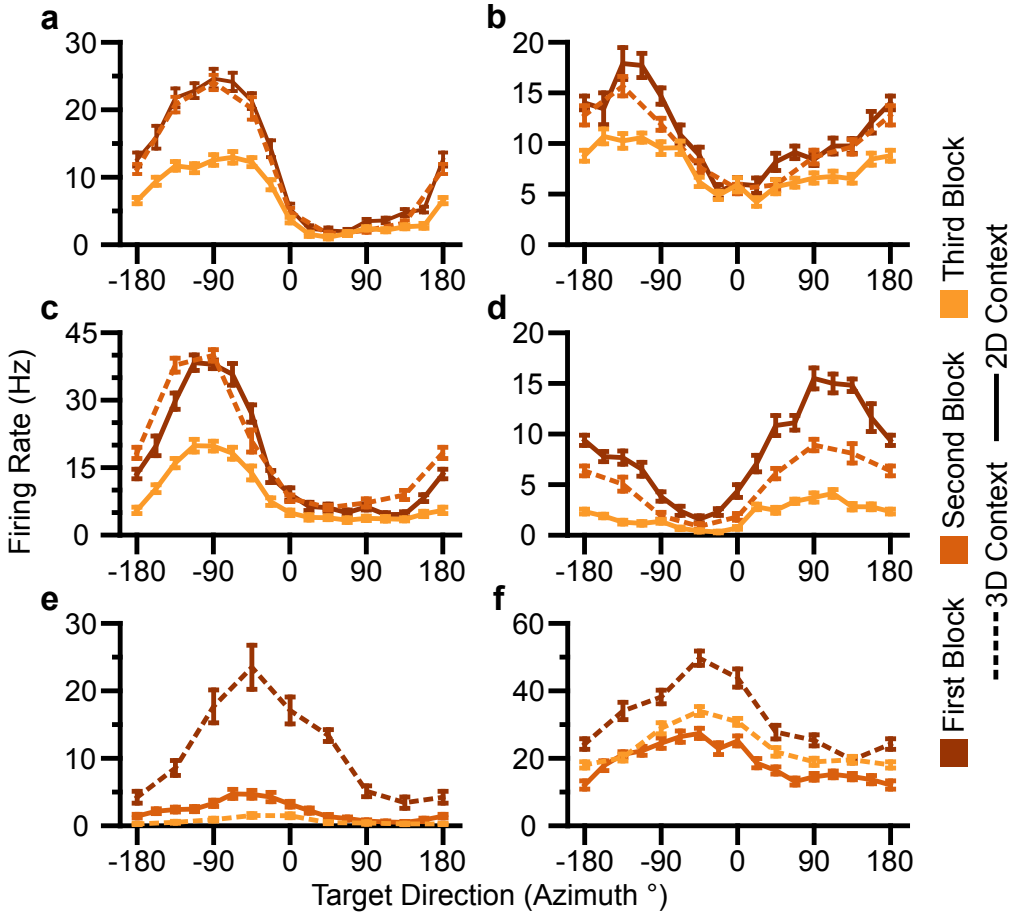

Figure 3.2: Units removed from analysis due to signal loss. Tuning curves from the first, second, and third block of trials are shown as the curves from dark to light orange. Firing rates are drawn as the mean ± s.e.m. across the trials in the block. Blocks from the 3D context are drawn as dashed lines and those from the 2D context are drawn as solid lines. (**a-e**) Five units from Monkey A. (**f**) One unit from Monkey C.

observed for all 26 targets during the 3D context. This finding is even more striking when considering the firing rates for the set of 8 targets that were identical between contexts. The units show greater maximal firing rates and lower minimal firing rates in the 2D context compared to the 3D context for the BCI task.

To quantify this change, we computed the planar tuning ranges as the difference between the minimum and maximum average firing rate amongst the set of 8 identical targets for the two contexts. We found that 334 of 471 units in Monkey A and 230 of 409 units in Monkey C exhibited an increase in planar tuning range in the 2D context relative to the 3D context. The mean $\pm$ standard error of the mean (s.e.m.) increase in tuning range was 4.02 $\pm$ 0.33 Hz for Monkey A and 0.81 $\pm$ 0.25 Hz for Monkey C (Figure 3.5).

The order of the 2D and 3D contexts do not affect these findings. In a subset of recording sessions, an additional block of 2D context trials preceded the blocks of 3D context and 2D context trials analyzed in this work. Similarly, in another subset of recording sessions, an additional block of 3D context trials followed the block of 3D context and 2D context trials analyzed in this work. We used these additional blocks of trials to study whether the order of the contexts changed the finding of increased planar tuning range in the 2D context. In Figure 3.6, we plotted the tuning ranges to the set of eight identical targets in the 2D and 3D contexts for the blocks where the 2D block of trials preceded the 3D block of trials. We found that the result of increased tuning range during the 2D context was invariant to the order of the contexts.

The findings also hold when considering only the sessions using either the PVA decoder or the OLE decoder. In a subset of recording sessions for Monkey A, an OLE decoder was used instead of a PVA decoder. We used these sessions to study whether the result of increased tuning range in the 2D context changed with a change in decoder type. In Figure 3.7, we plotted the tuning ranges to the set of eight identical targets in the 2D and 3D contexts for only the sessions for Monkey A that used a PVA decoder and only the sessions for Monkey A that used an OLE decoder. We found that the result of increased tuning range during the 2D context was invariant to the choice of OLE versus PVA decoders.

Additionally, when considering only the sessions where the entire population was identical between contexts, the units still show an increase in tuning range. In a subset of recording

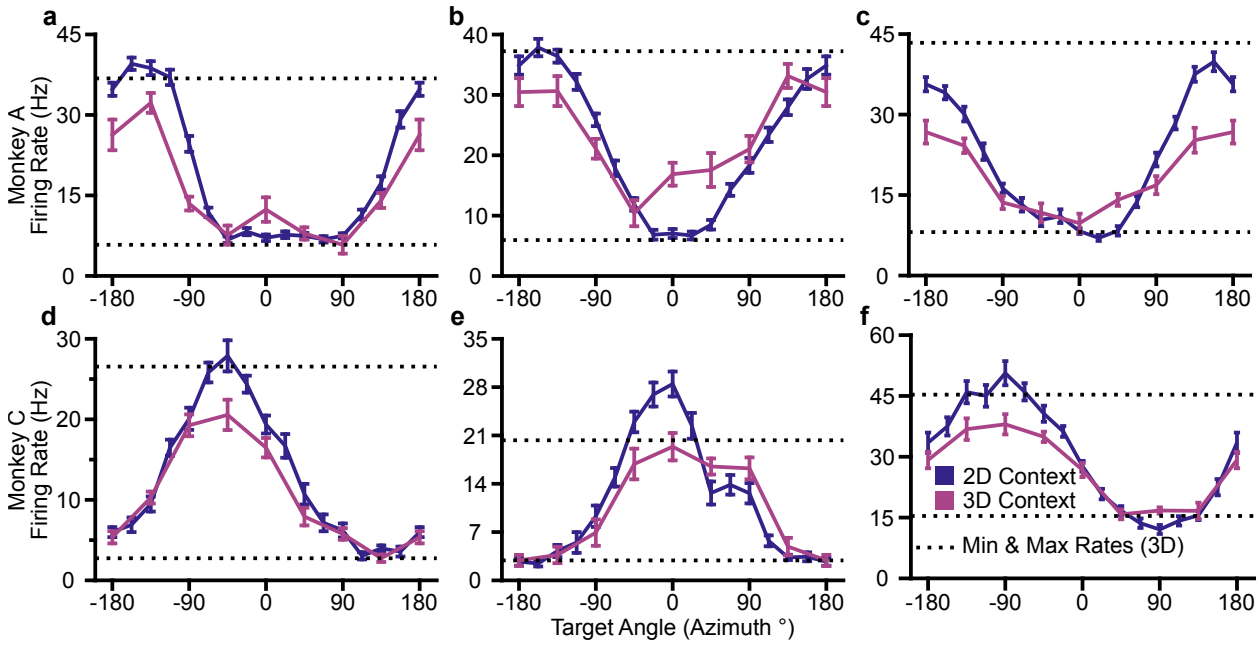

Figure 3.3: Tuning differences between the 2D and 3D contexts. (**a-f**) Selected tuning curves for the targets in the xy-plane during the 3D (pink) and 2D (dark blue) contexts from Monkey A (top row) and Monkey C (bottom row). Firing rates show the mean ± s.e.m. for each target (n_{3D} = 10(**a-e**), 12(**g**); n_{2D} = 27(**a,b**), 15(**c-f**)). The dashed horizontal lines show the minimum and maximum target-averaged firing rates for all 26 targets in the 3D context. Note that the unit shown in (**g**) had an elevation angle, ϕ, of $\approx 75°$.

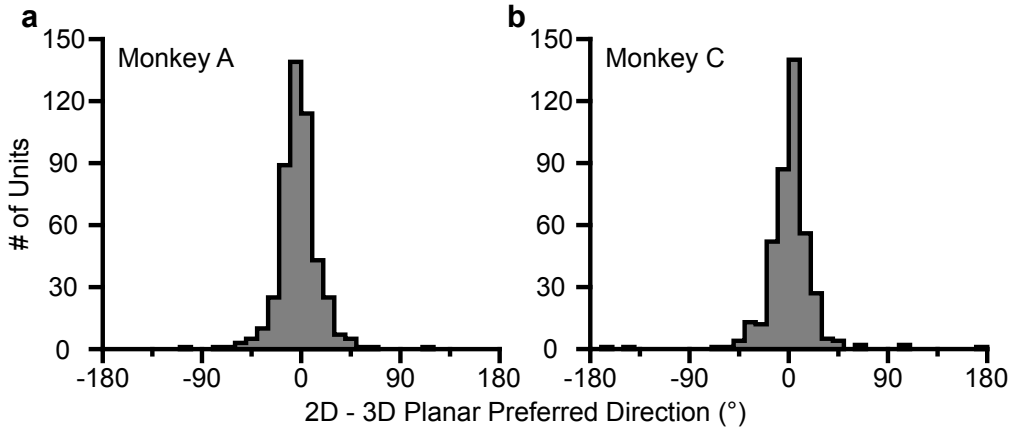

Figure 3.4: Changes in azimuthal preferred direction. (**a**) Monkey A. (**b**) Monkey C. Firing rates from active control in the target presentation to acquisition time windows were used to fit log-linear tuning models independently for the 2D and 3D contexts. The preferred direction from the 2D context was compared to the x and y-components of the preferred direction from the 3D context to calculate the change in the azimuthal preferred direction. The changes are insignificant under the Moore test of paired samples of angles[103, 66] for both Monkey A ($R' = 0.817$, $n = 471$, $P > 0.1$) and Monkey C ($R' = 0.887$, $n = 409$, $P > 0.05$). The two units from Monkey A with a large magnitude change in planar preferred direction ($> 90°$) had preferred directions with an elevation angle of $\approx 77°$, and $79°$ under the 3D context. The five units from Monkey C with a large magnitude change in planar preferred direction ($> 90°$) had preferred directions with an elevation angle of $\approx 80°, 81°, 85°, 87°$, and $89°$ under the 3D context.

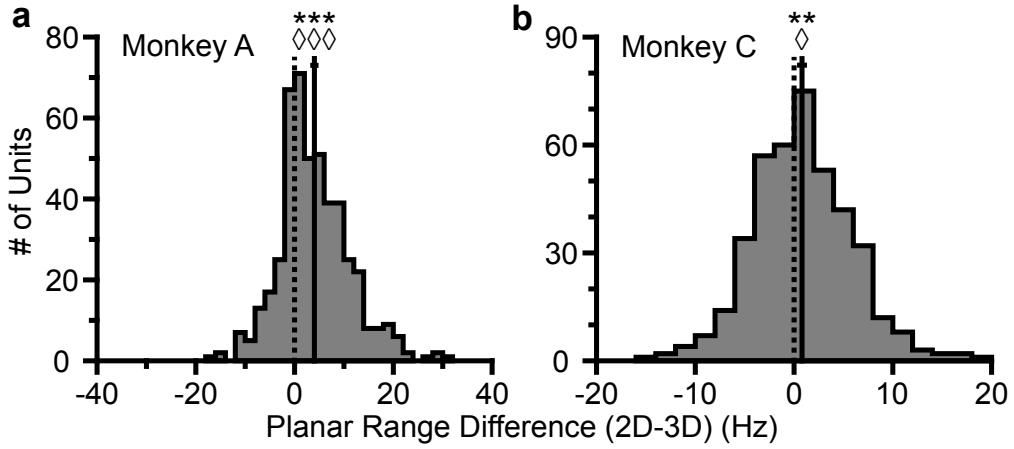

Figure 3.5: Tuning range differences between the 2D and 3D contexts. (**a,b**) Histograms of the differences in tuning ranges for the set of 8 identical targets between the 2D and 3D context for Monkey A (left) and Monkey C (right). For both panels: solid vertical lines, means of distributions; solid horizontal lines, mean ± s.e.m.; dashed vertical lines, point of equality between the two tuning ranges. $W_A = 88059$, $^{***}P \ll 10^{-20}$, $S_A = 334$, $\lozenge\lozenge\lozenge P < 10^{-18}$, $n_A = 471$, $W_C = 48975$, $^{**}P = 0.0032$, $S_C = 230$, $\lozenge P = 0.0134$, $n_C = 409$. W, Wilcoxon signed-rank tests, S, sign tests, n, number of analyzed units.

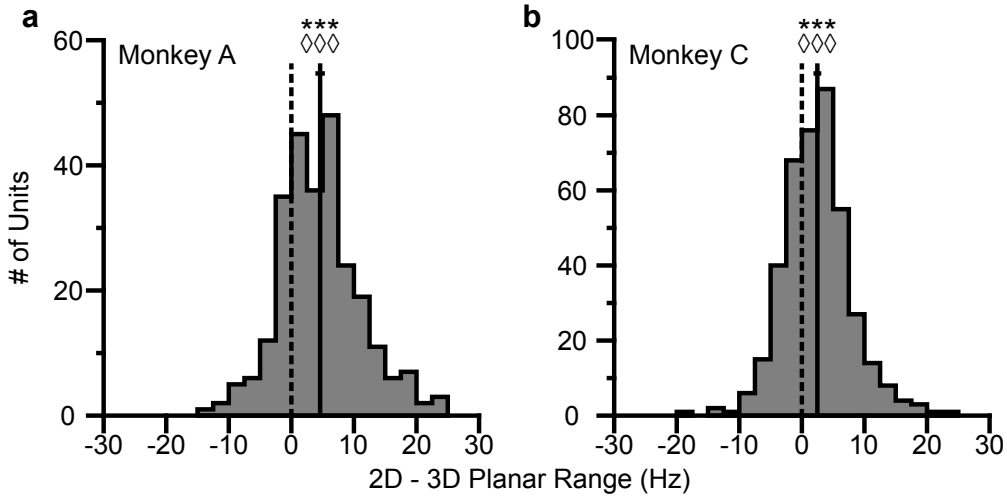

Figure 3.6: Tuning range change is invariant to the block order of the contexts. The plots compare the tuning ranges for Monkey A (**a**) and Monkey C (**b**) for the set of identical targets in the 2D and 3D context when blocks of 2D trials that preceded blocks of 3D trials. For both panels: solid vertical lines, means of distributions; solid horizontal lines, mean ± s.e.m.; dashed vertical lines, point of equality between the two tuning ranges. $W_A = 29248$, $^{***}P << 10^{-20}$, $S_A = 201$, $\lozenge\lozenge\lozenge P < 10^{-17}$, $n_A = 262$, $W_C = 62834$, $^{***}P < 10^{-17}$, $S_C = 276$, $\lozenge\lozenge\lozenge P < 10^{-11}$, $n_C = 409$. W, Wilcoxon signed-rank tests, S, sign tests, n, number of analyzed units.

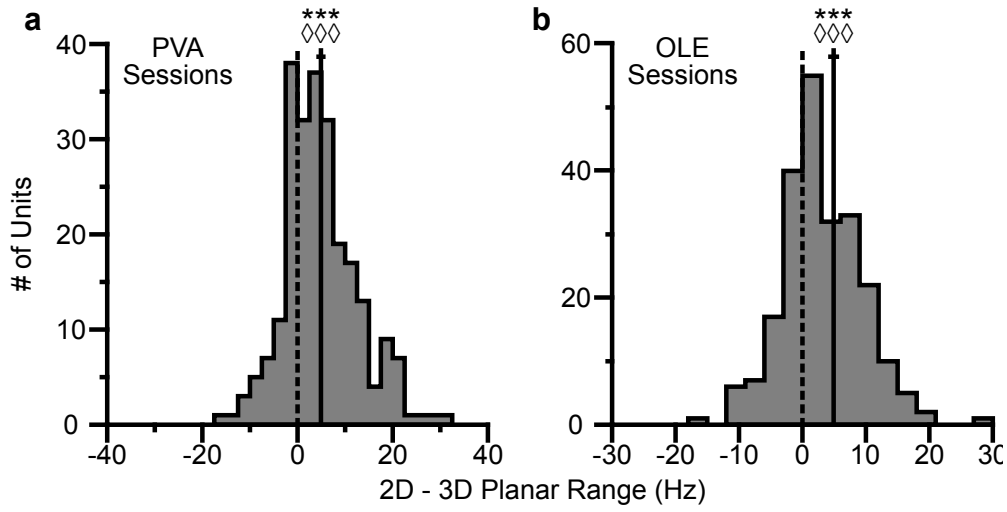

Figure 3.7: Tuning range change is invariant to the choice of PVA or OLE decoders. For Monkey A, separate recording sessions used either a PVA or OLE decoder. The plots compare the tuning ranges for the set of identical targets in the 2D and 3D context for the recording sessions that used the PVA decoder (**a**) and the recording sessions that used the OLE decoder (**b**). For both panels: solid vertical lines, means of distributions; solid horizontal lines, mean ± s.e.m.; dashed vertical lines, point of equality between the two tuning ranges. $W_{PVA} = 23856$, $^{***}P < 10^{-17}$, $S_{PVA} = 174$, $\lozenge\lozenge\lozenge P < 10^{-11}$, $n_{PVA} = 240$, $W_{OLE} = 20273$, $^{***}P < 10^{-10}$, $S_{OLE} = 160$, $\lozenge\lozenge\lozenge P < 10^{-8}$, $n_{OLE} = 231$. W, Wilcoxon signed-rank tests, S, sign tests, n, number of analyzed units.

sessions, the entire population used in controlling BCI task was identical between the two contexts. These sessions were those where the decoder was calibrated only once for the entirety of the recording session. We used these sessions to study whether the result of increased tuning range in the 2D context changed when the population was identical between the two contexts. In Figure 3.8, we plotted the tuning ranges to the set of eight identical targets in the 2D and 3D contexts for the sessions from Monkey A and Monkey C where the populations were identical between the contexts. We found that the result of increased tuning range during the 2D context was invariant to the matched populations between contexts.

The changes in tuning ranges are also apparent when looking at firing rates from a single recording session from either Monkey A (Figure 3.9) or Monkey C (Figure 3.10). The 2D and 3D planar tuning ranges for these recording sessions are compared in Figure 3.11.

3.3.2 Tuning range increases are driven by dynamic range adaptation

We next investigated the mechanisms that might be driving the context-dependent firing rate changes we observed during the BCI task. We considered three possible mechanisms: (1) a re-aiming mechanism, in which subjects aim at points other than the targets[48], (2) a change in intended speed between the two contexts[67], or (3) dynamic range adaptation[7]. These strategies each make different predictions about how tuning changes will correlate across populations of simultaneously recorded cells. Below we discuss each of these mechanisms in turn.

Re-aiming refers to the process of aiming at a virtual target different than the one that is presented. Under re-aiming, tuning curves are assumed to remain fixed, but firing rates to identical targets can change if their re-aiming points are different across contexts. Re-aiming processes have been found to explain the majority of short-term adaptation to visuomotor rotations experienced under BCI control[9]. Why might re-aiming occur between the 3D and 2D contexts? Under the 3D context, re-aiming would likely result in movement of the cursor away from the target, and thus would not likely occur. In the 2D context, however, aiming points anywhere along the z-axis that maintain a constant projection in the xy-plane would all result in a straight movement. However, if there are biases in the distributions of

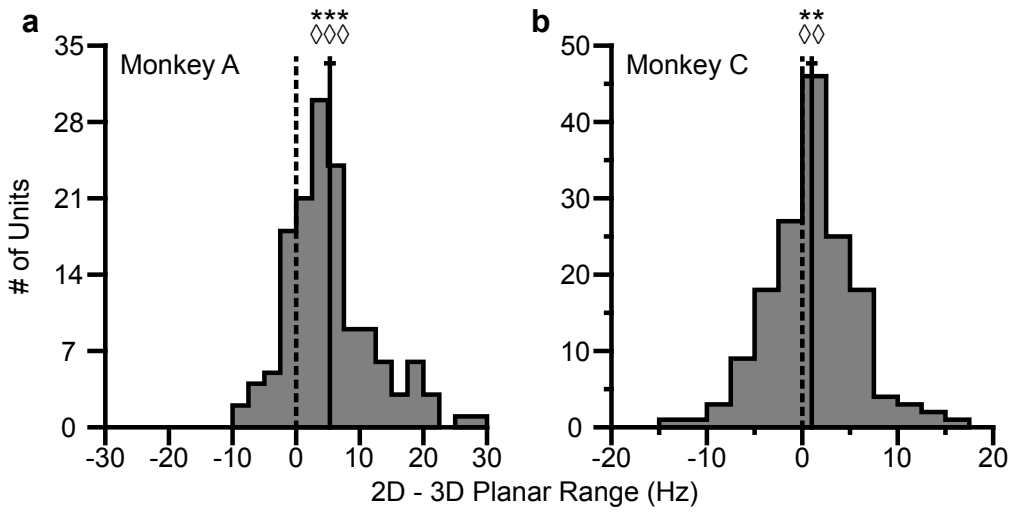

Figure 3.8: Tuning range change is invariant to decoders using an identical population. The plots compare the tuning ranges for Monkey A (**a**) and Monkey C (**b**) for the set of identical targets in the 2D and 3D context for the subset of recording sessions where the population used for BCI control was identical between the two contexts. For both panels: solid vertical lines, means of distributions; solid horizontal lines, mean ± s.e.m.; dashed vertical lines, point of equality between the two tuning ranges. $W_A = 8962$, $^{***}P < 10^{-14}$, $S_A = 113$, $\lozenge\lozenge\lozenge P < 10^{-11}$, $n_A = 142$, $W_C = 7799$, $^{**}P = 0.0084$, $S_C = 99$, $\lozenge\lozenge P = 0.0019$, $n_C = 158$. W, Wilcoxon signed-rank tests, S, sign tests, n, number of analyzed units.

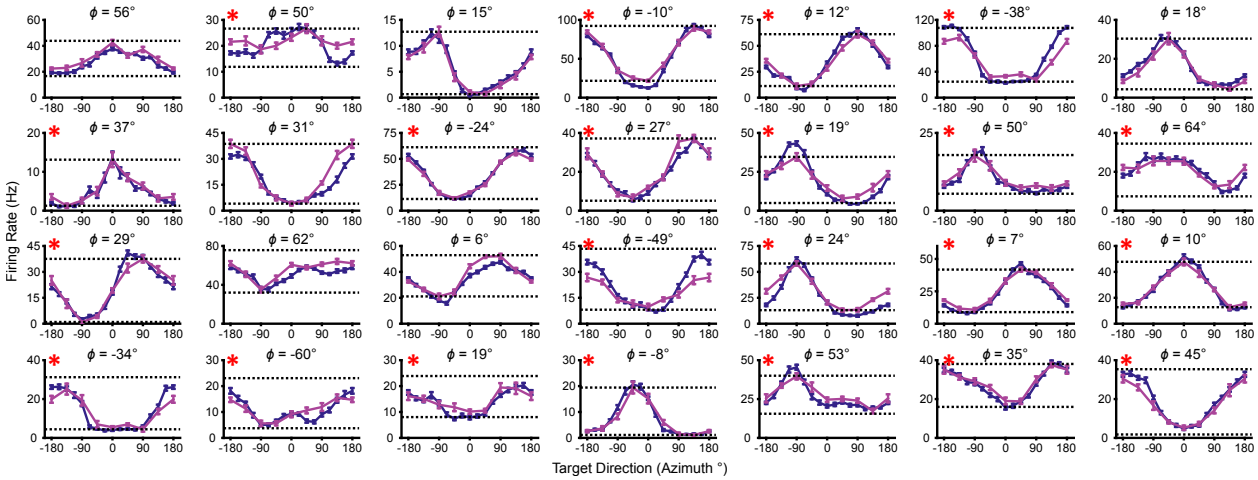

Figure 3.9: Tuning range changes for Monkey A for one recording session. The plots show the tuning curves for the targets lying on the xy-plane in the 2D (dark blue) and 3D (pink) contexts. The firing rates are shown as the mean ± s.e.m. ($n_{2D} = 24$; $n_{3D} = 10$). The minimum and maximum average firing rates amongst the set of all 26 targets from the 3D context are drawn as the dotted horizontal lines. The titles above each plot show the elevation angle, ϕ, that the unit's preferred direction vector estimated from the 3D data makes with the xy-plane. Units that showed a greater tuning range amongst the set of identical targets in the 2D context than the 3D context are marked with a red asterisk at the top-left corner of the plot.

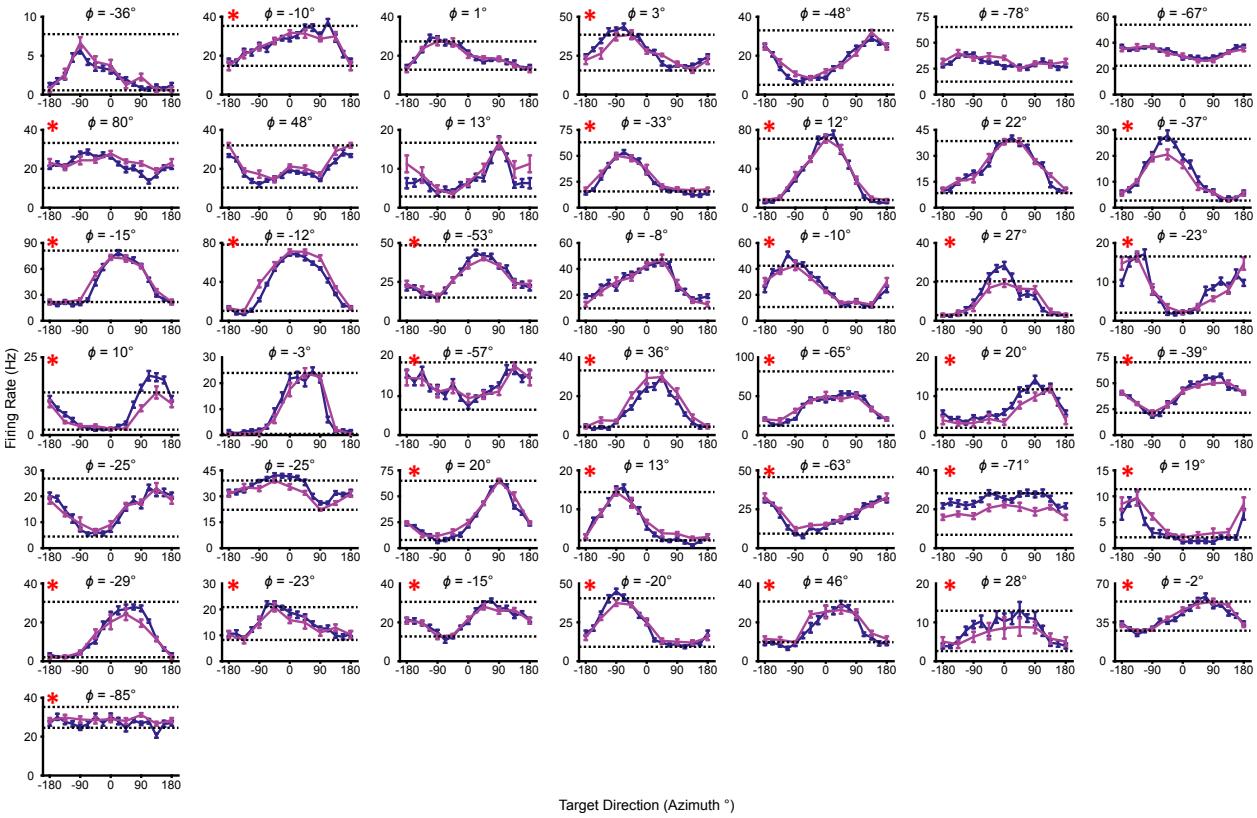

Figure 3.10: Tuning range changes for Monkey C for one recording session. The plots show the tuning curves for the targets lying on the xy-plane in the 2D (dark blue) and 3D (pink) contexts. The firing rates are shown as the mean ± s.e.m. ($n_{2D} = 16$; $n_{3D} = 10$). The minimum and maximum average firing rates amongst the set of all 26 targets from the 3D context are drawn as the dotted horizontal lines. The titles above each plot show the elevation angle, ϕ, that the unit's preferred direction vector estimated from the 3D data makes with the xy-plane. Units that showed a greater tuning range amongst the set of identical targets in the 2D context than the 3D context are marked with a red asterisk at the top-left corner of the plot.

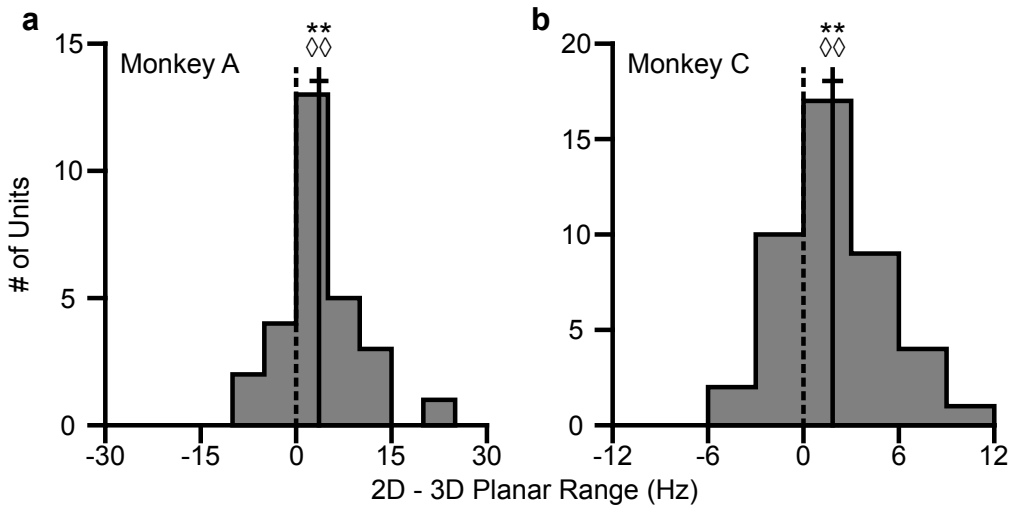

Figure 3.11: Difference in tuning ranges in single sessions. The plots show the histograms for the difference tuning ranges for the set of 8 identical targets between the 2D and 3D context for Monkey A (**a**) and Monkey C (**b**) for the recording sessions corresponding to the data shown in SI Figures 3.9 and 3.10. For both panels: solid vertical lines, means of distributions; solid horizontal lines, mean ± s.e.m.; dashed vertical lines, point of equality between the two tuning ranges. $W_A = 333$, $^{**}P = 0.0031$, $S_A = 22$, $\lozenge\lozenge P = 0.0037$, $n_A = 28$, $W_C = 731$, $^{**}P = 0.0018$, $S_C = 31$, $\lozenge\lozenge P = 0.0054$, $n_C = 43$. W, Wilcoxon signed-rank tests, S, sign tests, n, number of analyzed units.

preferred directions, such re-aiming might allow the subject to push the cursor faster along the path to the target than aiming directly would.

Under the re-aiming mechanism, units would undergo either an increase or decrease in tuning range, dependent upon the value of the unit's preferred direction. We illustrate these direction dependent changes for an example scenario in Figure 3.12a. The color on the sphere indicates the relative tuning range change for a unit with a preferred direction at that point. The preferred directions of three example units are shown as the light green points on the sphere. Although the three units have nearly the same azimuthal preferred directions (near 45°), the elevation angle of the preferred direction vectors are positive for the first two units and negative for the third. Under the re-aiming mechanism, the re-aiming point for the target with an azimuthal direction of 45° in the 2D context would be above that target, closer to the preferred directions of the first two units and farther from the preferred direction of the third unit. Consequently, the first two units would have an increased firing rate and the third unit would decrease its firing rate in the 2D context to the target with an azimuthal direction of 45°. The tuning curves for these three units for the 3D and 2D contexts under the re-aiming mechanism are drawn under the re-aiming sphere. In this hypothetical example, the first two units demonstrate an increased tuning range in the 2D context, while the third unit demonstrates a decreased tuning range.

Change in intended speed refers to the process of encoding different speeds in the firing rates. Moran and Schwartz demonstrated that movement speed has both an additive and multiplicative effects on the firing rate[67]. They modeled the relationship between movement velocity, $\boldsymbol{v}$, and neural firing rate, r_i, with the following equation:

$$r_i = b_{0,i} + ||\boldsymbol{v}||b_{s,i} + m_i \boldsymbol{v} \cdot \boldsymbol{p}_i \tag{3.20}$$

where $||\boldsymbol{v}||$ is the movement speed and $b_{s,i}$ scales the additive effect of the speed. Unlike the traditional linear tuning model[33], the modulation depth, m_i, scales not only the directional tuning effects but also the multiplicative effect of speed. The decoding algorithms used in these studies convert the firing rates of the population into cursor velocity. A more detailed description of the decoding algorithms is provided in the preceding methods section. Briefly, more extreme firing rates (i.e., very low and high firing rates relative to baseline) would

increase the speed of the cursor. Subsequently, increases in intended cursor speed during the 2D context would increase the tuning range of the units.

We illustrate the relative change in tuning range as a function of preferred direction predicted by change in intended speed in Figure 3.12b. Unlike the re-aiming mechanism, the relative change in tuning range expected does not vary with preferred direction. Instead, the relative change in tuning range is identical for all units. Following Equation 3.20, the tuning range for a unit, ρ_i, is the difference between the maximum and minimum firing rate, r_i, over the range of targets, $\boldsymbol{d}$, in the xy-plane. Because of the subtraction, only the multiplicative effects of speed remain in the tuning range, $\rho_i = 2m_i||\boldsymbol{v}||\cos(\phi_i)$. Thus, if the intended speed during the 2D context is twenty percent greater than that in the 3D context, the 2D tuning range will be twenty percent greater than the 3D planar tuning range.

Dynamic range adaptation refers to the process of the units adjusting their tuning curves to utilize their full tuning range, $2m_i$, in the given task context. This process is akin to the dynamic range adaptation observed in sensory cortices, where neurons adjust their tuning functions to optimally encode the range of input stimuli. In the 2D context, the z-dimension is no longer relevant. Subsequently, the portion of the tuning range allocated to encoding the z-dimension during the 3D context may be utilized to encode targets in the xy-plane during the 2D context.

We illustrate the relative change in tuning range as a function of preferred direction predicted by dynamic range adaptation in Figure 3.12c. Unlike a change in intended speed, the relative change in tuning range expected due to dynamic range adaptation varies with the elevation angle, ϕ, of the preferred direction. Under dynamic range adaptation, the 2D tuning range would be equal to the full tuning range, $2m_i$, whereas the 3D planar tuning range is scaled by the cosine of the elevation angle, $2m_i\cos(\phi_i)$. We refer to this as a "dose-response" effect. Increasing the "dose" of the elevation angle leads to an increased response of tuning range change.

To evaluate whether the results were consistent with a re-aiming strategy, we searched for scenarios like units 1 and 3 illustrated in Figure 3.12a. Specifically, we looked for a pair of units with nearly identical 2D preferred directions whose 3D preferred directions were mirrored across the xy-plane. As explained above, the re-aiming strategy predicts

that one unit would show an increased firing rate to the planar target in the 2D context compared to the 3D context while the other unit would show a decreased firing rate. In the alternative hypotheses, both units would show increased firing rates to the planar target in the 2D context. Results from a pair of units matching this scenario are shown for Monkey A (Figure 3.13a,b) and Monkey C (Figure 3.13c,d). Activity for these example pairs of units is inconsistent with the re-aiming strategy. Both units demonstrate maximal firing rates to the planar target in the 2D context.

To study whether the results were consistent with the re-aiming strategy at the population level, we developed an algorithm to predict the optimal aiming points for the population in the 2D context, based upon the firing rates in the 3D context. We applied this analysis to the recording sessions where the entire population was identical between the two contexts. For Monkey A, of the 87 units predicted to increase tuning range, 66 were observed to increase (21 type A discordant pairs). Of the 55 units predicted to decrease tuning range, 8 were observed to decrease (47 type B discordant pairs). For Monkey C, of the 86 units predicted to increase tuning range, 57 were observed to increase (29 type A discordant pairs). Of the 72 units predicted to decrease tuning range, 30 were observed to decrease (42 type B discordant pairs). If the re-aiming model matched the data, we would expect the noisy pairs to be equally distributed between type A and type B discordance. We tested this using McNemar's test. We found significant results for one monkey (A: $P = 0.0016$) and a trend for more units increasing tuning range than predicted by re-aiming for the second monkey (C: $P = 0.1229$). This suggests that the tuning changes were inconsistent with re-aiming.

In order to distinguish whether the results were consistent with a change in intended speed or dynamic range adaptation, we investigated whether the results demonstrated a dose-response effect. Although the accuracy of the speed encoding model is debated[12], it is hard to see how randomly distributed speed tuning across the population would lead to a dose-response effect. We plotted the ratio of the 3D planar to 2D ranges against the absolute value of the elevation angle. We found weighted linear fits with a negative slope (Figure 3.14). These slopes were significant as evaluated with an F-test against a constant model hypothesis for Monkey A ($P < 10^{-12}$) and Monkey C ($P = 0.00125$). We repeated this analysis using the cosine of the elevation angle rather than the absolute value (Figure 3.15).

We found weighted linear fits with a positive slope which were also significant with an F-test (Monkey A: $P < 10^{-13}$; Monkey C: $P = 0.00299$). These results are inconsistent with the speed hypothesis and consistent with the dynamic range adaptation hypothesis. The results suggest that the units in the population are using the portion of the tuning range that encoded and controlled the z-dimension in the 3D context to contribute to the encoding and control of the x and y-dimensions relevant in the 2D context of the BCI task. When we compared the full tuning ranges from the 2D and 3D contexts, we found that more than half of the units (54.8%) had greater full tuning range in 2D than 3D for Monkey A, whereas less than half of the units (41.8%) had greater full tuning range in 2D than 3D for Monkey C (Figure 3.17). This suggests that this adaptation effect is nearly complete for Monkey A and partial for Monkey C.

3.3.3 Change in Population Structure

The results from the analyses of neuron pairs suggest that the observed dynamic range adaptation ought to lead to a change in the patterns of correlation that the population naturally exhibits. To further investigate this, we modeled these patterns of correlation using factor analysis. We created separate factor analysis models of the population for the 2D and 3D contexts from the set of unique targets[102]. For each trial from the set of identical targets, we calculated the leave-one-out prediction error of the firing rates under the models created from the two contexts. We labeled the models as concordant when the trial context matched the context from which the model was created and discordant when the trial and model contexts were mismatched. We found that the leave-one-out prediction error is significantly greater for the discordant models than with the concordant models (Figure 3.18a,b,d,e). This result suggests that the patterns of correlation in the population activity changes with the change in context.

Recently, work by Sadtler, et al.[82] demonstrated the role of intrinsic manifolds in BCI tasks. These manifolds describe the lower dimensional subspace in which population activity commonly lies and can be predictive of BCI mappings that are quickly learnable. In our work, we estimated separate manifolds for the 3D and 2D contexts. We then computed the average

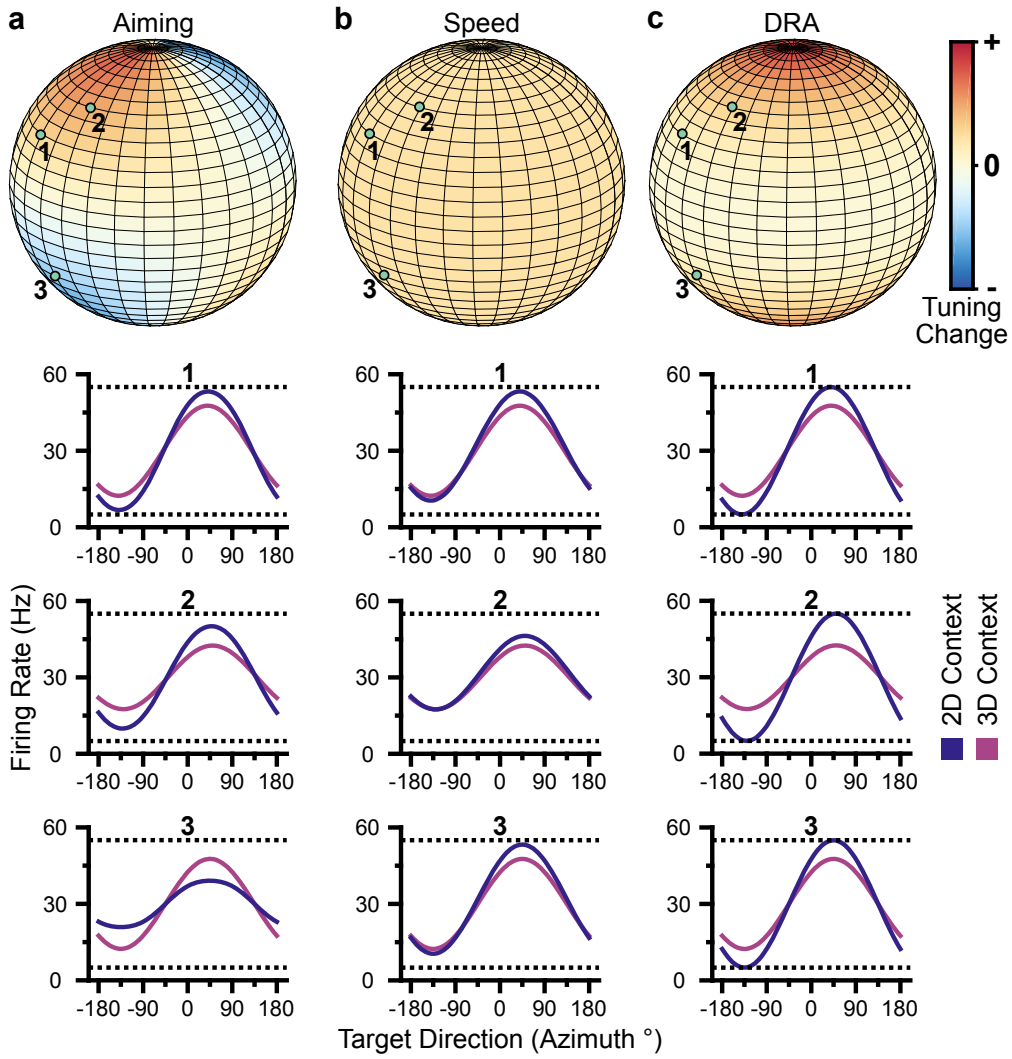

Figure 3.12: Hypotheses for tuning changes. (**a**) Illustration of the aiming strategy hypothesis. (**b**) Illustration of the speed hypothesis. (**c**) Illustration of the dynamic range adaptation hypothesis. For each hypothesis, the first row shows heat maps of the relative change in tuning range as a function of preferred direction. For illustrative purposes, the heat map in (**a**) is shown as $\frac{\text{2D Range}-\text{3D Planar Range}}{\text{3D Range}}$ and scaled in the range $[-0.25, 0.25]$. The other heat maps are shown as $1 - \frac{\text{3D Planar Range}}{\text{2D Range}}$ and scaled in the range $[-1, 1]$. The bottom three rows show example changes in tuning functions for three units with preferred directions drawn as the light green points on the heat maps.

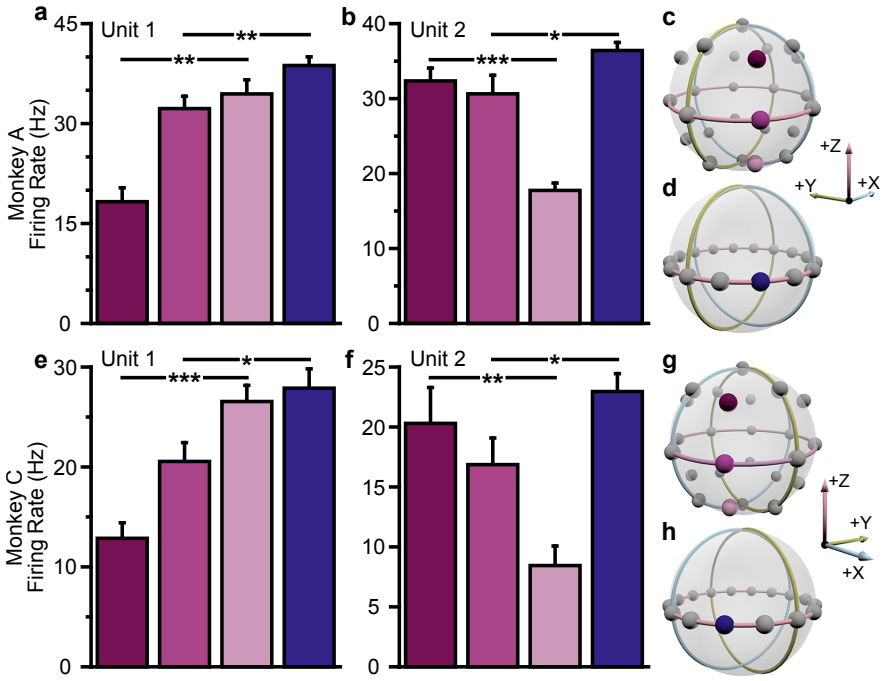

Figure 3.13: Evidence for dynamic range adaptation. (**a,b**) Firing rates from Monkey A for the units from Figure 3.3a,b. Both units have an azimuthal PD near $-135°$. The first three bars show the firing rates in the 3D context for the target that lay at $-135°$ on the xy-plane (pink) and the two targets immediately above (dark pink), and below (light pink) that target (**c**). The firing rate in the 2D context to the target at $-135°$ is shown in the fourth bar (**d**). Unit 1 had a preferred direction below the xy-plane ($U_{1;Z} = 61$, $^{**}P = 0.001$). Unit 2 had a preferred direction above the xy-plane ($U_{2;Z} = 154$, $^{***}P < 10^{-3}$). Despite this difference, both units showed an increased firing rate to the planar target in the 2D context compared to the 3D context ($U_{1;2D,3D} = 114$, $^{**}P = 0.0098$, $U_{2;2D,3D} = 126$, $^{*}P = 0.0299$). A similar set of plots for the units from Monkey C shown in Figure 3.3d,e are shown in (**e,f**). The corresponding targets are shown in (**g,h**). Both units had an azimuthal PD near $-45°$. Unit 1 had a preferred direction below the xy-plane ($U_{1;Z} = 69$, $^{***}P < 10^{-3}$). Unit 2 had a preferred direction above the xy-plane ($U_{2;Z} = 164$, $^{**}P = 0.0028$). Despite this difference, both units showed an increased firing rate to the planar target in the 2D context compared to the 3D context ($U_{1;2D,3D} = 89$, $^{*}P = 0.0165$, $U_{2;2D,3D} = 95$, $^{*}P = 0.0374$). The firing rates are plotted as the mean $\pm$ s.e.m. (U, Mann-Whitney U tests, n_{2D} and n_{3D} trials are the same from Figure 3.3a,b,d,e.)

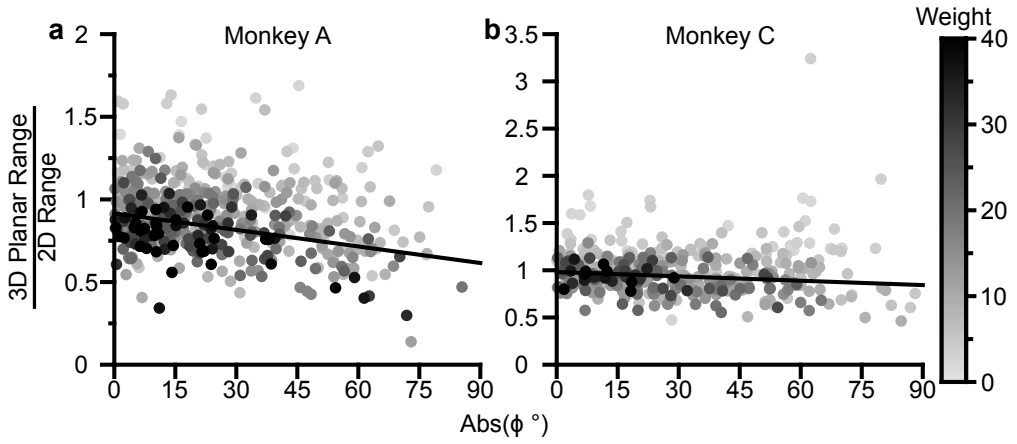

Figure 3.14: Firing rate changes vary with elevation angle. Dose-response effects in the tuning changes are shown for Monkey A (**a**) and Monkey C (**b**). The ratio of 3D planar to 2D dynamic ranges are plotted against the absolute value of the elevation angle (ϕ) of the PD vectors. The weighted linear fits for the data points are shown in black. The fits have negative slopes. $b_A = -0.0033$, $F_A = 53.9$, $P < 10^{-12}$, $n_A = 471$, $b_C = -0.0015$, $F_C = 10.6$, $P = 0.00125$, $n_C = 409$. b, slope, F, F-test versus constant model, n, number of analyzed units. The darkness of the points correspond to the weights used for the linear fits with the legend shown to the right. To provide contrast, the upper threshold of colormap for the weights was set at 40. The tuning curves for the two points that lie significantly off the trend line in (**b**) are shown in Figure 3.16.

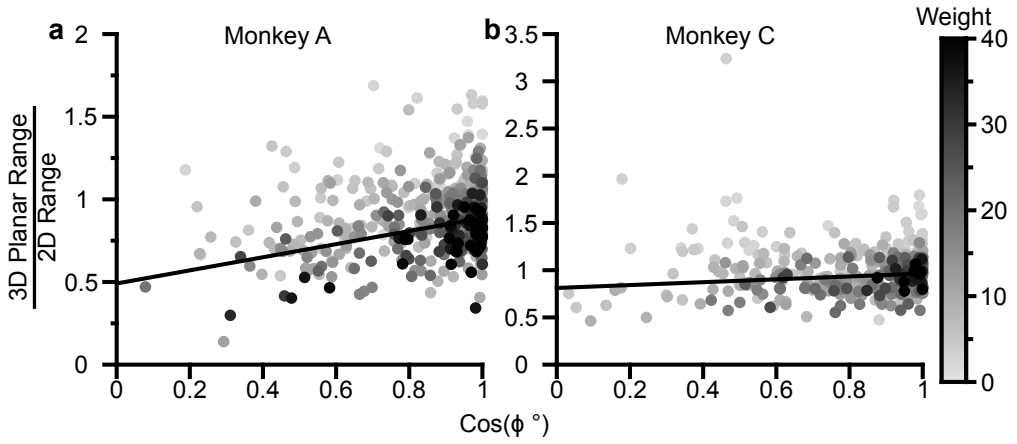

Figure 3.15: Firing rate changes vary with cosine of elevation angle. Dose-response effects in the tuning changes are shown for Monkey A (**a**) and Monkey C (**b**). The ratio of 3D planar to 2D dynamic ranges are plotted against the cosine of the elevation angle (ϕ) of the PD vectors. The weighted linear fits for the data points are shown in black. The fits have positive slopes. $b_A = 0.397$, $F_A = 63.6$, $P < 10^{-13}$, $n_A = 471$, $b_C = 0.152$, $F_C = 8.92$, $P = 0.00299$, $n_C = 409$. b, slope, F, F-test versus constant model, n, number of analyzed units. The darkness of the points correspond to the weights used for the linear fits with the legend shown to the right. To provide contrast, the upper threshold of colormap for the weights was set at 40. The tuning curves for the two points that lie significantly off the trend line in (**h**) are shown in SI Figure 3.16.

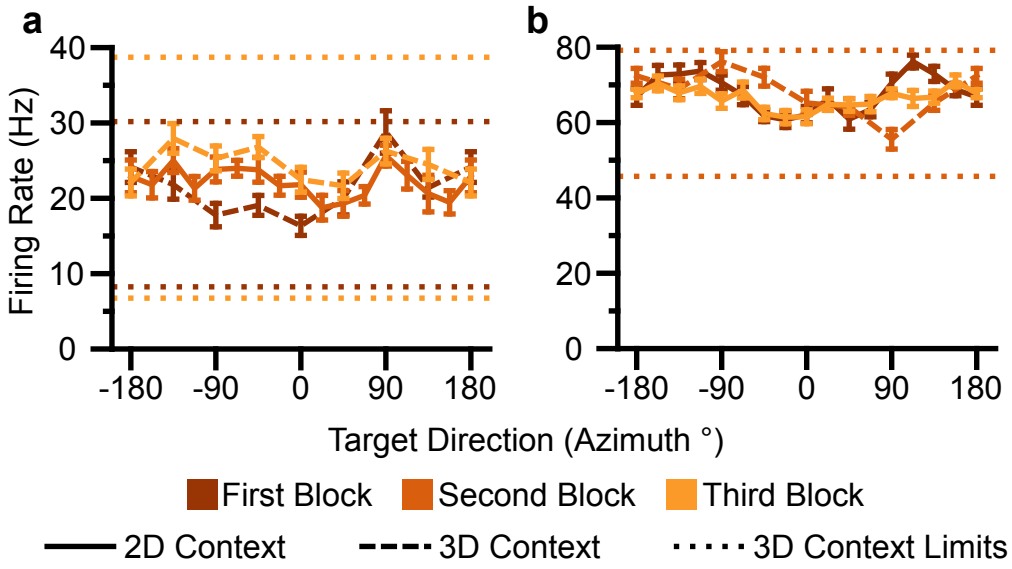

Figure 3.16: Outlier units from dose-response analysis. The plots show the tuning curves for the targets lying on the xy-plane in the 2D (solid line) and 3D (dashed line) contexts. The firing rates are shown as the mean $\pm$ s.e.m. The minimum and maximum average firing rates amongst the set of all 26 targets from the 3D context are drawn as the dotted horizontal lines. The tuning curves and the minimum and maximum lines are colored (dark to light orange) according to the block order of the data (first to third block). The tuning curves show a noisy response to targets in the xy-plane with decreased estimated ranges in the 2D context.

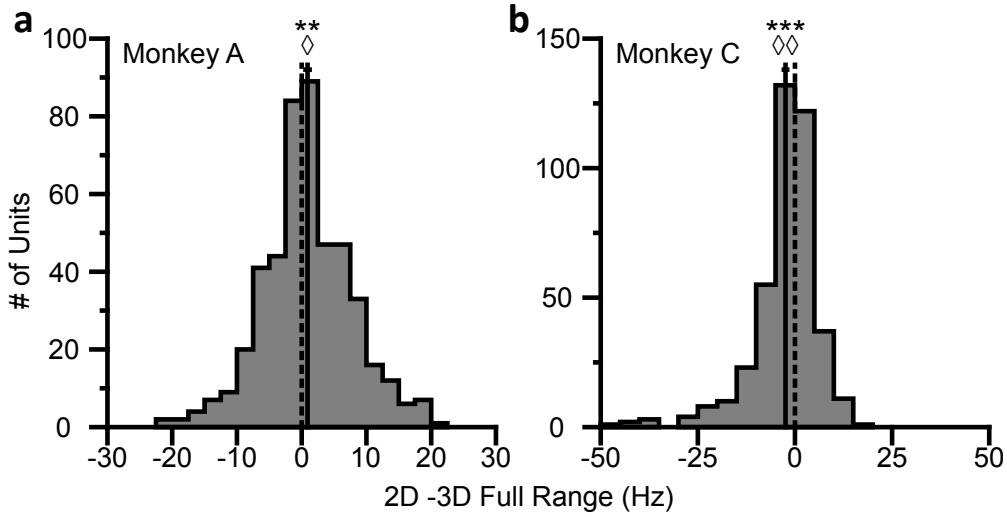

Figure 3.17: Histograms of the differences in full tuning ranges between the 2D and 3D context for Monkey A (**a**) and Monkey C (**b**). Full tuning ranges were calculated from the full set of 26 targets for the 3D context and from the full set of 16 targets for the 2D context. For both panels: solid vertical lines, means of distributions; solid horizontal lines, mean ± s.e.m.; dashed vertical lines, point of equality between the two tuning ranges. $W_A = 63402$, $^{**}P = 0.0081$, $S_A = 258$, $\lozenge P = 0.0426$, $n_A = 471$, $W_C = 31208$, $^{***}P < 10^{-5}$, $S_C = 171$, $\lozenge\lozenge P = 0.0011$, $n_C = 409$. W, Wilcoxon signed-rank tests, S, sign tests, n, number of analyzed units.

principal angle between the manifolds in comparison to the bootstrapped distributions from within each context (Figure 3.18c,f). The average principal angle between manifolds from the different contexts was greater than the principal angle within each context. Although the difference was small, it was significant over the many bootstrap samples. The results were the same when analyzing the minimum principal angle between manifolds (Figure 3.21). These results add more evidence to the hypothesis that the population utilized distinct patterns of activity between the 3D and 2D contexts.

3.4 DISCUSSION

Neurons in sensory areas encode and transmit information about the external environment[6]. Sensory neurons also undergo dynamic range adaptation with contextual changes in the environment[72, 17]. It has been suggested that dynamic range adaptation allows neurons to optimize their encoding of information[97, 7].

In our study, M1 neurons demonstrate significant changes in their firing rates to identical targets, when the task context switches from 3D to 2D. These changes are widespread across the recorded population. The observed changes are not consistent with a re-aiming strategy during the 2D context. Furthermore, the observed changes are not consistent with changes in intended speed between the two contexts. Instead, the observed changes appear to be consistent with dynamic range adaptation.

During the 2D context, the z-dimension gets added to the task-irrelevant null space. Without the observed adaptation, the portion of the dynamic range encoding the z-dimension during the 3D context would not be utilized during the 2D context. Our results showed that units begin to utilize that portion of the dynamic range to encode targets in the xy-plane as the task context switches from 3D to 2D. These results are markedly similar to the dynamic range adaptations that occur in sensory regions. Just as neurons in the retina and visual cortex adjust their tuning to encode the current range of light intensities, the recorded units adjusted their tuning to encode the current range of targets in the given context of the BCI task.

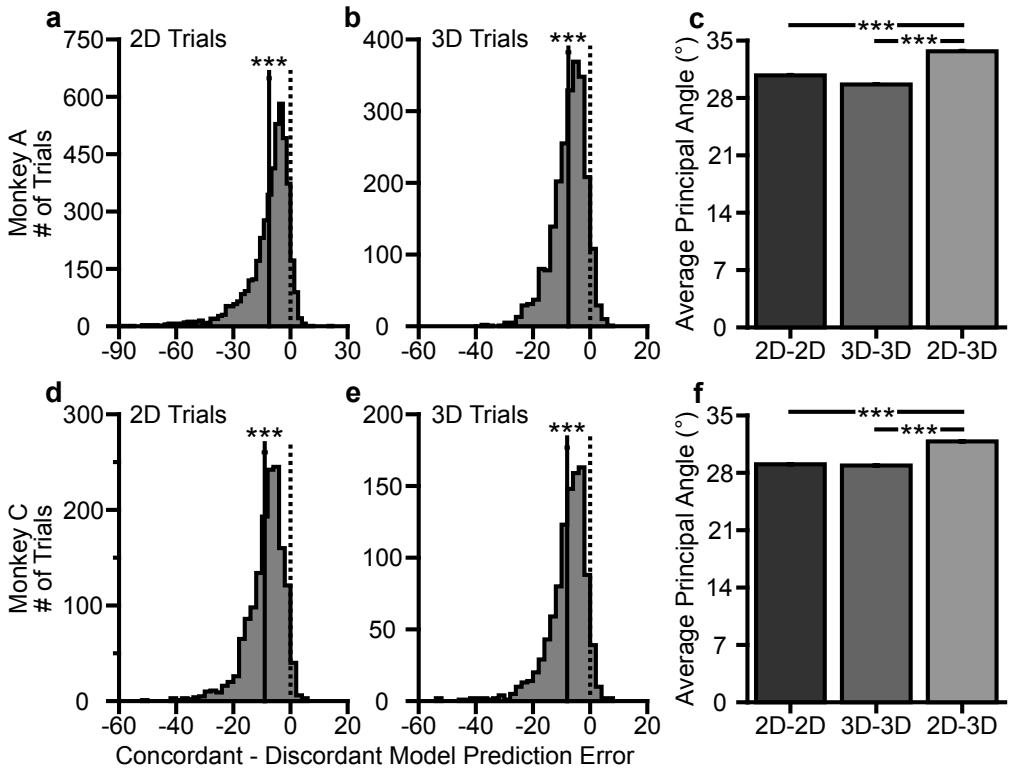

Figure 3.18: Changes in population structure for Monkey A (first row) and Monkey C (second row). (**a,b,d,e**) Histograms of the difference in prediction error between the concordant and discordant factor analysis models for the 2D trials (**a,d**) and 3D trials (**b,e**). For the four panels: solid vertical lines, means of distributions; solid horizontal lines, mean ± s.e.m.; dashed vertical lines, point of equality between the two prediction errors. $W_{A;2D} = 1.6 \times 10^5$, $^{***}P \ll 10^{-20}$, $n_{A;2D} = 4567$, $W_{A;3D} = 37257$, $^{***}P \ll 10^{-20}$, $n_{A;3D} = 2281$; $W_{C;2D} = 5050$, $^{***}P \ll 10^{-20}$, $n_{C;2D} = 1505$, $W_{C;3D} = 5809$, $^{***}P \ll 10^{-20}$, $n_{C;3D} = 1025$. W, Wilcoxon signed-rank tests, n, number of analyzed trials. (**c,f**) Average principal angles within the 2D (dark gray) and 3D (medium gray) intrinsic manifolds and between the 2D and 3D intrinsic manifolds (light gray). Data are plotted as mean ± s.e.m. of the average principal angles. $U_{A;2D} = 2.7 \times 10^8$, $^{***}P \ll 10^{-20}$, $U_{A;3D} = 2.5 \times 10^8$, $^{***}P \ll 10^{-20}$, $n_A = 1.8 \times 10^4$, $U_{C;2D} = 9.1 \times 10^7$, $^{***}P \ll 10^{-20}$ $U_{C;3D} = 9.1 \times 10^7$, $^{***}P \ll 10^{-20}$, $n_C = 1.1 \times 10^4$. U, Mann-Whitney U tests.

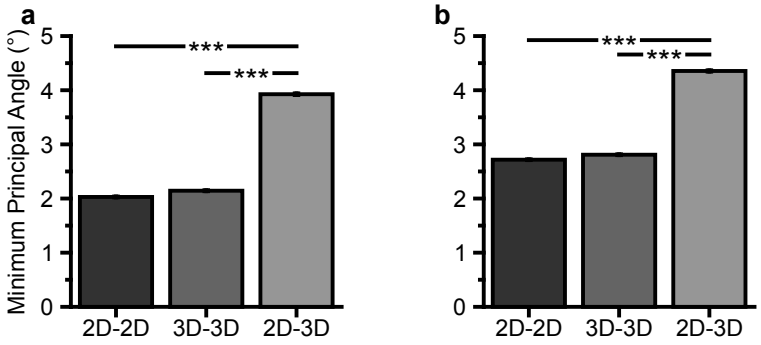

Figure 3.19: Minimum principal angles between intrinsic manifolds. The average minimum principal angle calculated between the 2D and 3D contexts are shown in light gray versus the distributions estimated within the 2D context (dark gray) and 3D context (gray) for Monkey A (**a**) and Monkey C (**b**). The between context principal angles are significantly greater than the estimated within context distributions for both monkeys (Wilcoxon rank sum, Monkey A: 2D $P \ll 10^{-20}$; 3D $P \ll 10^{-20}$, Monkey C: 2D $P \ll 10^{-20}$; 3D $P \ll 10^{-20}$).

Researchers have described dynamic range adaptation in sensory systems as functioning to optimize information throughput of the neural populations[7, 24, 97]. Because the recorded populations directly controlled cursor movement and we limited our analyses to successful trials, there was no measurable difference in the information transmitted by the population between the two contexts for the set of identical targets. However, when we estimated the information transmitted by individual units, we found that the information transmission increased from the 3D context to the 2D context (Figure 3.22). This trend was significant for Monkey A but not significant for Monkey C. This trend is due to the fact that increases in the tuning range increase the information transmission of the units[68, 8]. This may also be visualized by the increased slope of the tuning curves when plotting the firing rates against the cosine of the difference between the target direction and preferred direction for the planar targets (Figure 3.23). Just as the slopes of tuning curves in the visual system increase to transmit more information about a more narrow range of light intensities, the slopes of the tuning curves of the M1 units increase to transmit more information about a

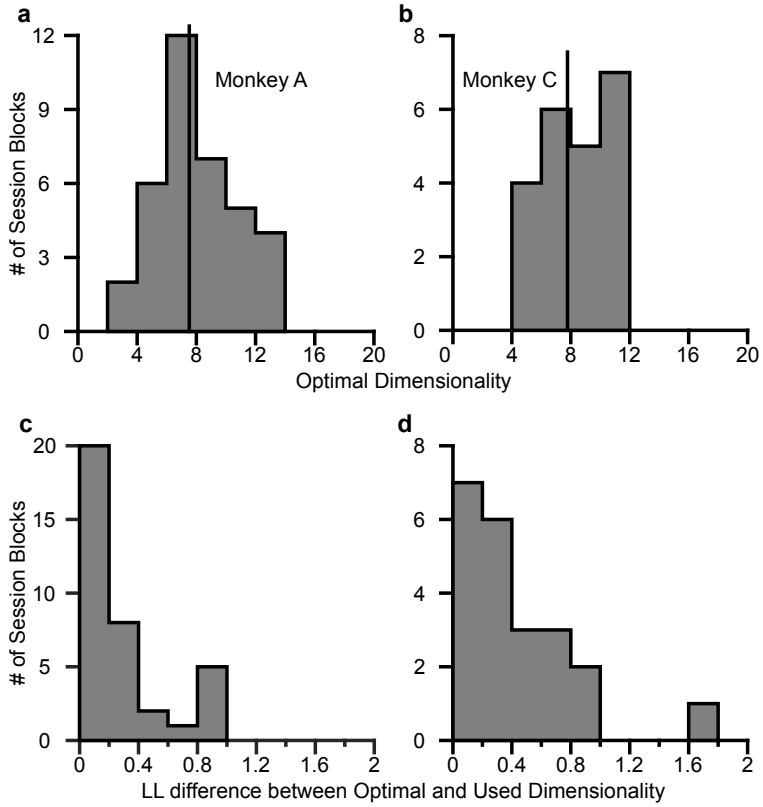

Figure 3.20: Selection of factor analysis models for non-overlapping target set. (**a,b**) Optimal factor analysis dimensionality from 4-fold cross validation analysis for Monkey A (left) and Monkey C (right). We analyzed the square-root transformed time-averaged responses to the sets of unique targets in each context (2D: 8 unique targets; 3D: 18 unique targets). For each session and each context, we split the data into four equal folds. For each fold and for each candidate dimensionality from 1 to the population size, factor analysis models were created from 75% of the data. The models were used to calculate the log-likelihood of the remaining 25% of the data. The optimal dimensionality was taken as the candidate dimensionality the maximized the log-likelihood averaged across the four folds. The mean optimal dimensionality across the contexts and sessions was 7.64 for Monkey A and 7.86 from Monkey C (**c,d**) Differences in the log-likelihood of the data at the used dimensionality (8D) and at the optimal dimensionality for each context of each session. The units are the number of standard errors of log-likelihood for the optimal dimensionality model.

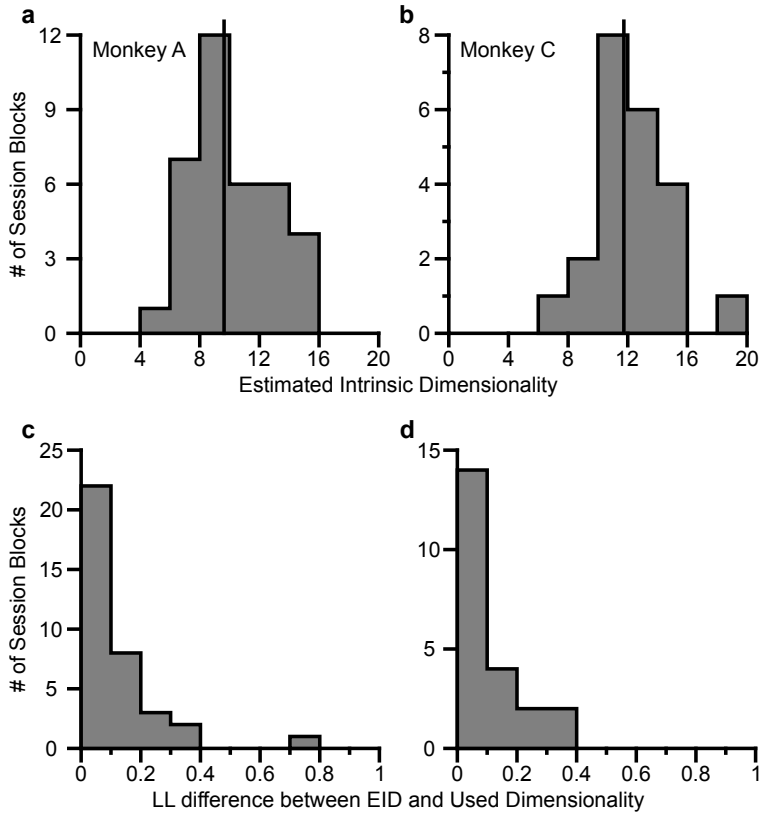

Figure 3.21: Properties of the intrinsic manifold. (**a,b**) Estimated intrinsic dimensionality (EID) from 4-fold cross validation analysis for Monkey A (left) and Monkey C (right). For each session and task context, the square-root transformed 40 ms spike bin data was split into four equal folds. For each fold and for each candidate dimensionality from 1 to the population size, factor analysis models were created from 75% of the data. The models were used to calculate the log-likelihood of the remaining 25% of the data. The estimated intrinsic dimensionality was taken as the candidate dimensionality the maximized the log-likelihood averaged across the four folds. The mean EID across the contexts and sessions was 9.75 for Monkey A and 11.86 from Monkey C (**c,d**) Differences in the log-likelihood of the data at the used dimensionality (Monkey A: 10D; Monkey C: 12D) and at the estimated intrinsic dimensionality for each context of each session. The units are the number of standard errors of log-likelihood for the EID model.

more narrow range of target directions. It is possible that this phenomenon is limited to isometric tasks such as that studied by Hepp-Reymond, et al[39]. The arms of the monkeys were loosely restrained during the BCI task. Initial, preliminary studies of a reaching version of the same task did not show the same effect as in the BCI version.

Overall, M1 populations exhibited distinct patterns of activity to optimally encode task-relevant information under changing contexts. The populations changed their correlation structure as the task context switched. These changes in the correlation structure, or manifold[82], suggest that the dynamic range adaptation of units in the motor cortex might reflect independent processes at the level of individual neurons. Both monkeys were proficient at both 2D and 3D BCI control prior to this combined study, although Monkey C was less experienced with the 3D context. Because of this we did not observe the time-course of the adaptation process[97]. Nonetheless, the changes in the tuning ranges occurred as fast as could be measured. Future studies could measure the time-course of the adaptation in naive monkeys across multiple recording sessions. It is possible that the dynamic range utilized during BCI control could become a metric of BCI learning.

The results found in this work support the hypothesis that neurons in M1 serve to efficiently transmit contextually encoded information. Motor learning in dynamic environments can be viewed as learning efficient ways to encode information. Changes in the environmental context, such as tool use, can lead to changes in the association between M1 activity and motor output[77]. Even during typical reaches in a static environment, M1 neurons efficiently encode information about the task. The common linear tuning function[33] maximizes the output entropy for a uniform distribution of target directions in a 3D environment. This "histogram equalization" maximizes the information transmission in the low noise limit[58, 68]. In our studies, the units in M1 have limited dynamic ranges with which to encode cursor movement under the different contexts. Rather than using a subset of the available tuning ranges, the population adaptively displays new coding schemes that more fully utilize the ranges of the units comprising the population. This adaptive response of the M1 population allows for the efficient encoding of task relevant information in changing environments.

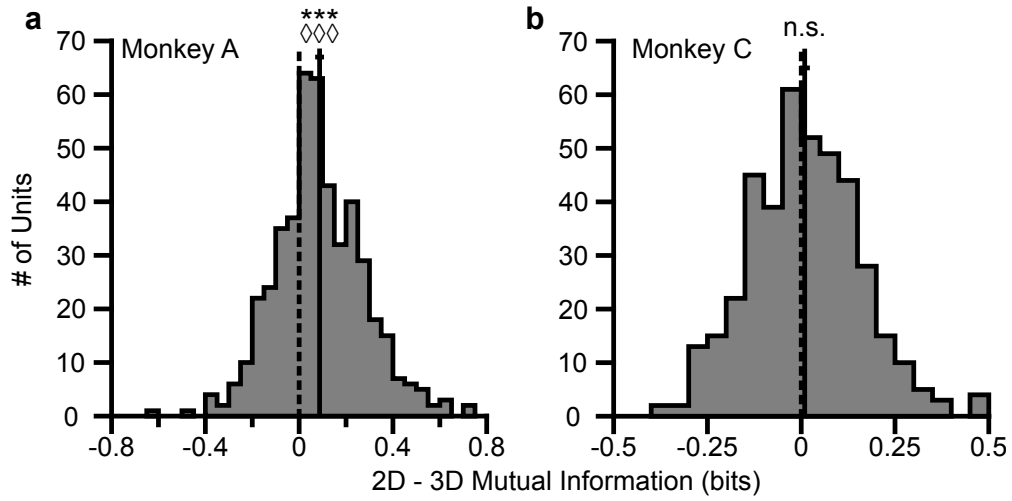

Figure 3.22: Change in mutual information between contexts for Monkey A (**a**) and Monkey C (**b**). The plots show the histograms of the difference between the mutual information estimated from the set of common targets in the 2D context and that from the common targets in the 3D context. For both panels: solid vertical lines, means of distributions; solid horizontal lines, mean ± s.e.m.; dashed vertical lines, point of equality between the two estimates of mutual information. $W_A = 82811$, $^{***}P < 10^{-19}$, $S_A = 329$, $\lozenge\lozenge\lozenge P < 10^{-16}$, $n_A = 471$, $W_C = 44354$, n.s. $P = 0.3094$, $S_C = 210$, n.s. $P = 0.621$, $n_C = 409$. W, Wilcoxon signed-rank tests, S, sign tests, n, number of analyzed units.

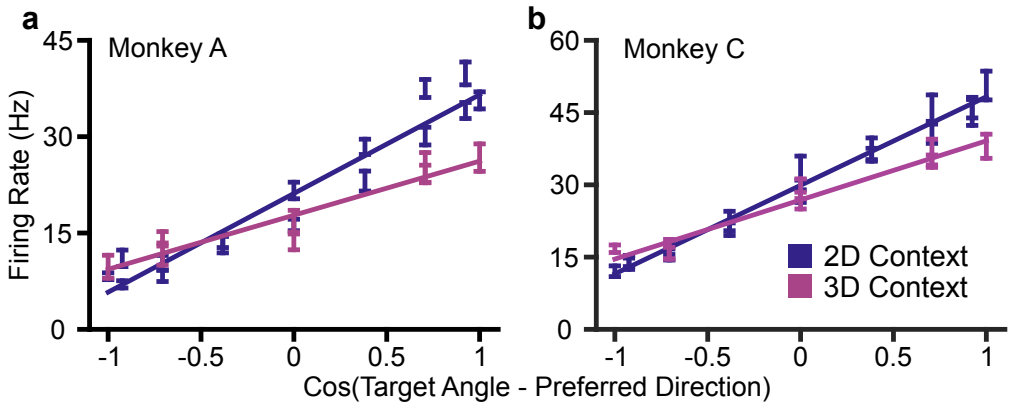

Figure 3.23: Slopes of tuning curves increase for the 2D context compared to the 3D context. (**a**) The plots show selected tuning curves from Monkey A (**a**) and Monkey C (**b**). The units are identical to those shown previously in Figure 3.3c,f. For each plot, the preferred direction was estimated as the target direction for the greatest average firing rate during the 3D context, amongst the set of planar targets. The fit lines were calculated from ordinary linear regression on all the trial data processed in a similar manner. The data points show the trial-averaged firing rates ± s.e.m. The number of trials per target is identical to that in Figure 3.3c,f. Because of the symmetry of the cosine function, the data for distinct targets that are mirrored across the preferred direction are plotted separately at the same point along the abscissa.

4.0 GENERAL DISCUSSION

4.1 INFORMATION IN THE MOTOR CORTEX

In Chapter 2, I formulated a unique method to compute the information transmitted about a movement task by a neural population. I used this method to estimate the information transmitted about a center-out arm-reaching task by a motor cortical population. Lastly, I estimated the information for varying sizes of target sets in both two- and three-dimensional reaching tasks.

In an information theoretic framework, increasing the size of the target set had the effect of increasing the stimulus information. As the information of the stimulus increased, the mutual information between the stimulus and the neural response (i.e., the information transmitted by the population about the task) increased. However, as the information of the stimulus continued to increase, the information transmitted by the population about the task began to reach a limit. For example, when the stimulus information was near 4.5 bits (22 distinct targets) a population from Monkey N was only capable of transmitting around 3.5 bits (11 distinct levels). These findings are in agreement with similar findings in sensory neurons by Werner and Mountcastle[100] and in mental judgements as reviewed by Miller[64]. As Miller famously wrote, the nervous system making judgements on input stimuli reached a limit of transmitting around 7 distinct levels.

It is important to note that these limits are not the equivalent of Shannon's "channel capacity" for the neural population. The channel capacity is computed across the range of possible stimulus distributions. In my study, as well as the early studies mentioned above, the information was always measured with a uniform stimulus distribution. Although the number of stimulus levels or targets changed across measurements, each was equally probable

for a given measurement. The change in the number of stimulus levels represented a change in the information channel itself. Instead of representing channel capacity, the limits represent a limit in the number of discretized, equally likely stimuli a neural population is capable of encoding within a closed range of stimulus values.

This raises the question of why these limits exist. They may be related to the noise in the neural response. Although the firing-rate response of the population varies with the distinct targets[33, 34, 50, 85], or movement directions, there is still noise in the neural response[25]. This noise may be due to multiple different factors including imperfections in the recording system and sorting parameters as well as the stochastic nature of neural firing. As more stimuli are added within the closed range of stimulus values, the stimuli themselves are crowded closer together. Similarly, the varying responses of the population to the set of stimuli also becomes crowded closer together. The responses are bound by the physiological ranges of possible firing rates. As a result of the nearly steady range in noise, the closer values in the firing rates responses become less distinguishable. Eventually, with a large enough stimulus set, the population response can provide no more information with the addition of more stimuli to the set.

It may seem counterintuitive that the limit in the information transmitted by the population is reached when the information of the stimulus set is much greater than the limit. In other words, in the plots showing the estimate of mutual information against the stimulus information, the mutual information does not abruptly diverge from the unity line and immediately plateau. Instead, the mutual information gradually diverges from the unity line before eventually reaching a plateau. This is due to the fact that the value of the mutual information represents the upper limit on the amount of information that can be decoded from the population response. Mutual information considers the probabilistic nature of the population responses to the target stimuli. Instead of considering only whether the decoded stimulus is correct or not, the mutual information considers the probability that each stimulus in the set was the original input stimulus. For example, the population from Monkey N during one recording session reached a limit of around 3.5 bits of information (11 distinct levels) when the input stimulus information was near 4.5 bits (22 distinct levels). However, when the input stimulus information is near the limit of 3.5 bits, the information transmitted

by the population is only around 3.2 bits (9 distinct levels). In other words, because of the noise in the population, no decoder may be 100% perfect with an 11 target task even though the population can transmit 11 targets worth of information during a 22 target task.

Another finding from the study was that when the size of the population increased, the limit on the information transmitted by the population increases. This is due to the fact that the additional units in the population provide additional coding range with which to transmit information about the movement direction. However, using the method I developed for estimating the information, it appears that this increase in information also approaches a limit. In other words, an infinitely large population would not be able to transmit all the information contained in a large target set. This may be explained by the correlated nature of the neural encoding. Under a cosine-tuning model, the upper limit on the entropy of large, noiseless neural populations increases minimally with additional neurons in the population.

This result was found by calculating the upper limit of entropy for simulated noiseless populations of between 200 and 50000 cosine-tuned neurons, in steps of 100. Initially, 50000 random preferred directions were generated from a uniform circular distribution. Each neuron was assumed to have a modulation depth of 16 Hz. To center the responses, the baseline firing rates of the units were all set to zero. The firing rates of the population were then calculated in response to 1000 unique targets uniformly dispersed on the unit circle. For a population of n neurons, the response to the uniformly distributed 2D targets forms a 2D ellipse in an n-dimensional space. For each population size, I found the plane occupied by the ellipse using three points randomly selected from the population responses. I then projected the ellipse into the 2D plane. If the targets are distributed as a uniform circular distribution, then the population responses would be uniformly distributed along the ellipse. Thus, the entropy of the population response would be equal to the logarithm of the circumference of the ellipse.

I calculated he upper limit of the noiseless population entropy, $H(X)$, from the upper limit for the circumference of an ellipse:

$$H(X) \leq \log(2\pi a) \tag{4.1}$$

where a is half of the length of the major axis of the ellipse. This value was estimated as the distance from the origin to the point farthest from the origin. The upper limit of the population entropy is plotted against the population size in Figure 4.1. This curve is well fit by a power law, $y = ax^b + c$, where x is the population size, y is the upper limit of the entropy, and a, b, and c are regression constants. The fit power law for the curve shown in Figure 4.1 has regression constants ($\pm 95\%$ confidence interval) of $a = 364 \pm 91$, $b = 0.0019 \pm 0.0005$, $c = -358 \pm 91$ bits. Doubling the average modulation depth of the population has the effect of raising the curve by one bit.

Notably, the fit exponent, b in the power law is positive, meaning that the curve does not approach an asymptote. Nonetheless, the value is close to zero and, as can be seen in Figure 4.1, the upper limit of the population entropy increases very gradually for large populations. It is important to note that the noiseless population entropy is not equal to the mutual information between the population response and target stimuli. In a noisy population, where the noise is additive and independent, the population response may be considered as the sum of random variables, $R = X + E$, where X is again the noiseless population response and E is the noise. Subsequently, the mutual information may be rewritten as:

$$\begin{aligned} I(R;S) &= H(R) + H(R|S) \\ &= H(X+E) + H(E) \\ &= H(X) - H(E|X+E) \end{aligned} \tag{4.2}$$

However, the upper limit of the noiseless population entropy does not also form an upper limit of the mutual information. This is due to the fact that entropy for continuous variables may be negative. In other words, the entropy of the noise conditioned on the noisy response could be negative which would cause the mutual information to be greater than the noiseless population entropy. In fact, if there was zero noise, the conditional entropy would be negative infinity. Thus, the mutual information would be infinite, meaning that an infinite number of unique targets could be decoded from the population response.

The findings from this work suggest that the conditional entropy, $H(E|X+E)$, is not only positive but also increases with population size, assuming the noise is additive and

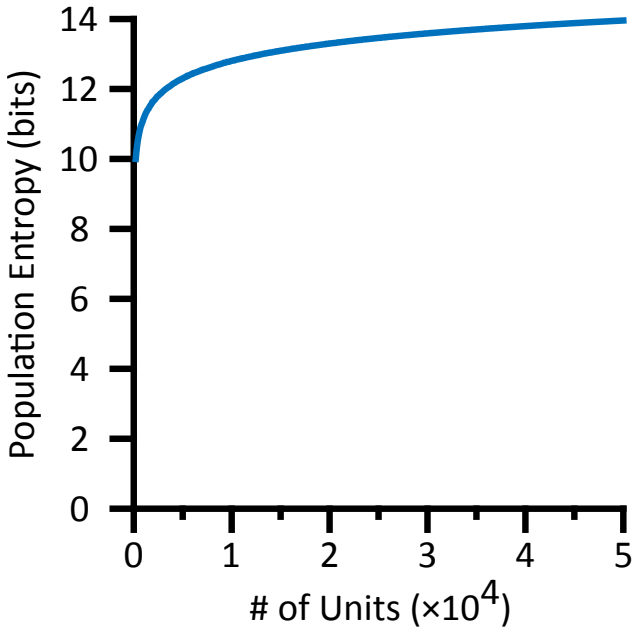

Figure 4.1: Population entropy versus population size. The blue curve shows the calculated upper limit for the entropy of the simulated neural population. The neurons were simulated in a 2D task with cosine tuning and modulation depths of 16 Hz. The preferred directions of the neurons were randomly drawn from a uniform circular distribution.

independent. This increase would explain the observation of an asymptote of the mutual information with increasing population size. Nonetheless, it is also possible that the modeled dimensionality of eight factors may be poorly-suited for extrapolating results beyond the recorded population size.

A third striking finding from the study was that when the task context switched from 2D to 3D, the limit on information transmitted by the population with increasing stimulus information increased. The populations were capable of transmitting more information in the 3D than the 2D context. A likely explanation for this difference is the relationship amongst information transmission, signal, and noise. The information transmitted increases when the signal increases and the information transmitted increases when the noise decreases. In the case of the switch in context from 2D to 3D, both likely occurred.

First, the noise likely decreases as the context changes from 2D to 3D. Noise can be considered as all information that is not related to the signal. During the 2D task, the signal only related to the movements in the xy-plane. However, during the 3D task, the signal also related to the movements in the z-dimensions. During the 2D task, the monkeys' arms were not constrained to stay within the xy-plane. Subsequently, movements in the z-dimension during the 2D context created noise for the estimation of information transmission. However, during the 3D context, the movement in the z-dimension is no longer part of the noise in the system.

This change in noise between two contexts directly translates to a second point. What was once noise in the 2D context becomes the signal in the 3D context. In the classic linear tuning model, the modulation depth of a neuron in a 2D context is a fraction of the modulation depth in the 3D context. This fraction is equal to the cosine of the angle, ϕ, between the neuron's preferred direction vector and the xy-plane. This increase in modulation depth is the equivalent of an increase in the signal for information transmission. The greater range in tuning allows for more information to be transmitted by each neuron in the population. This result raises the question of how rigidly constrained are the tuning ranges of neurons when the task context changes.

4.2 ADAPTATION IN BRAIN-COMPUTER INTERFACES

In Chapter 3, I found that units recorded from primary motor cortex undergo dynamic range adaptation when context changes in a BCI task. As the task context changes from 3D to 2D, the tuning range to identical targets in the xy-plane increases. These results demonstrate that the tuning ranges are not rigidly constrained during changes in task context and suggest that the portion of the tuning range that encodes the z-dimension during the 3D context becomes utilized in the 2D context to encode the targets in the xy-plane. By leveraging the simultaneous nature of the recordings, I was able to test a number of hypotheses about the mechanisms that might explain these results. I concluded that the observed changes are a motor system analogue to the phenomenon of dynamic range adaptation observed throughout various sensory systems.

A striking finding from this work is that the units in the population appear to change their correlation structure as each unit individually adapts its dynamic range. In other words, during the 2D context, the units are not constrained by the inter-unit dynamics observed during the 3D task. Considering the tuning functions of the units as scaled vectors in a 3D space, each vector rotates independently down into the xy-plane. The vectors do not rotate together as a whole, maintaining their respective angles from one-another. Although this process of independent rotation of the vectors was not complete for all units in both monkeys, the results suggest that this was the nature of the observed changes in tuning between contexts.

These results have interesting implications for brain-computer interface work. The work demonstrates that the units controlling a BCI task are capable of adapting their tuning functions to changes in the task. They allocate tuning range to the features that need to be encoded for task success. This result implies that the units are limited only by their maximum tuning range available to encode information. It is perhaps unsurprising, in light of these results, that many studies have found that the tuning ranges observed during BCI tasks are greater than the ranges of the same units observed during arm reaches. During the arm reaches, the units may also be encoding features of arm movements other than purely direction. However, during BCI control, those other features are irrelevant to successful

completion of the task. They are the "null-space" of the BCI task. Subsequently, the units allocate the portion of their tuning range that encoded those features during arm movements to encoding only the task-relevant features for BCI control.

The ability of the population to change its correlation structure may also be useful for BCI research. Sadtler, et al. demonstrated that BCI mappings outside of a population's intrinsic manifold could be learned, although with greater difficulty[82]. Taken together, these studies show that neural populations are not constrained by their initially observed correlation structure. Instead, the populations may adapt or learn new dynamics to increase performance and information throughput. It is possible that the population structure may adapt so as to break past the informational asymptote for large populations found in the arm reaching study.

This work also supports the hypothesis that motor cortex functions to transmit contextually encoded information about desired movement output. It demonstrates that the motor cortex can function similar to visual and other sensory areas, adjusting the tuning properties of neurons to adapt to changes in the distribution of stimuli needing to be encoded. Unlike the sensory areas, those stimuli for motor cortex are desired output movements. This capability raises the interesting questions of the role it plays in actual limb movements in dynamic environments as well as the mechanisms that facilitate the process of dynamic range adaptation in motor control.

4.3 FUTURE DIRECTIONS

This work detailed a unique method for estimating the information transmitted by a neural population despite a limited number of trials per stimulus condition. This method provides a strong foundation for future studies on information transmission in the motor cortex and other brain areas. Further work utilizing this method could help answer some of the questions raised by this work. One such question is the accuracy of the factor analysis model for populations larger than those measured in these studies. Although this would require many more trials per stimulus condition, such a study would be useful in determining the accuracy

of the asymptote of information transmission for large populations extrapolated from this work.

A second question that could be answered with the information estimation method is how the information transmission of neural populations changes with increases in task dimensionality beyond three-dimensional arm movements. Unfortunately, due to training difficulties, this study was unable to investigate an extension of the task design into four dimensional movements. However, with further training, such a study as well as further extensions to higher dimensional movements should be feasible. Results from these studies could reveal whether another asymptotic limit of information transmission is approached as the task dimensionality increases. The results from the BCI studies suggest that such a limit exists as a function of the dynamic ranges of the units comprising the population.

The results from the BCI studies also raise novel research opportunities. There is the possibility that the dynamic range adaptation is a learned phenomenon. Although the changes in tuning range were observed as rapidly as could be measured, both monkeys had prior experience controlling a BCI in each task context, although not in the same recording session. Repeating this study in monkeys that are naive to the BCI task in the 2D context could reveal whether the dynamic range adaptation is truly immediate or requires more long-term learning of the new output movement statistics. If the adaptation is a learned phenomenon, the study could be combined with unit tracking across days to measure the learning process of dynamic range adaptation. In fact, this result could be broadly applied to the studying learning in BCI tasks as the dynamic range utilized by units during the task becomes a measure of the learning process.

The ability of the populations in M1 to undergo dynamic range adaptation raises the question of how much of a role it plays in motor control. It is possible that the tuning functions observed in research studies are adaptations to the distributions of targets studied in the task. In fact, for single neurons, the cosine tuning model is the optimal encoder of movement directions uniformly distributed in 3D space. This work highlights the ability of the motor cortex to contextually encode information. It opens up opportunities to further explore this ability and the role it plays in controlling movements in dynamic environments.

BIBLIOGRAPHY

[1] L. F. Abbott, E. T. Rolls, and M. J. Tovee. Representational capacity of face coding in monkeys. *Cereb Cortex*, 6(3):498–505, 1996.

[2] J. Accot and S. Zhai. Beyond Fitts' law: models for trajectory-based HCI tasks. In *Proceedings of the ACM SIGCHI Conference on Human factors in computing systems*, pages 295–302. ACM, 1997.

[3] J. Accot and S. Zhai. More than dotting the i's—foundations for crossing-based interfaces. In *Proceedings of the SIGCHI conference on Human factors in computing systems*, pages 73–80. ACM, 2002.

[4] J. G. Beebe-Center, M. Rogers, and D. O'connell. Transmission of information about sucrose and saline solutions through the sense of taste. *The Journal of Psychology*, 39(1):157–160, 1955.

[5] A. Bjorck and G. H. Golub. Numerical methods for computing angles between linear subspaces. *Math Comput*, 27(123):579–594, 1973.

[6] A. Borst and F. E. Theunissen. Information theory and neural coding. *Nat Neurosci*, 2(11):947–57, 1999.

[7] N. Brenner, W. Bialek, and R. de Ruyter van Steveninck. Adaptive rescaling maximizes information transmission. *Neuron*, 26(3):695–702, 2000.

[8] N. Brunel and J.-P. Nadal. Mutual information, fisher information, and population coding. *Neural Computation*, 10(7):1731–1757, 1998.

[9] S. M. Chase, R. E. Kass, and A. B. Schwartz. Behavioral and neural correlates of visuomotor adaptation observed through a brain-computer interface in primary motor cortex. *J Neurophysiol*, 108(2):624–44, 2012.

[10] S. M. Chase, A. B. Schwartz, and R. E. Kass. Bias, optimal linear estimation, and the differences between open-loop simulation and closed-loop performance of spiking-based brain-computer interface algorithms. *Neural Networks*, 22(9):1203–13, 2009.

[11] A. Cherian, M. O. Krucoff, and L. E. Miller. Motor cortical prediction of EMG: evidence that a kinetic brain-machine interface may be robust across altered movement dynamics. *J Neurophysiol*, 106(2):564–75, 2011.

[12] M. M. Churchland, J. P. Cunningham, M. T. Kaufman, J. D. Foster, P. Nuyujukian, S. I. Ryu, and K. V. Shenoy. Neural population dynamics during reaching. *Nature*, 487(7405):51–6, 2012.

[13] S. T. Clanton, A. J. McMorland, Z. Zohny, S. M. Jeffries, R. G. Rasmussen, S. N. Flesher, and M. Velliste. *Seven Degree of Freedom Cortical Control of a Robotic Arm*, pages 73–81. Springer, 2013.

[14] J. L. Collinger, B. Wodlinger, J. E. Downey, W. Wang, E. C. Tyler-Kabara, D. J. Weber, A. J. McMorland, M. Velliste, M. L. Boninger, and A. B. Schwartz. High-performance neuroprosthetic control by an individual with tetraplegia. *Lancet*, 381(9866):557–64, 2013.

[15] E. R. F. W. Crossman. Entropy and choice time: The effect of frequency unbalance on choice-response. *Q J Exp Psychol*, 5:41–65, 1953.

[16] E. R. F. W. Crossman and P. J. Goodeve. Feedback control of hand-movement and fitts' law. *The Quarterly Journal of Experimental Psychology*, 35(2):251–278, 1983.

[17] I. Dean, N. S. Harper, and D. McAlpine. Neural population coding of sound level adapts to stimulus statistics. *Nat Neurosci*, 8(12):1684–9, 2005.

[18] A. P. Dempster, N. M. Laird, and D. B. Rubin. Maximum likelihood from incomplete data via EM algorithm. *J Roy Stat Soc B Met*, 39(1):1–38, 1977.

[19] R. P. Dum and P. L. Strick. Motor areas in the frontal lobe of the primate. *Physiol Behav*, 77(4-5):677–82, 2002.

[20] R. Eckhorn and B. Popel. Rigorous and extended application of information theory to the afferent visual system of the cat. I. Basic concepts. *Kybernetik*, 16(4):191–200, 1974.

[21] R. Eckhorn and B. Popel. Rigorous and extended application of information theory to the afferent visual system of the cat. II. Experimental results. *Biol Cybern*, 17(1):71–7, 1975.

[22] E. V. Evarts. Pyramidal tract activity associated with a conditioned hand movement in the monkey. *J Neurophysiol*, 29(6):1011–27, 1966.

[23] E. V. Evarts. Relation of pyramidal tract activity to force exerted during voluntary movement. *Journal of neurophysiology*, 31(1):14–27, 1968.

[24] A. L. Fairhall, G. D. Lewen, W. Bialek, and R. R. de Ruyter Van Steveninck. Efficiency and ambiguity in an adaptive neural code. *Nature*, 412(6849):787–92, 2001.

[25] A. A. Faisal, L. P. Selen, and D. M. Wolpert. Noise in the nervous system. *Nat Rev Neurosci*, 9(4):292–303, 2008.

[26] L. Faivishevsky and J. Goldberger. Dimensionality reduction based on non-parametric mutual information. *Neurocomputing*, 80(0):31–37, 2012.

[27] P. M. Fitts. The information capacity of the human motor system in controlling the amplitude of movement. *J Exp Psychol*, 47(6):381–91, 1954.

[28] P. M. Fitts and J. R. Peterson. Information capacity of discrete motor responses. *J Exp Psychol*, 67:103–12, 1964.

[29] D. Flament and J. Hore. Relations of motor cortex neural discharge to kinematics of passive and active elbow movements in the monkey. *J Neurophysiol*, 60(4):1268–84, 1988.

[30] W. R. Garner. An informational analysis of absolute judgments of loudness. *J Exp Psychol*, 46(5):373–80, 1953.

[31] W. R. Garner and H. W. Hake. The amount of information in absolute judgements. *Psychol Rev*, 58(6):446–59, 1951.

[32] A. P. Georgopoulos, J. Ashe, N. Smyrnis, and M. Taira. The motor cortex and the coding of force. *Science*, 256(5064):1692–5, 1992.

[33] A. P. Georgopoulos, J. F. Kalaska, R. Caminiti, and J. T. Massey. On the relations between the direction of two-dimensional arm movements and cell discharge in primate motor cortex. *J Neurosci*, 2(11):1527–37, 1982.

[34] A. P. Georgopoulos, R. E. Kettner, and A. B. Schwartz. Primate motor cortex and free arm movements to visual targets in three-dimensional space. II. Coding of the direction of movement by a neuronal population. *J Neurosci*, 8(8):2928–37, 1988.

[35] A. P. Georgopoulos and J. T. Massey. Cognitive spatial-motor processes. 2. Information transmitted by the direction of two-dimensional arm movements and by neuronal populations in primate motor cortex and area 5. *Exp Brain Res*, 69(2):315–26, 1988.

[36] S. Goldman. *Information theory*. Prentice-Hall electrical engineering series. Prentice-Hall, New York,, 1953.

[37] H. W. Hake and W. R. Garner. The effect of presenting various numbers of discrete steps on scale reading accuracy. *J Exp Psychol*, 42(5):358–66, 1951.

[38] R. V. L. Hartley. Transmission of information. *Bell System Technical Journal*, 7(3):535–563, 1928.

[39] M. Hepp-Reymond, M. Kirkpatrick-Tanner, L. Gabernet, H. X. Qi, and B. Weber. Context-dependent force coding in motor and premotor cortical areas. *Exp Brain Res*, 128(1-2):123–33, 1999.

[40] M. Hepp-Reymond, U. Wyss, and R. Anner. Neuronal coding of static force in the primate motor cortex. *Journal de physiologie*, 74(3):287, 1978.

[41] W. E. Hick. On the rate of gain of information. *Q J Exp Psychol*, 4:11–26, 1952.

[42] D. H. Howes and R. L. Solomon. Visual duration threshold as a function of word-probability. *J Exp Psychol*, 41(6):401–10, 1951.

[43] D. H. Hubel and T. N. Wiesel. Receptive fields, binocular interaction and functional architecture in the cat's visual cortex. *J Physiol*, 160:106–54, 1962.

[44] M. F. Huber, T. Bailey, H. Durrant-Whyte, and U. D. Hanebeck. On entropy approximation for gaussian mixture random vectors. In *Multisensor Fusion and Integration for Intelligent Systems, 2008. MFI 2008. IEEE International Conference on*, pages 181–188, 2008.

[45] G. W. Huntley and E. G. Jones. Relationship of intrinsic connections to forelimb movement representations in monkey motor cortex: a correlative anatomic and physiological study. *J Neurophysiol*, 66(2):390–413, 1991.

[46] R. A. Ince, R. Senatore, E. Arabzadeh, F. Montani, M. E. Diamond, and S. Panzeri. Information-theoretic methods for studying population codes. *Neural Networks*, 23(6):713–27, 2010.

[47] E. Jankowska, Y. Padel, and R. Tanaka. Projections of pyramidal tract cells to alpha-motoneurones innervating hind-limb muscles in the monkey. *J Physiol*, 249(3):637–67, 1975.

[48] B. Jarosiewicz, S. M. Chase, G. W. Fraser, M. Velliste, R. E. Kass, and A. B. Schwartz. Functional network reorganization during learning in a brain-computer interface paradigm. *Proc Natl Acad Sci USA*, 105(49):19486–91, 2008.

[49] S. Kakei, D. S. Hoffman, and P. L. Strick. Muscle and movement representations in the primary motor cortex. *Science*, 285(5436):2136–9, 1999.

[50] R. E. Kettner, A. B. Schwartz, and A. P. Georgopoulos. Primate motor cortex and free arm movements to visual targets in three-dimensional space. III. Positional gradients and population coding of movement direction from various movement origins. *J Neurosci*, 8(8):2938–47, 1988.

[51] E. T. Klemmer and F. C. Frick. Assimilation of information from dot and matrix patterns. *J Exp Psychol*, 45(1):15–19, 1953.

[52] S. Koyama, S. M. Chase, A. S. Whitford, M. Velliste, A. B. Schwartz, and R. E. Kass. Comparison of brain-computer interface decoding algorithms in open-loop and closed-loop control. *J Comput Neurosci*, 29(1-2):73–87, 2010.

[53] S. W. Kuffler. Discharge patterns and functional organization of mammalian retina. *J Neurophysiol*, 16(1):37–68, 1953.

[54] I. Kurtzer, T. M. Herter, and S. H. Scott. Random change in cortical load representation suggests distinct control of posture and movement. *Nat Neurosci*, 8(4):498–504, 2005.

[55] M. N. Kvale and C. E. Schreiner. Short-term adaptation of auditory receptive fields to dynamic stimuli. *J Neurophysiol*, 91(2):604–12, 2004.

[56] F. Lacquaniti, C. Terzuolo, and P. Viviani. The law relating the kinematic and figural aspects of drawing movements. *Acta Psychol (Amst)*, 54(1-3):115–30, 1983.

[57] S. Landgren, C. G. Phillips, and R. Porter. Cortical fields of origin of the monosynaptic pyramidal pathways to some alpha motoneurones of the baboon's hand and forearm. *J Physiol*, 161:112–25, 1962.

[58] S. Laughlin. A simple coding procedure enhances a neuron's information capacity. *Z Naturforsch C*, 36(9-10):910–2, 1981.

[59] I. S. MacKenzie. A note on the information-theoretic basis of Fitts' law. *J Mot Behav*, 21(3):323–30, 1989.

[60] I. S. MacKenzie. Fitts' law as a research and design tool in human-computer interaction. *Hum-Comput Interact*, 7(1):91–139, 1992.

[61] I. S. MacKenzie and W. Buxton. Extending Fitts' law to two-dimensional tasks. In *Proceedings of the SIGCHI conference on Human factors in computing systems*, pages 219–226. ACM, 1992.

[62] U. Maoz, E. Portugaly, T. Flash, and Y. Weiss. Noise and the two-thirds power law. In *Advances in Neural Information Processing Systems*, pages 851–858.

[63] M. Maravall, R. S. Petersen, A. L. Fairhall, E. Arabzadeh, and M. E. Diamond. Shifts in coding properties and maintenance of information transmission during adaptation in barrel cortex. *PLoS Biol*, 5(2):e19, 2007.

[64] G. A. Miller. The magical number seven plus or minus two: some limits on our capacity for processing information. *Psychol Rev*, 63(2):81–97, 1956.

[65] G. A. Miller and F. C. Frick. Statistical behavioristics and sequences of responses. *Psychol Rev*, 56(6):311–24, 1949.

[66] B. R. Moore. A modification of the rayleigh test for vector data. *Biometrika*, 67(1):175–180, 1980.

[67] D. W. Moran and A. B. Schwartz. Motor cortical representation of speed and direction during reaching. *J Neurophysiol*, 82(5):2676–92, 1999.

[68] J.-P. Nadal and N. Parga. Nonlinear neurons in the low-noise limit: a factorial code maximizes information transfer. *Network: Computation in neural systems*, 5(4):565–581, 1994.

[69] H. Nyquist. Certain factors affecting telegraph speed. *American Institute of Electrical Engineers, Transactions of the*, XLIII:412–422, 1924.

[70] H. Nyquist. Certain topics in telegraph transmission theory. *American Institute of Electrical Engineers, Transactions of the*, 47(2):617–644, 1928.

[71] E. R. Oby, C. Ethier, and L. E. Miller. Movement representation in the primary motor cortex and its contribution to generalizable emg predictions. *J Neurophysiol*, 109(3):666–78, 2013.

[72] I. Ohzawa, G. Sclar, and R. D. Freeman. Contrast gain control in the cat's visual system. *J Neurophysiol*, 54(3):651–67, 1985.

[73] A. Onken, S. Grunewalder, M. H. Munk, and K. Obermayer. Analyzing short-term noise dependencies of spike-counts in macaque prefrontal cortex using copulas and the flashlight transformation. *PLoS Comput Biol*, 5(11):e1000577, 2009.

[74] S. Panzeri, R. Senatore, M. A. Montemurro, and R. S. Petersen. Correcting for the sampling bias problem in spike train information measures. *J Neurophysiol*, 98(3):1064–72, 2007.

[75] I. Pollack. The information of elementary auditory displays. *The Journal of the Acoustical Society of America*, 24(6):745–749, 1952.

[76] I. Pollack. The information of elementary auditory displays. II. *The Journal of the Acoustical Society of America*, 25(4):765–769, 1953.

[77] M. M. Quallo, A. Kraskov, and R. N. Lemon. The activity of primary motor cortex corticospinal neurons during tool use by macaque monkeys. *J Neurosci*, 32(48):17351–64, 2012.

[78] R. Quian Quiroga and S. Panzeri. Extracting information from neuronal populations: information theory and decoding approaches. *Nat Rev Neurosci*, 10(3):173–85, 2009.

[79] J. A. Rathelot and P. L. Strick. Subdivisions of primary motor cortex based on cortico-motoneuronal cells. *Proc Natl Acad Sci U S A*, 106(3):918–23, 2009.

[80] A. Rees and A. R. Palmer. Rate-intensity functions and their modification by broadband noise for neurons in the guinea pig inferior colliculus. *J Acoust Soc Am*, 83(4):1488–98, 1988.

[81] G. A. Reina, D. W. Moran, and A. B. Schwartz. On the relationship between joint angular velocity and motor cortical discharge during reaching. *J Neurophysiol*, 85(6):2576–89, 2001.

[82] P. T. Sadtler, K. M. Quick, M. D. Golub, S. M. Chase, S. I. Ryu, E. C. Tyler-Kabara, B. M. Yu, and A. P. Batista. Neural constraints on learning. *Nature*, 512(7515):423–6, 2014.

[83] J. N. Sanes and J. P. Donoghue. Plasticity and primary motor cortex. *Annu Rev Neurosci*, 23:393–415, 2000.

[84] A. B. Schwartz. Direct cortical representation of drawing. *Science*, 265(5171):540–2, 1994.

[85] A. B. Schwartz, R. E. Kettner, and A. P. Georgopoulos. Primate motor cortex and free arm movements to visual targets in three-dimensional space. I. Relations between single cell discharge and direction of movement. *J Neurosci*, 8(8):2913–27, 1988.

[86] C. E. Shannon. A mathematical theory of communication. *Bell Syst Tech J*, 27(3):379–423, 1948.

[87] C. E. Shannon. Communication in the presence of noise. *Proceedings of the IRE*, 37(1):10–21, 1949.

[88] R. Shapley and C. Enroth-Cugell. Visual adaptation and retinal gain controls. *Progress in retinal research*, 3:263–346, 1984.

[89] D. J. Simons. Response properties of vibrissa units in rat SI somatosensory neocortex. *J Neurophysiol*, 41(3):798–820, 1978.

[90] N. J. A. Sloane. Spherical codes: Nice arrangements on a sphere in various dimensions. http://neilsloane.com/packings/index.html, 2015.

[91] S. M. Smirnakis, M. J. Berry, D. K. Warland, W. Bialek, and M. Meister. Adaptation of retinal processing to image contrast and spatial scale. *Nature*, 386(6620):69–73, 1997.

[92] R. W. Soukoreff, J. Zhao, and X. Ren. *The Entropy of a Rapid Aimed Movement: Fitts Index of Difficulty versus Shannons Entropy*, pages 222–239. Springer, 2011.

[93] D. M. Taylor, S. I. Tillery, and A. B. Schwartz. Direct cortical control of 3d neuroprosthetic devices. *Science*, 296(5574):1829–32, 2002.

[94] M. Velliste, S. Perel, M. C. Spalding, A. S. Whitford, and A. B. Schwartz. Cortical control of a prosthetic arm for self-feeding. *Nature*, 453(7198):1098–101, 2008.

[95] P. Viviani and R. Schneider. A developmental study of the relationship between geometry and kinematics in drawing movements. *J Exp Psychol Hum Percept Perform*, 17(1):198–218, 1991.

[96] K. Voelkel. Entropy mutual information relative entropy relation diagram. https://commons.wikimedia.org/wiki/File:Entropy-mutual-information-relative-entropy-relation-diagram.svg, Oct. 2010.

[97] B. Wark, B. N. Lundstrom, and A. Fairhall. Sensory adaptation. *Curr Opin Neurobiol*, 17(4):423–9, 2007.

[98] A. T. Welford. The measurement of sensory-motor performance: Survey and reappraisal of twelve years' progress. *Ergonomics*, 1960.

[99] A. T. Welford. *Fundamentals of skill*. Methuen's manuals of modern psychology. Methuen, London,, 1968.

[100] G. Werner and V. B. Mountcastle. Neural activity in mechanoreceptive cutaneous afferents: Stimulus-response relations, Weber functions, and information transmission. *J Neurophysiol*, 28:359–97, 1965.

[101] B. Wodlinger, J. E. Downey, E. C. Tyler-Kabara, A. B. Schwartz, M. L. Boninger, and J. L. Collinger. Ten-dimensional anthropomorphic arm control in a human brain-machine interface: difficulties, solutions, and limitations. *J Neural Eng*, 12(1):016011, 2014.

[102] B. M. Yu, J. P. Cunningham, G. Santhanam, S. I. Ryu, K. V. Shenoy, and M. Sahani. Gaussian-process factor analysis for low-dimensional single-trial analysis of neural population activity. *J Neurophysiol*, 102(1):614–35, 2009.

[103] J. H. Zar. *Biostatistical analysis*. Prentice-Hall/Pearson, Upper Saddle River, N.J., 5th edition, 2010.